Robustness assessment of leak detection and localization in water distribution networks under stochastic water demand

by

J.E. van Steen

In fulfilment of the requirements for the degree of Master of Science in

Civil Engineering

at the Delft University of Technology

Personal information: **J.E. van Steen**   TU Delft, Civil Engineering
                                                     Student number: 4594622
                                                     Tel: +31681368100
                                                     Email: jipvansteen@gmail.com

Thesis Committee :   **Dr. ir. E. Abraham**,   TU Delft, CEG,
                     Chairman   Water Management

                     Dr. D.B. Steffelbauer,   TU Delft, CEG,
                     Supervisor   Water Management

                     Ir. S. Balkema,   Royal HaskoningDHV
                     Company supervisor

                     Prof. dr. J.P. van der Hoek,   TU Delft, CEG,
                     Supervisor   Water Management

Abstract

Globally, water demand is rising and resources are diminishing. In the context of climate change and a growing world population, a further increase in water scarcity seems inevitable. Aiming towards a sustainable future, water should be used as efficiently as possible by minimizing water losses, which can be higher than 50% in some drinking water networks. To minimize water losses it is crucial to detect, localize and repair leaks as soon as possible.

Leaks can be efficiently and automatically tracked down in the early stages by using leak detection and localization techniques. These techniques are based on coupling information from flow and pressure measurements with the hydraulic model of the drinking water network. The success of such methods depends to a great extend on the estimation of the uncertain water demand in the area. The water demand within a hydraulic model is usually estimated in a deterministic fashion, which lacks the ability to realistically describe the fluctuations in water demand. To include realistic fluctuations in water demand, this study proposes a novel approach by estimating the water demand in a stochastic way by simulating it with SIMDEUM. This stochastic demand model uses information of water users and water-use appliances from Dutch statistics to simulate realistic domestic drinking water demands and its stochastic variations. With this approach, this study aims to assess the influence of a realistic stochastic demand model on the robustness of leak detection and localization algorithms.

The applied case study is a residential area in the Netherlands, consisting of a drinking water network with an inflow and six pressure sensors. The corresponding hydraulic model uses stochastic demand loading conditions as inputs. The model represents the network reliably when the SIMDEUM software with local statistics is used instead of average Dutch household statistics. By conducting a Monte Carlo analysis, the influence of stochastic demand on the variability of simulated flow and pressures is determined.

Artificial leaks are simulated and the influence of stochastic demand on the performance of leak detection and leak localization is analyzed. The leak detection method consists of setting up confidence intervals per sensor from Monte Carlo simulations and checking whether data falls within these intervals. The leak localization method is based on simulating artificial leaks on all possible locations in the model and comparing the resulting simulated pressures for each simulation to the observed data by using Pearson's correlation coefficient. The position of the leak in the simulation most similar to the observations is most likely to be near the real leak position.

The results show that the stochastic demand variability is strongly linked to the performance of leak detection and localization. The leak detection and localization is most sensitive during the night due to low nocturnal demand fluctuations and least sensitive during the morning peak, when diurnal demand fluctuations are highest. Moreover, the results show that the position and size of the leak significantly influence the performance of leak detection and localization.

This study shows that stochastic water demand can be used to quantify the influence of realistic demand variations on the performance of leak detection and localization. Hence, it is recommended to assess the robustness of more leak detection and localization techniques by using stochastic water demand. Furthermore, it gives insight into the expected variability in pressure throughout the network, hence, can prove to be useful in optimal sensor placement.

Acknowledgements

Table of Contents

1. Introduction

This chapter serves as introduction to the study, in which the problem statement and research questions are discussed followed by an introduction into the topic in the form of a literature review, for the readers that are not familiar with the subject.

Drinking water that flows out of your tap comes from an underground network of pipelines, as illustrated in Figure 1.1. Such an underground network that distributes water is known as a Water Distribution Network (WDN), a schematic representation of such a network is shown in Figure 1.2. A pump is used at the beginning of a WDN such that the water gets distributed at a high enough pressure in the entire network. The source of the water that gets distributed is usually a water purification plant or a distribution reservoir. However, not every drop of water that enters the network reaches the customer, an average of 23% in Europe gets lost before reaching the customer (EurEau 2017). Leakage is the major component of these water losses in developed countries (Farley et al. 2001). Detecting, localizing and repairing leaks leads to minimizing valuable water loss. Furthermore, lower distribution losses result in savings on energy, hence lead to financial benefits and reducing the carbon footprint. Moreover, reducing the amount of leaks reduces its potential destructive impact on the surrounding infrastructure. Hence, the necessity to detect, localize and repair leaks is emphasized.

Figure 1.1: Underground water pipes, image adopted from Cochran 2020
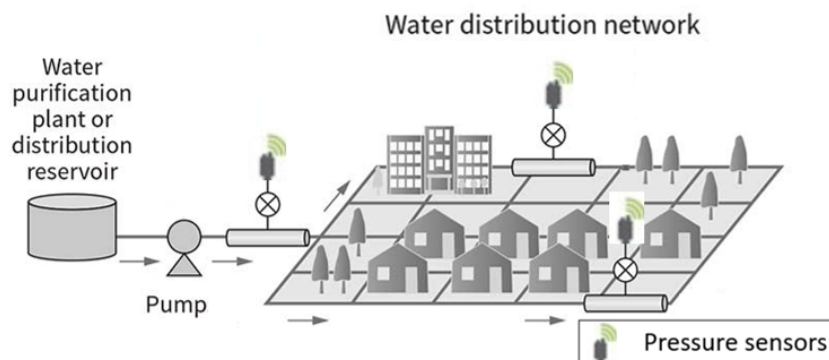
Figure 1.2: Sketch of a WDN, image adopted from Scan 2020

1.1 Problem statement

Leaks in WDNs result in valuable water loss, higher pump energy and a potential destructive impact on the surrounding infrastructure. Hence, it is of importance to trace leaks as soon as possible. WDNs are usually pressurized, hence if a leak appears in the network, it causes a change in inflow and pressure in the network. These changes can be measured by installed flow and pressure sensors in the network. Model-based leak localization techniques use these measurements in combination with a hydraulic model of the WDN to compare simulations with the sensor measurements to trace back the leaks location.

Various leak localization techniques have been published in the literature. The success of these techniques depends, among other (e.g. amount, locations and accuracy of installed sensors), largely on the estimation of the uncertain water demand in the area. In addition to leaks, water demand affects the inflow and pressure in the network. Because water demand in the area is usually unknown, it needs to be estimated within the hydraulic model. The water demand is usually estimated in a deterministic fashion, which often neglects the realistic fluctuations in water demand. To include these fluctuations in the estimation, a new approach is proposed in which the water demand is estimated in a realistic stochastic manner.

The stochastic demand simulator SIMDEUM (Blokker 2006) is used in this study to simulate realistic domestic drinking water demands. This software uses statistical information of users and end-uses to simulate realistic water usage patterns on a micro scale (tap, toilet or shower). SIMDEUM is preferred above other stochastic demand software because it uses statistical information based on Dutch statistics, hence directly applicable to Dutch areas. Furthermore, simulations from this software are in good correspondence to measured water demands (Blokker et al. 2009).

With the water demand simulator software, realistic stochastic demand and variations in demand are simulated. The hydraulic model with these stochastic demand loading conditions is used to conduct Monte Carlo simulations. By means of these simulations and by simulating artificial leaks, the influence of stochastic demand on model-based leak localization techniques can be analyzed. The aim of this study is to analyze the robustness and limitations of leak detection and leak localization techniques with respect to realistic stochastic demand loading conditions.

Low water demand during the night leads to smaller pressure drops, but also contains low fluctuations. High demand occurring during the day lead to higher pressure drops but also higher fluctuations. Coupling realistic stochastic demand software with leak detection and localization techniques give insight into their performance under the influence of different demand conditions. The time during the day in which the performance improves, or the leak sizes that can still be detected and localized can be analyzed. Hence, the robustness of the leak detection and localization techniques can be assessed.

1.2 Research objective

The main research question that this study aims to answer is stated as follows:

**How does the use of stochastic demand models in leak detection
and model-based leak localization methods influence their performance?**

To systematically address this issue, four sub-questions are formulated that need to be answered consecutively:

1. How does the stochastic demand influence fluctuations in pressure and flow in a simulated system?
2. How do these pressure and flow fluctuations influence leak detectability when leaks are simulated?
3. How do these pressure and flow fluctuations influence the leak localization performance when leaks are simulated?

1.2.1 Collaboration with RoyalHaskoningDHV

This study is conducted in collaboration with the engineering company Royal HaskoningDHV (RHDHV). This study is conducted within the research branch of the *Aquasuite BURST Find* group. *Aquasuite* is a product of RHDHV and it consists of a monitoring and control software platform aiming to monitor, control and optimize water systems. Different products within Aquasuite are available serving specific purposes. The Dutch water sector controls a lot of valuable assets and has an enormous amount of information and data being generated by these assets. Aquasuite can provide smart data management to make efficient use of this big data. Several water utility companies in the Netherlands have bought their product, resulting in Aquasuite software controlling about 70% of the drinking water produced in the Netherlands.

Aquasuite BURST is one of these products, relatively new and still in development. As the name already reveals, it aims to detect and localize leaks in water distribution networks. Aquasuite BURST can be generally split up into two branches: *BURST Alert* and *BURST Find*. The former focuses on the detection of leakages, while the latter focuses on the localization of leaks. Definitions concerning water losses are elucidated in section Section 1.3.1. Within the BURST program, new innovations are developed to reduce water loss together with six water companies who have installed sensors in some of their networks. The Aquasuite BURST program members are Brabant Water, WML, Oasen, Waterbedrijf Groningen, PWN and Dunea.

Hence within the BURST program, water distribution networks are available with installed pressure and flow sensors. Some networks have collected data of over a year, suitable for analysis within the contours of this study. In collaboration with RHDHV and the BURST program members, this study aims to gain insight into the uncertainties of water demand on leak detection and localization through the implementation of stochastic demand in a water distribution network. Insight into the influence of uncertain water demand on leak detection and localization performance is relevant research within the development of *BURST Find*.

1.3 Background

This section provides the necessary background information needed to understand the process and methodology of this study. It serves as an introduction into the topic in the form of a literature review. In the first subsection, the necessary terminology related to water distribution and water losses is discussed. Thereafter a brief overview is given of the literature concerning leakage control, hydraulic modelling, leak detection and localization

methods, deterministic and stochastic water demand modelling.

1.3.1 Terminology concerning water losses

A drinking water utility produces and distributes water. Drinking water is commonly transmitted using underground pipelines. An underground network of pipelines is referred to as a WDN. Due to a variety of reasons, a leak can appear in the network which can cause a significant loss of water. Examples of causes that lead to a leak are damaged pipes, lack of maintenance or an increase in pressure. To minimize the effects of leaks, it is of major importance to detect and locate the leak as soon as possible.

The standard terminology concerning the components of the water balance of a WDN is set up by the International Water Association (IWA) and is illustrated in Table 1.1.

Table 1.1: Standard water balance of a WDN, adopted from Lambert and Hirner 2000

Water Balance Table of IWA				
System Input Volume	Authorized Consumption	Billed Authorized Consumption	Billed Metered Consumption	Revenue Water
			Billed Unmetered Consumption	
		Unbilled Authorized Consumption	Unbilled Metered Consumption	**Non-Revenue Water (NRW)**
			Unbilled Unmetered Consumption	
	Water Losses	Apparent Losses	Unauthorized Consumption	
			Customer Metering Inaccuracies	
			Systematic Data Handling Errors	
		Real Losses	Leakage on Transmission and Distribution Mains	
			Leakage and Overflows at Utility's Storage Tanks	
			Leakage on Service Connections up to point of Customer metering	

The system input of a WDN is the starting point of the water balance. It can be split up into *Revenue Water* and *Non-Revenue Water (NRW)*. The billed metered consumption together with the billed un-metered consumption form the revenue water. The NRW is calculated by subtracting the revenue water from the system input of the network. Hence, it describes where the water utility actually loses money, because no money is received for this water. *Water losses* are part of the NRW, and they can be subdivided into *apparent losses* and *real losses*. Apparent losses contain unauthorized consumption (illegal water use, or water theft) and metering inaccuracies. Real losses is the volume that is physically lost from the system. In this study, the focus lies on detecting and locating real losses, or more specifically on leaks in transmission and distribution mains.

Beside from the generally accepted standard terminology from the IWA, different studies in the literature use different terminologies regarding water losses or referring to similar methods for finding leaks. To clarify the terminology used in this study, the definitions of leaks, leakages, leak detection and leak localization are clarified in the following paragraphs, adopted from Steffelbauer 2018.

In WDNs, water is lost through holes, cracks or breaks in pipes or water escapes the pipe system through faulty joints and fittings between pipes. In the literature, this is often called leak or leakage. Hence to emphasize the difference between the two, the term *leak* is the physical hole in a pipe through which water is lost. The term *leakage* is the process of water escaping the system through a leak. In this study, no distinction is made between the different forms of leaks (holes, cracks, faulty joints etc.) because it is not of importance how the water is lost.

Leak detection refers to the task of realizing that a leak occurred somewhere in the system, hence to become aware of a leak somewhere present in the system without finding its location. If a leak is detected, the location of the leak is of interest. *Leak localization* refers to the process of finding the approximate location of a leak in a certain area. Finding the approximate location is already valuable since only a part of the network has to be searched for the leak instead of the entire system where a leak is detected. *Leak pinpointing* means finding the exact location of the leak.

There are different kind of leaks, and they can generally be split up into three categories. *Bursts* or large leaks have a large discharge and are usually noticed relatively fast due to the destructive impact on its surrounding. *Small leaks* have a low discharge and usually a longer duration because it can take a longer time before the leak is detected (it can take more time for the impact of the leak to become noticeable). *Background leaks* are considered to have an even smaller discharge, they are assumed to be continuous leakages that usually go unnoticed.

It does not necessarily mean that small leaks have a smaller impact than large leaks. Because of the size of the leak, a small leak is generally harder to detect and can over time transform into a large leak. Hence in the end, small leaks can have the same impact as large leaks (Moors et al. 2016). It is therefore of importance to automatically detect leaks in an early stage such that water is saved and small leaks do not turn into bursts.

1.3.2 Leakage control

An average of 23% of treated water in Europe gets lost before reaching the customer (EurEau 2017) and leakage is the major component of water loss in developed countries (Farley et al. 2001). Beside the fact that detecting, localizing and repairing leaks leads to minimizing valuable water loss, lower distribution losses also result in savings on energy due to a decrease in pump use needed to distribute the water. Hence leading to financial benefits and reduction of the carbon footprint. Furthermore, reducing the amount of leaks reduces its potential destructive impact on the surrounding infrastructure. Hence leakage control is of great importance in WDNs.

Leakage control has been of importance since the positioning of the underground pipe network, though the used techniques have developed and changed over time. A clear distinction of two strategies can be made within leakage control: passive leakage control and active leakage control. In passive leakage control, action is only taken when the leak is visible at the surface or when customers report leak-related complaints (e.g. a low water pressure at their tap). The downside of this strategy is that as soon as leaks become visible, serious damage is often already done to the surrounding infrastructure. Furthermore, not all leakages appear at the surface. Hence, this strategy leads to high total water losses compared to the active leakage control (Farley and Trow 2003).

The preference is therefore usually given to active leakage control. Active leakage control focuses on regularly examining the distribution system for leakages to reduce the impact of leaks. There are various known active leakage control methods for detecting and locating leaks, ranging from ground-penetrating radar to acoustic listening devices (Farley and Trow 2003). Although all of these methods have their own advantages and disadvantages, all the available techniques for active leakage control are generally expensive, labour intensive, time consuming, pipe-material dependent, only applicable during the night and result in long leakage detection and leak localization times (brief overview in Steffelbauer 2018, extensive review in Puust et al. 2010).

Hence, researchers have been looking for different methods that can detect and localize leaks in an automated and more efficient way. A relatively new technique is model-based localization. Essential in this technique is a hydraulic model that is able to simulate the

behaviour of a WDN.

1.3.3 Hydraulic modelling of a WDN

A mathematical hydraulic model is a simplification of a real-world system to help analyze the system's hydraulic behaviour. A hydraulic model can be created to simulate the behaviour of a WDN given different operating conditions in a pressurized pipe network. Such a hydraulic model computes the flow and head loss at all links in the network and the pressure at every node in the WDN. This is achieved by solving a large set of non-linear equations depending on what physical principles are assumed (like the conservation of mass and energy).

Different types of hydraulic models can be used, as discussed in Kapelan 2002: the steady flow model, the quasi-steady flow model, the unsteady in-compressible flow model and the unsteady compressible flow model. The steady flow model performs steady-state simulations in which conservation of energy and conservation of mass are assumed. The quasi-steady flow model simulates changes of a WDN over time, although it applies a steady-state simulation at every time-step. The other two unsteady or transient models adapt the energy conservation principle and are generally more complex than the steady flow models.

This study will apply the quasi-steady hydraulic flow model to simulate changes of a WDN over time. As a side note, one should keep in mind that a mathematical model is always an approximation of reality, no matter how complex and accurate it aims to be (Kapelan 2002).

To set up an hydraulic model, the model first needs to be configured. Configuration of the network involves creating a hydraulic model from structural (e.g. position pipes or location domestic drinking water connections) and geometrical data (e.g. diameter or roughness of the pipes). Furthermore, a formula needs to be chosen from the multiple formulas that can be used in the hydraulic model to calculate head loss. Head loss in the network is caused by two phenomena: friction and local losses.

Friction head losses are simply the result of flow through a straight pipe due to wall friction. In this study, the Hazen-Williams (HW) equation is used to calculate this head loss, which is given in International System of Units (SI) as follows:

$$h_L = \frac{32}{3} C^{-\gamma} d^{-\beta} Q^{\gamma} L \tag{1.1}$$

where h_L (m) is the pipe headloss, C (−) is the HW roughness coefficient, $\gamma = 1.852$ and $\beta = 4.871$ are constants, d (m) the pipe diameter, L (m) the pipe length and Q (m^3/s) the flow rate of water in the pipe.

The other type of head loss, the local losses, are traditionally referred to as minor losses with the (sometimes incorrect) implication that the majority of the system head loss is associated with the friction in straight pipes. They are the result of flow through components other than straight pipes; for example entries, exits, bends, fittings and valves. The head loss caused by local losses could be formulated with a local loss coefficient added to Equation 1.1.

However, the roughness coefficient in the HW equation and the minor loss coefficient are usually both unknown for a network. It is generally impossible to distinguish between the two, hence in this study only the HW roughness coefficient is taken into account, which thereby implicitly includes the local losses. This incorporation of the local losses into the HW roughness coefficients means that the roughness coefficients are likely to be slightly higher (yielding in less friction head loss) in practice than the theoretical values in the hydraulic model due to the negative exponent of the roughness coefficient in Equation 1.1.

After the configuration of the hydraulic model, it needs to be calibrated to improve the accuracy of the estimated network characteristics so that it can mimic the WDN accurately. A

well calibrated hydraulic model is a prerequisite in performing model-based leak localization (Meseguer et al. 2014). Calibration of a hydraulic model has been studied a lot the past four decades, resulting in numerous publications in this field. A review of the wide variety of calibration methods the literature has to offer can be found in Savic et al. 2009 and Kapelan 2002. Although a lot can be read in the literature about calibrating a model, it is emphasized that the process of calibration is neither unique nor straight-forward and its success is partly based on the modelers experience and intuition (Ostfeld et al. 2012).

For the calibration in this study, pressure and flow measurements in the network are used. During the calibration of the model, observed and simulated flows as well as observed and simulated pressures are compared. To minimize the difference between the two, model parameters are adjusted during the calibration in which an optimization method is applied to minimize the differences.

1.3.4 Leak detection and localization

WDNs are usually pressurized, hence leaks cause a change in inflow into the system and a change in pressure in the network. The water that flows out of the leak has to be compensated by an increase in inflow of the system due to the continuity (or water balance) equation. Furthermore, the flow through the leak causes an increase in flow velocities in parts of the system which are upstream of the leak (Steffelbauer 2018). Higher velocities lead to higher friction losses, hence result in pressure drops. Leak detection and localization techniques are founded on these physical effects, they exploit the fact that pressure and flow change when a leak occurs.

By using sensors in the network that measure the pressure and flow, leak detection and localization can in essence work in a complete automated way. If a leak appears in the network, it can warn the responsible water utility of the leak happening in the area and ideally give an approximate location of the leak. This is a much more efficient way than the older time- and labour-intensive leakage control methods. Hence, reducing the detection and localization time of a leak, yielding in less water loss.

The success of model-based leak localization depends largely on the configuration of the network, the accuracy of estimated network characteristics (e.g. pipe roughness), the accuracy of the sensors and the accuracy of estimated demand patterns (Pudar and Liggett 1992). The former two relate to the configuration and calibration of the hydraulic model (discussed in the previous subsection) and the latter one is the main topic of this study. Accurate demand modelling can have a positive effect on the accuracy of leak detection and localization, this will be further elucidated in Section 1.3.5.

Leak detection

If a leak appears in the WDN, the first step is to detect the leak; to become aware of the leak being present in the network. As already stated, measurements in the field are necessary to detect leaks automatically. The smaller the monitored area, the easier a leak can automatically be detected. A network can be subdivided into smaller compartments. A smaller compartment is called a District Metered Area (DMA). There is a relation between the size of the monitored area and the size of the leaks that can be detected automatically (Bakker et al. 2014b; Bakker 2014). For the detection of leaks, various diverse methods can be used (Puust et al. 2010).

To keep it simple, this study solely looks at statistics to detect leaks, discussed in detail in Section 2.3. The corresponding fluctuations at the sensors can be deduced from conducting hydraulic simulations with different demand loading conditions. With Monte Carlo simulations, the corresponding fluctuations at the sensors are computed and confidence intervals at the sensors are set up. If a measurement at a sensor exceeds its confidence

interval, a detection alarm is triggered.

Leak localization

After one has become aware of a leak happening in the system, the next step is to find the leak's approximate location. When a leak is altering a system's flow and pressure response in some way, these alterations are in theory discernible at other locations in the network and they have the potential to reveal useful information about the location of the leak (Colombo et al. 2009). If these alterations provide a clear and unique fingerprint, a leak can be theoretically localized by comparison of the pressure signals registered by sensors relative to the signal that would be observed if the system did not contain the leak.

There are various model-based leak localization methods published in the literature. A general distinction can be made between transient methods and steady-states methods. An extensive review of transient methods can be found in Puust et al. 2010. The success of transient methods are usually limited due to the fact that a WDN is often highly looped, contains many valves, tanks and pumps, which yields in damping of the transient waves.

A steady-state leak localization method can be found in Quevedo et al. 2011 in which pressure residuals are obtained by comparing measurements and simulated pressures from the model. This method is further elucidated in Meseguer et al. 2014, and is validated by Mirats-Tur et al. 2014 and Moors et al. 2016. This approach requires accurate estimates of the water demands in the area because of its influence on pressure variations and therefore also leak localization performance (Meseguer et al. 2014; Mirats-Tur et al. 2014; Perez et al. 2014). A uniform and a factorized demand model were applied with this approach, in which the factorized demand model yielded in better results (Moors et al. 2018). Stochastic demand can prove to be valuable in this approach, hence, the method of Quevedo et al. 2011 is chosen as leak localization method in this study.

The leak localization method is explained here in a nutshell. When the hydraulic model is calibrated and a leak is detected in the system, changes in measurements can be observed at the pressure sensors, which are inconsistent with the simulated measurements from the calibrated model. By running simulations in which artificial leaks are placed on all possible locations in the network, the resulting simulated measurements for each simulation are compared to the observed data. The simulation in which the simulated measurements has the highest similarity to the observed measurements is the best fit to the real case. Hence the position of the leak in this simulation is most likely to be the position of the real leak. The leak localization method is explained in more detail in Section 2.4.

The model-based leak localization method of Quevedo et al. 2011 works in practice, although the results are not always accurate. This is due to the fact that the accuracy does not solely depend on the used leak localization technique. Other complicated issues arise that have their effect on the results of model-based leak localization. The accuracy of model-based leak localization depends, among others (e.g. optimal sensor placement, discussed in Cheng et al. 2017 or Cugueró-Escofet et al. 2017), largely on demand modelling. The problem within demand modelling is that the spatially and temporally varying demand needs to be known or estimated. Hence being able to accurately model the water demand can positively influence the accuracy of leak localization. The main focus of this study lies in this area, hence demand modelling will be further discussed in the next subsection.

1.3.5 Demand modelling in leak detection and localization

The success of leak detection and localization depends highly on the uncertainties present in the system. One of the main sources of uncertainty is the water demand in the network. Water demand throughout the system is usually unknown; spatially and temporally. The water demand as well as a potential leak affect the pressure and the flow in the system in a

similar way. Hence, if a change in pressure and flow is observed, it can be challenging to distinguish the two potential causes. Therefore, accurate demand modelling can improve the accuracy of the leak detection and localization.

The most accurate way of determining the water demands in the network would be to massively and continuously measure the consumption of all water-using buildings (households, offices, stores, schools, etcetera) that are attached to the network. To achieve this, smart meters should be placed at every building that is able to withdraw water from the network and the data should become available and analyzed directly. A sudden change in the system, uncorrelated to the water demand fluctuations, can therefore directly be linked to a leak after which the leak localization can be applied.

Measuring water demand this extensively is usually not realistic. Placing smart meters throughout the network is labour intensive and expensive. Furthermore, setting up a system in which the data of all the smart meters is continuously imported and synced, and is able to directly analyse this amount of data is at least challenging. Therefore some estimation is usually made to predict this demand.

Different strategies can be used to make a prediction of the water demand in the area. A general distinction is made between using deterministic and stochastic water demand. No randomness is involved in the former while the latter is inherently based on probability.

Deterministic water demand

An overview of traditional deterministic water demand forecasting literature can be found in Donkor et al. 2014. An example of a deterministic demand forecast model is described in Bakker et al. 2013, which predicts the total water demand in the area. Although the domestic drinking water demand is usually measured only a couple of times per year, the total water demand over the total area can be determined by performing a water balance calculation. Because the inflow to the area is usually measured with a much higher frequency, one can equate this to the total water demand with the implicit assumption that all water reaches the customers (and no change in storage is happening). Background leaks are therefore incorporated in this total water demand.

In performing model-based leak localization, some estimation has to be made for the location specific water demand in the area, because this influences the localization of the leak. A strategy to predict the water demand that incorporates spatial variance is generally more difficult. The most direct and rough way to do this is to assume a homogeneously distributed consumption at any time. Hence, the measured inflow which should be equivalent to the net water demand according to the water balance, gets evenly distributed over the amount of junctions in the model. Hence, this strategy does not take any spatial variance into account (only temporal variance).

Another more accurate strategy would be to look at the latest water billing information (factorized demand model) in the area for each household, calculate how much water a household used and sum the amount of water spend by all households connected to a node in the network. An example of a study that applied this strategy can be found in Moors et al. 2018. This yields in a water consumption for each node based on the last-measured period, thus spatial variance of water demand is included in the area.

By implicitly assuming that the water demand per node will not deviate much in the future from the last-measured period, this water demand for each node can be scaled back to daily consumption (or even hour or second water demand, if wanted). Hence this value is a scalar and is known as the base demand factor. To include the temporal variance of the nodal water demand, a demand pattern is constructed from the inflow pattern by applying the continuity equation, shown in Equation 1.2 and Equation 1.3.

$$Q_{inflow}(t) = D_{tot}(t) = \sum_i D_{n_i}(t) = \sum_i (B_{n_i} \cdot D_{P_i}(t)) = \sum_i (B_{n_i}) \cdot D_{Pat}(t) \qquad (1.2)$$

Hence the demand pattern for all nodes is calculated as follows:

$$D_{Pat}(t) \equiv \frac{Q_{inflow}(t)}{\sum_i B_{n_i}} \qquad (1.3)$$

where $Q_{inflow}(t)$ is the inflow discharge, assumed to be equivalent to the total demand $D_{tot}(t)$. $D_{n_i}(t)$ is the demand throughout the day for node i, B_{n_i} is the base demand factor for node i, $D_{P_i}(t)$ is the demand pattern for node i and $D_{Pat}(t)$ the characteristic demand pattern for the entire area. If the base demand factor B_{n_i} is given in terms of daily consumption, $D_{Pat}(t)$ has to be a daily pattern.

It is disputable whether the strategies above give a reliable enough representation of the water demand in the area, since they do not cover demand fluctuations. It accounts to some extend for the spatial and temporal variance. However, the uncertainty as well as the implications on the accuracy of leak detection and localization are unknown. Beside from the strategies explained above, Donkor et al. 2014 analyzed a large sample of other deterministic water demand forecasting methods and models. They concluded that more attention should be given to probabilistic forecasting methods to reflect the level of uncertainty in demand forecasts.

Stochastic water demand

Researchers started approaching water demand modelling in a stochastic manner around thirty years ago. Bao and Mays 1990 were amongst the first in characterizing water demand using Monte Carlo sampling to generate synthetic data. In the years after, a fair amount of studies were conducted into representing the residential water demand by means of probabilistic methods, hence describing water demand in a more realistic way.

One of the models in the literature is for example the stochastic demand model proposed by Gargano et al. 2016, which generates stochastic water demand of single residences as displayed at the house water meter. It does not distinguish demand pulses relating to the different activities in the residence.

Another more detailed stochastic demand model is SIMDEUM (Blokker et al. 2009; Blokker 2010), which stands for simulation of water demand and end-use model. End-uses are activities in which water is tapped from the network (e.g. flushing the toilet, using the dishwasher or brushing teeth). This end-use approach to determine water demand patterns is based on statistical information of users and water-using appliances instead of water demand measurements. Hence, difference in water use behaviour leads to different water use patterns.

SIMDEUM is able to predict water demand patterns on small timescale (1 second) and small spatial scale (end-use level). The model can simulate water demands for diverse residential areas if statistical information about that area and its inhabitants is present. The statistical input data that the model uses is by default based on average Dutch statistics. Hence, applying this model to an area in a different country would involve collecting country-specific data to modify its parameters, which might be a challenge (e.g. modifying the average water-using appliances).

SIMDEUM is preferred above other stochastic demand models in this study because it uses Dutch average statistics, hence, directly applicable to Dutch areas. Furthermore, it has been validated with measurements in several studies in the Netherlands (Blokker 2010; Blokker et al. 2017). A limitation of SIMDEUM is that numerous parameters are needed to set up and run simulations. Collecting this significant amount of specific data is challenging

as some of the required parameters are variable, difficult to collect and prone to inaccurate estimations (Blokker et al. 2018). All in all, SIMDEUM is able to simulate realistic demands and realistic variations in those demands, within days, between days and between nodes. It can provide leak-free reference demand patterns, is able to realistically describe the water demand in a network and is proposed to be used in leakage modelling (Blokker et al. 2017). A detailed explanation of the model and how it is used is given in Section 2.1.

This study aims to assess the influence of realistic stochastic water demand on the performance of leak detection and localization. This novel approach to assess the performance of leak detection and localization under realistic demand fluctuations is, to the best knowledge of the author, new in the literature. Since it is unknown how realistic demand fluctuations influence the performance of leak detection and localization algorithms, an assessment of the robustness of these algorithms under realistic demand fluctuations is essential in improving these algorithms.

2. Methodology

A schematic overview of the methods and their connections are shown in Figure 2.1, including the sections where the methods can be found. Stochastic demand simulations on household level are computed using SIMDEUM (Blokker 2006), explained in detail in the first section. The applied case study is discussed in the second section, consisting of a network with inflow and pressure sensors. The corresponding hydraulic model of this network uses stochastic demand simulations as inputs. By conducting a Monte-Carlo analysis, the influence of stochastic demand on the variability of simulated inflow and pressure is determined. Leak simulations serve as basis for testing the effect of stochastic demand on the robustness of leak detection and localization algorithms. The leak detection method consists of setting up confidence intervals from a multitude of simulations and checking whether data falls within these intervals, discussed in the third section. The leak localization method is based on measuring additional pressure disturbances at the sensors caused by the occurrence of a leak. By running simulations in which artificial leaks are placed on all possible locations in the network, the resulting simulated pressures for each simulation are compared to the observed data. Pearson's correlation coefficient is used to determine which simulation is most similar to the observations, hence the corresponding leak node is most likely to be near the real leak position. The leak localization method is further elucidated in the fourth section.
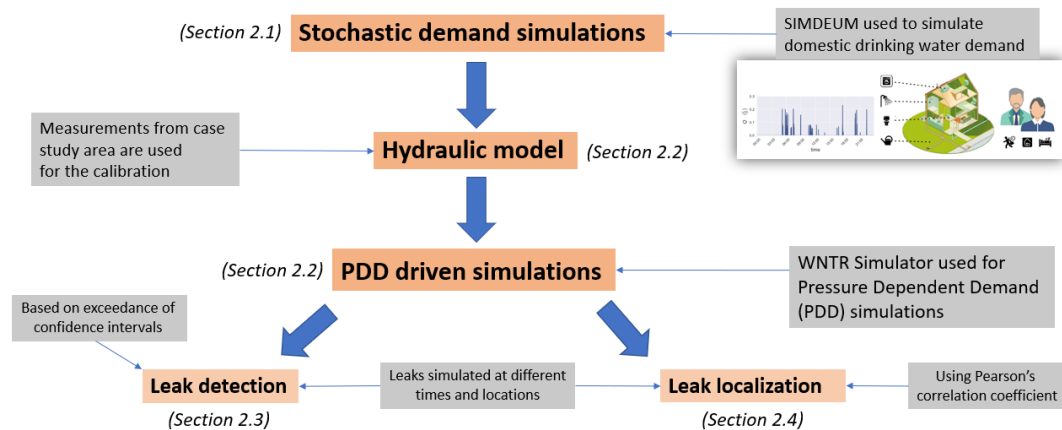
Figure 2.1: Schematic overview methodology

2.1 Stochastic demand simulations

This study uses SIMDEUM (Blokker 2006; Blokker et al. 2009; Blokker 2010), for stochastic demand simulations. SIMDEUM is a water demand end-use model developed by KWR Watercycle Research Institute. SIMDEUM can be used to simulate realistic residential water uses on small time (1 second) and spatial scales (at the end-use/device level). End uses are activities in which water is tapped from the network (e.g. flushing the toilet). The demand simulations are based on statistical information of users and water-using appliances.

2.1.1 Mathematics and statistics behind SIMDEUM

SIMDEUM simulates each end-use (toilet, shower, washing machine, dishwasher, kitchen tap, bathroom tap, bathtub and outside tap) as a pulse depending on the intensity, duration and frequency of the end-use. The intensity and duration are either technical data (size of toilet cistern, different programs of dishwasher or washing machine) or depend on user behaviour. Frequency and time of use depend on people's daily schedules (e.g. time of getting up, leaving the house). To simulate the domestic drinking water demand, all pulses are combined with a given probabilities over the day (related to the residents' activities, time of uses of specific end-uses and frequency of use).

There are eight different types of end-uses defined in SIMDEUM; the toilet, the shower, the washing machine, dishwasher, kitchen tap, bathroom tap, bathtub and outside tap. The users are divided into groups based on household size, age, gender, and occupation. Three household types are discerned: one-person households, two or more person households with no children and family households (households with two adults and children). For every household type, the number of people, the men/women fraction and the division over the different age groups is based on Dutch statistics and census data, see Table 2.1.

Table 2.1: Default household statistics (Blokker 2006)

		One person households	Two person households	Families with children
Number of people per household		1	2	3.75[a]
Number of households (%)		34	30	36
Gender division: male/female (%)		46/54	50/50	50/50
Age division (%)	Children (0–12 years old)	0	0	25
	Teens (13–18 years old)	0	0	16.5
	Adults (19–64 years old)	70	70	58.5
	Subdivision: % of adults with job away from home	Male: 67.5	Both persons: 49	Both parents: 39
			Only male: 26	Only father: 52
		Female: 52.4	Only female: 6	Only mother: 3
			Neither person: 18	Neither parent: 5
	Seniors (>65 years old)	30	30	0

[a]On average.

The way in which SIMDEUM creates water demand is described in two equations:

$$Q = \sum_{k=1}^{M} \sum_{j=1}^{N} \sum_{i=1}^{F_{jk}} B(I_{ijk}, D_{ijk}, \tau_{ijk}) \tag{2.1}$$

$$B(I_{ijk}, D_{ijk}, \tau_{ijk}) = \begin{cases} I_{ijk}, & \tau_{ijk} < T < \tau_{ijk} + D_{ijk} \\ 0, & elsewhere \end{cases} \tag{2.2}$$

in which Q is the total water use of a household over time and B is a water pulse related to specific end-uses. To elucidate the different parameters: k is an index over all end uses from 1 to M, j is an index over all users from 1 to N and i is an index over all water use events per day F_{jk}, which is user and end-use dependent. D_{ijk} (s) is the pulse duration, I_{ijk} (m^3/s) is the pulse intensity and τ is the starting time of the end use. Hence, the total water demand Q (m^3/s) over the day is calculated by summing all available end uses M, all users N and per end-use.

The frequency of use (F_{jk}) for each end-use is based on a residential water-use survey and is modeled as a discrete statistical distribution (Blokker et al. 2009). The pulse intensity (I_{ijk}) and pulse duration (D_{ijk}) are partly based on the survey and partly from technical information of water-using appliances. The pulse intensity is described as either a fixed number or a uniform distribution, depending on the end-use. The pulse duration is described

as a log-normal distribution, a chi-squared distribution or a fixed number, again depending on the end-use.

The usage time (τ_{ijk}) is correlated to the end uses and the diurnal pattern of the users. Rough diurnal patterns are based on a time-budget survey that describes activities like their sleep-wake rhythm and their time spent at home (see Table 2.2). The averages and standard deviations of their activities are deduced from the time-budget survey. The users' activity times are assumed to be strongly related to people's ages and occupation for week-days, for weekend days less so. Therefore, a general diurnal pattern is set up for all users during weekend days.

Table 2.2: Default diurnal patterns (Blokker 2006)

		Weekday							Weekend day
		Child	Teen	Adult with job away from home	Adult without job away from home	Senior	Total	
Time of getting up	μ	7:00	7:00	7:00	8:00	8:00	7:00	9:00
	σ	1:00	1:00	1:00	1:00	1:00	1:00	1:30
Time of leaving the house	μ	8:30	8:15	8:00	13:00	13:00	8:00	13:00
	σ	0:30	0:30	0:45	3:00	3:00	1:00	3:00
Duration of being away	μ	7 h	8 h	9.5 h	10 h	10 h	8.5 h	10 h
	σ	2 h	2 h	3.25 h	4.5 h	4.5 h	1 h	4.5 h
Duration of sleep	μ	10 h	9 h	7 h	8 h	8 h	8 h	9 h
	σ	1 h	1 h	1 h	1 h	1 h	1 h	1.5 h

These diurnal patterns are converted to probability density functions of water-use events with multiple conditions (e.g. the probability of the start of water use during absence is zero). The Cumulative Distribution Function (CDF) of such a probability density function, scaled between zero and one, is then able to produce the random starting time of water use (τ) under these conditions. The CDF of all end-uses are constructed in this way (based on the diurnal pattern from Table 2.2). For the kitchen tap, dishwasher and the washing machine, the CDF is afterwards multiplied with its corresponding known usage pattern.

It is emphasized that, the resulting demand patterns vary for every simulation since they are sampled from probability distributions. Since the default statistics used in SIMDEUM are based on average Dutch statistics, the resulting domestic drinking water demands are suitable for Dutch households. The statistics can be modified to make SIMDEUM applicable to other countries.

By default, the parameters of SIMDEUM are based on Dutch average statistics. Since values for these parameters can differ for different areas, SIMDEUM's parameters can be adapted to match the outputs better to measurements within a specific case study area. Two kind of settings can be easily changed in SIMDEUM that modify the general demand outcome, the household statistics and the diurnal patterns. The household statistics comprise of the composition of households, as shown in Table 2.1, the amount of households and the different types of households present. The diurnal patterns that can be modified are shown in Table 2.2. The parameters that are adapted in this study are the unemployment rate, the diurnal patterns of the residents and the negligence of the outside water use (outside water tap).

2.2 Case study area

The case study is a District Metered Area (DMA) in Duindorp, an urban domestic area located in the city district Scheveningen, part of the city Den Haag (Zuid-Holland, the Netherlands). The DMA is operated by the water utility Dunea. The total pipe length of the DMA sums up to 13.9 kilometers, with diameters ranging from 20mm to 250mm and the main pipe materials are PVC(A) or (H)PE. An overview of the DMA and its location can be

found in Figure 2.2. More details about the case study area can be found Appendix B.
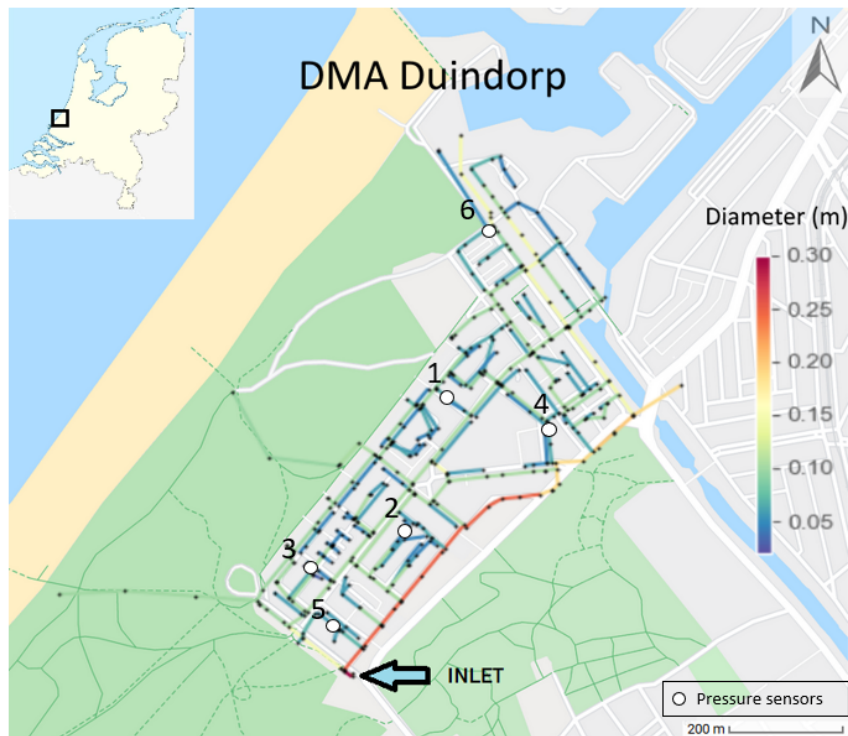

Figure 2.2: Network DMA Duindorp

2.2.1 Measurement devices

An inflow and six pressure sensors are installed in DMA Duindorp. The locations shown in Figure 2.2. Each pressure sensor is numbered for convenience such that they can be easily referred to later in this study. The accuracy of the inflow sensor is 0.5 m^3/h, the accuracy of all pressure sensors is approximately 0.6 meter head. More details about the sensors can be found Appendix B.

The smallest common frequency of all measurement devices is 5 minutes, hence, all sensor data is resampled to a 5 minute frequency and the same frequency is set at the hydraulic model simulations such that they can be easily compared. An extensive time series analysis concerning the measurement data in DMA Duindorp is described in Appendix C.

2.2.2 Hydraulic model

The configuration of the pipe network, including structural and geometrical data of the DMA Duindorp is available as a hydraulic model in EPANET. The hydraulic model is simulated with the Water Network Tool for Resilience (WNTR), designed to simulate and analyze resilience of water distribution networks. More details concerning the used software can be found in Appendix A. Headlosses are computed with Hazen-Williams (HW) (Equation 1.1) and demands are simulated with a Pressure Dependent Demand (PDD) model.

WNTR is able to run two types of simulations: Demand Driven (DD) and Pressure Dependent Demand (PDD) driven simulations. If node demands in the hydraulic model are assumed to always be satisfied, the pressure throughout the network depends on the node demands and hydraulics can be run using Demand Driven (DD) simulations. However, this assumption becomes unreasonable if low pressure conditions appear. A pipe leak can for example result in low pressure conditions such that the demand cannot always be met. Hence, in conditions of low pressure in the network, customers do not always receive the requested

amount of demand and a Pressure Dependent Demand (PDD) simulation is more realistic.

The following pressure-demand relationship (Wagner et al. 1988):

$$d = \begin{cases} 0, & p \leq P_0 \\ D_f \cdot \sqrt{\frac{p-P_0}{P_f-P_0}}, & P_0 \leq p \leq P_f \\ D_f, & p \geq P_f \end{cases} \tag{2.3}$$

where d (m^3/s) is the actual demand, D_f (m^3/s) is the desired demand, p (m) is the pressure, P_f (m) is the nominal pressure and P_0 (m) is the minimum pressure. If the pressure goes below the minimum, the customer is not able to receive any water. If the pressure is above the minimum but below the nominal pressure, the customer still cannot receive the desired demand, but is able to receive some amount of water depending on the pressure. If the pressure is above the nominal pressure, the customer receives the desired demand and the result is the same as a demand driven simulation. The nominal and minimum pressure throughout the entire network are fixed in this study at $P_0 = 0$ m and $P_f = 20$ m, both in meters heads.

Adding leaks to a pressure dependent demand simulation is done in WNTR using the following formula (proposed by Crowl and Louvar 2001), where the mass flow rate of fluid through the hole is expressed as:

$$d_{leak} = C_d \cdot A \cdot p^\alpha \sqrt{\frac{2}{\rho}} \tag{2.4}$$

where d_{leak} (m^3/s) is the leak demand, C_d is the discharge coefficient, A (m^2) is the area of the hole of the leak, p (Pa) is the pressure, α is the emitter exponent and ρ (kg/m^3) the density of the fluid. C_d and α are unitless. The emitter exponent is fixed at $\alpha = 0.5$ and the density of water is fixed at $\rho = 1000$ kg/m^3.

The hydraulic model is calibrated to fit the inflow and pressure measurements in the DMA (see Appendix C for details). The calibration is performed in two consecutive steps. For both steps, the mean squared error between the observed pattern and the simulated pattern is minimized.

In the first step, both the daily consumption pattern and the billing information are implemented into the model. The simulated inflow is then compared with the observed inflow. The mismatch between the simulated inflow and the observed inflow is assumed to be the result of background leaks. Hence, background leaks are homogeneously distributed to the hydraulic model in the form of additional pressure dependent demand distributed over all nodes by using Equation 2.4.

In the second calibration step, pipe roughness coefficients are calibrated by comparing the simulated pressure patterns with the observed pressure patterns at the six pressure sensor locations. For the roughness calibration, the pipes are divided into different groups. Different criteria for groupings can be chosen (e.g. pipe diameter, pipe material) (Mallick et al. 2002). Since it was found by Lippacher 2018 that the best grouping for roughness calibration for leak localization was to group according to relative position in the network, this grouping criterion is chosen. Hence, all pipes are roughly divided based on their relative distance from the pump. Since there was a pressure mismatch between the measured inflow pressure and the remaining pressure sensors, the first group consist of the inflow pipes to decrease the incoming pressure. The roughness values in each group are then multiplied with the corresponding factor. By using Differential Evolution (DE), the four factors relating to the four groups are optimized through comparison of the simulated and observed pressures at the sensors.

A more extensive explanation of the calibration process of the hydraulic model is discussed Appendix D. The roughness coefficients range between 60 and 150, with a lower value for the inflow pipes to account for the high dissipation of energy needed in the calibration. The resulting calibrated model will be used throughout this study.

2.2.3 Implementation stochastic demand

Because DMA Duindorp covers exclusively the area Duindorp in its entirety, statistics of the residence of Duindorp are directly applicable to the DMA. Since SIMDEUM uses statistics of the area to simulate domestic drinking water demand, these statistics are used to create stochastic domestic drinking water demand.

The following statistics of Duindorp are publicly available and retrieved on October 23, 2019 from CBS 2019. There are 5875 registered citizens in Duindorp, of which 19% is younger than the age of 15, 9% between age 15-24, 57% between age 25-64, 15% of age 65+. There are 2825 households present in Duindorp, of which 1195 one-person households (42%), 625 households without kids (22%) and 1015 households with kids (36%). The average amount of people per households is 2.08. The total amount of households in Duindorp is verified by with the billing information retrieved from the water utility company, in which all the water bills are summed.

Since Duindorp is a domestic area, it is assumed that the water consumption in the network can be described by solely simulating domestic drinking water demand. Hence, it is assumed that there are no other large water users present in the network. The water demand of the 2825 households are simulated by using the Duindorp census data within SIMDEUM. The total water consumption in the network is then calculated by simply summing up all household water demands.

Furthermore, the amount of households that are connected to each node in the hydraulic model need to be known. It is derived from the known nodal base demand which originates from the billing information, as discussed in section B.1. For example, a node that has zero base demand is assumed to lack any connected households.

Knowing the amount of nodes with a demand (nodes with base demand larger than zero), the total amount of households need to be distributed over the amount of nodes that consume water. This is done as follows

$$H_{n_i} \equiv \left\lfloor \frac{B_{n_i}}{\sum\limits_i B_{n_i}} \right\rfloor \in \mathbb{N} \tag{2.5}$$

such that

$$P_{n_i}(t) = \sum_{j=1}^{H_{n_i}} P_{SIM_j}(t) \tag{2.6}$$

where H_{n_i} is the amount of connected households for node i, B_{n_i} is the base demand factor for node i, $P_{n_i}(t)$ is the consumption pattern throughout the day for node i and $P_{SIM_j}(t)$ is the simulated domestic drinking water demand for one household. If not all households are distributed by performing Equation 2.5, the left-over households are randomly allocated over the nodes with base demand larger than 0 such that:

$$\sum_i H_{n_i} = 2825 \tag{2.7}$$

All the simulated domestic drinking water demands are connected to the nodes in the network by following the process above. Hence, one hydraulic simulation includes the implementation of 2825 stochastic domestic drinking water demand simulations into the hydraulic model. Every simulation connects its newly simulated water demands to the

hydraulic model in the same way. By conducting a multitude of hydraulic simulations and plotting the results of the inflow and pressures at the sensors, it can be confirmed that the simulated patterns correspond to the observed patterns (as derived in section C.4).

2.2.4 Parameterizing stochastic demand model with measurement data

Besides demand and roughness calibration, to further decrease the mismatch between the hydraulic model and the measurements, SIMDEUM parameters can be adapted. If the simulated daily inflow does not correspond well enough to the observed daily inflow, this mismatch could be simply compensated by multiplying all the nodal consumptions with a certain pattern throughout the day such that the total inflow matches the total consumption. However, this would undermine the physical bases of SIMDEUM. Multiplying the domestic drinking water demands with a certain pattern would mean that various physically assumed constants in the stochastic demand simulator (like discharges of toilet use during the day) will not be constant.

To avoid jeopardizing the physical basis of SIMDEUM and still be able to reduce the mismatch, its parameters (e.g. the diurnal patterns of the residents) can be adapted to modify the water demand. To reduce the mismatch, the SIMDEUM parameters are changed according to a trial-and-error method.

Beside from potentially modifying the parameters of the stochastic demand simulator, every simulation (of all households) is different due to the fact that it is stochastic, hence yielding in different results at the sensors. By running a multitude of demand simulations and simulating the results at the sensors, the influence of the demand fluctuations on the sensors can be analyzed.

2.3 Leak detection method

The inflow and pressures at the sensors can be simulated for a multitude of stochastic demand simulations. A range can be set up at each sensor in which most of the simulated results lie. In this study, a confidence interval of 95% is set up. This means that 95% of the simulated results (in which the results are solely a consequence of the stochastic demand variation) are found within this band-width.

Hence every sensor has its own resulting 95% confidence interval. Due to the stochastic nature of the demand, single simulations can exceed the confidence interval. However, exceedance of this confidence interval for a certain continuous amount of time gives reason to believe that something is out of the ordinary. By defining a time threshold of allowed exceedance of the confidence interval, a tool is created to distinguish the potential leaks from the normal fluctuations as a result of the stochastic demand. A detection alarm is triggered at a sensor if its measured values lay outside the confidence interval for a continuous time period exceeding the predefined threshold. Hence, a simple heuristic leak detection method is created, applicable to sensor data that can be drawn from a normal or non-normal distribution.

To mathematically elucidate this heuristic leak detection method, the confidence interval is defined with the lower bound to be $l(t)$ and the higher bound to be $h(t)$, the measurement at the sensor which is checked on leakage is defined to be $x(t)$. Hence, the leak detection is mathematically performed with the following equations (Equations (2.8) and (2.9)):

$$f(t_i) = \begin{cases} 0, & l(t_i) \leq x(t_i) \leq h(t_i) \\ 1, & else \end{cases} \quad \forall i \in \{1, 2, ..., T\} \quad T \in \mathbb{N}^+ \quad (2.8)$$

$$g(t_j) = \begin{cases} 0, & \sum_{k=j}^{j+\tau-1} f(t_k) \neq \tau \\ 1, & \sum_{k=j}^{j+\tau-1} f(t_k) = \tau \end{cases} \quad \forall j \in \{1, 2, ..., T-\tau+1\} \quad T, \tau \in \mathbb{N}^+ \quad (2.9)$$

where $\tau \leq T$. The time window of the simulation consists of T amount of consecutive time steps and the leak detection is set to raise an alarm if τ amount of consecutive time steps are outside of their confidence interval. If $g(t_j) = 0 \quad \forall j \in \{1,2,...,T-\tau+1\}$, no detection alarm is triggered. A detection alarm is triggered for every $g(t_j) = 1$ with $j \in \{1,2,...,T-\tau+1\}$.

Essential in this method is to determine the amount of time steps τ, the predefined time threshold of exceedance. If a small time threshold is chosen, the leak detection method becomes too sensitive, raising a lot of false alarms. If a large time threshold is chosen, less alarms are generally triggered. However, the leak detection method will be less sensitive with respect to small leaks.

To illustrate the effect of this set threshold, examples are shown in Figures 2.3 and 2.4. Both show the simulated inflow data throughout the day in which $N_{sim} = 1000$ simulations are conducted. One random simulation is extracted and a leak has been added starting at 14:00 of discharge 5 m^3/h and lasting for 5 hours. This simulation is illustrated with the black line. The median and the 95% confidence interval of the remaining simulations is shown in blue and yellow. The time window in which a detection alarm is raised is colored light-blue. The only difference between both figures is the set time threshold of the leak detection method.

It can be seen from Figure 2.3, having a time threshold of 10 minutes, that a false alarm is triggered before the leak is happening. This is the result of a stochastic demand fluctuation, but labeled as a leak by the leak detection method. Figure 2.3 has a time threshold of 20 minutes, which results in no detection alarm. Hence, the leak detection method has become too insensitive to be able to detect the leak.

Hence, a trade-off needs to be made between sensitivity of the leak detection method and the amount of resulting false alarms. Hence, a false alarm analysis needs to be conducted to determine how often a false alarm is triggered for different time thresholds. The leak alarm analysis is applied on all sensors. The results of this analysis are discussed in Section 3.2. From this analysis, one time threshold for the leak detection method is chosen on the basis of an acceptable false alarm rate for all sensors.

The false alarm analysis comprises of determining what the false alarm rate is at different time thresholds. Monte Carlo simulations are conducted and the resulting sensor simulations are checked on detection alarms by using the detection method with the predefined time threshold. Any raised leak detection alarm is then a false alarm, since no leak has been simulated. By determining per sensor the fraction of simulations that yield in a detection alarm relative to the total amount of simulations, the false alarm rate is determined per sensor.
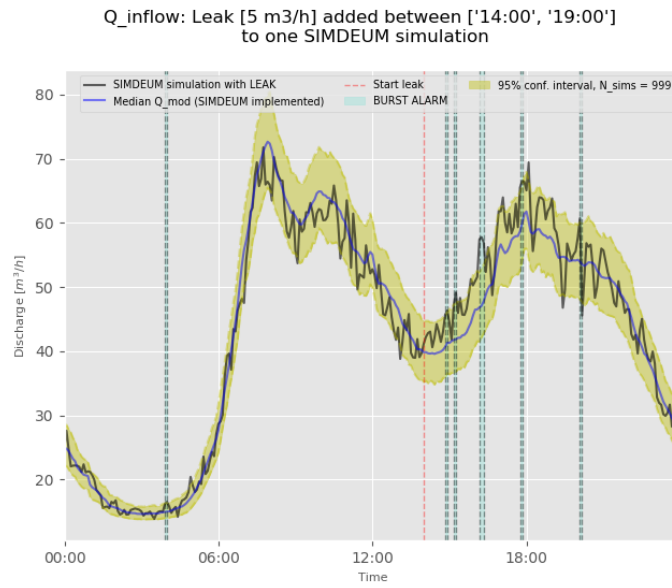
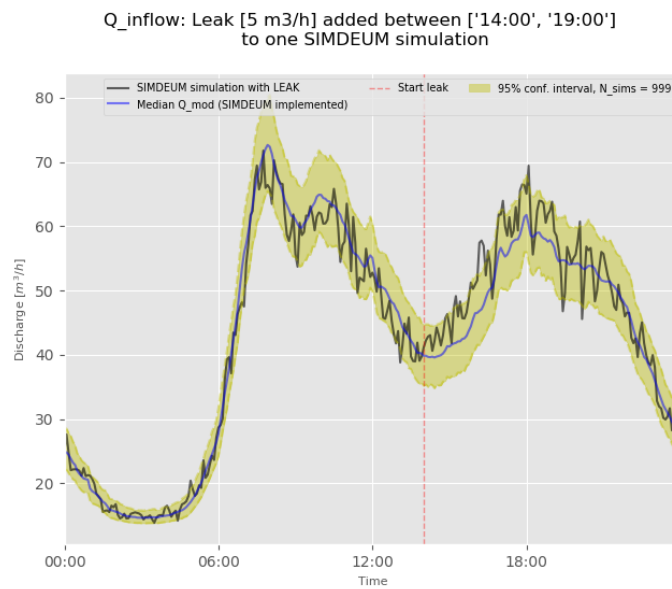Figure 2.3: Example leak detection at inflow sensor: time threshold of two timesteps: 10 minutes

Figure 2.4: Example leak detection at inflow sensor: time threshold of four timesteps: 20 minutes

2.4   Leak localization method

The method that is used in this study to localize leaks is proposed by Quevedo et al. 2011 and Meseguer et al. 2015. It is based on the use of a flow and pressure sensor at the inlet of the DMA, and pressure sensors inside the DMA. In a nutshell, the observed pressure disturbances are compared with the theoretical pressure disturbances caused by artificially created leaks at every possible node to determine which simulations are most similar to the observations. The locations of the artificially created leaks in these simulations (that show a high similarity to the observations) are more likely to contain the real leak than the other locations in the DMA.

Four assumptions that are made:
- Only a single-leak scenario is considered in this method. A scenario of multiple leaks at the same time is not covered in this method nor in this study.
- The leak discharge needs to be known or estimated which ideally is similar to the real leak. Therefore the leak discharge is assumed to be known and fixed in this study.
- A leak is considered to be situated at one of the nodes rather than somewhere along a pipe in the network.
- A leak can either be modelled with an emitter coefficient or as extra demand. The latter is chosen in this study because the leak discharge is preferred to be fixed.

2.4.1   Mathematical derivation

Consider a DMA with N nodes and S pressure sensors. The measured pressures at time t are stored in vector $p(t) \in \mathbb{R}^S$. The vector that contains the simulated pressures in a leak-free scenario at time t is defined as $\hat{p}_0(t) \in \mathbb{R}^S$. The residual vector $r(t) \in \mathbb{R}^S$ is determined by subtracting the predicted pressures considering a leak-free scenario from the measured pressure vector. They are described in Equation 2.10.

$$
\begin{aligned}
p(t) &= \begin{pmatrix} p_1(t) & p_2(t) & \dots & p_S(t) \end{pmatrix}^T, \\
\hat{p}_0(t) &= \begin{pmatrix} \hat{p}_{01}(t) & \hat{p}_{02}(t) & \dots & \hat{p}_{0S}(t) \end{pmatrix}^T, \\
r(t) = p(t) - \hat{p}_0(t) &= \begin{bmatrix} p_1(t) - \hat{p}_{01}(t) \\ p_2(t) - \hat{p}_{02}(t) \\ \vdots \\ p_S(t) - \hat{p}_{0S}(t) \end{bmatrix}
\end{aligned}
\tag{2.10}
$$

Artificial leaks are simulated consecutively at every possible node N with a known fixed leak discharge $Q_{leak} \in \mathbb{R}^+$. The leak matrix $L(t) \in \mathbb{R}^{N \times S}$ describes the resulting modelled pressures at every sensor for every simulation:

$$
L(t) = \begin{bmatrix} \hat{p}_{11}(t) & \dots & \hat{p}_{1S}(t) \\ \vdots & \ddots & \vdots \\ \hat{p}_{N1}(t) & \dots & \hat{p}_{NS}(t) \end{bmatrix}
\tag{2.11}
$$

The theoretical pressure disturbances are calculated by subtracting all rows of $L(t)$ with the leak free scenario $\hat{p}_0(t)$. The resulting matrix is called the Fault Signature Matrix (FSM) with $FSM(t) \in \mathbb{R}^{N \times S}$ described as follows:

$$
FSM(t) = \begin{bmatrix} \hat{p}_{11}(t) - \hat{p}_{01}(t) & \dots & \hat{p}_{1S}(t) - \hat{p}_{0S}(t) \\ \vdots & \ddots & \vdots \\ \hat{p}_{N1}(t) - \hat{p}_{01}(t) & \dots & \hat{p}_{NS}(t) - \hat{p}_{0S}(t) \end{bmatrix}
\tag{2.12}
$$

The rows of $FSM(t)$ describe the pressure deviations at the sensors as a result of a simulation with an artificial leak placed at node i. These simulated pressure deviations are now compared with the observed pressure deviations. Therefore, correlations between each row of $FSM(t)$ and the residual vector $r(t)$ are computed. The correlation is Pearson's correlation coefficient, which is defined for two variables X and Y as follows:

$$\rho_{X,Y} = \frac{cov(X,Y)}{\sqrt{cov(X,X)cov(Y,Y)}} = \frac{E[XY] - E[X]E[Y]}{\sqrt{E[X^2] - [E[X]]^2}\sqrt{E[Y^2] - [E[Y]]^2}} \tag{2.13}$$

where $cov(X,Y) = E[(X - \mu_X)(Y - \mu_Y)]$ is the covariance, $\mu_X = E(X)$ is the mean and $\sigma_X^2 = E[(X - E[X])^2] = E[X^2] - [E[X]]^2$ is the standard deviation.

The highest correlation represents a high likeliness that the actual leak can be found near the fixed leak node in that simulation. To find the highest correlation of all simulations, the following equation is solved:

$$\max_j(\rho_{r,FSM_j}(t)) \qquad j = 1,\ldots,N \tag{2.14}$$

The corresponding simulation with this maximum correlation value is therefore the best candidate to contain the correct leak location (at time t), which is the corresponding node following from Equation 2.14.

Pearson's correlation coefficient has a range between -1 and +1, describing the range of a total negative to a total positive linear correlation. A correlation coefficient of 0 means there is no linear correlation. In this study, only high Pearson correlations of above 0.5 are considered (as proposed by Perez et al. 2014), the rest is considered to be non-correlated, hence transformed to 0.

Until so far, the process of calculating Pearson's correlation coefficient for a single snapshot at time t is explained. However, the leak localization is usually performed over a certain time span, hence evaluated for multiple time steps. Performing this process for multiple time steps gives an extra dimension to this problem. The amount of time steps at which the leak localization should be applied on would logically follow from the time window in which a detection alarm is raised, hence the resulting time span of the leak detection. Suppose the leak detection raises an alarm for $\tau \in \mathbb{N}$ amount of consecutive time steps. This makes the detection time window consist of $T_W = \{t_1, t_2, \ldots, t_\tau\}$ in which the difference between two time steps is the frequency.

However, the leak detection and localization are performed separately in this study. The frequency is fixed at 5 minutes (as discussed in section B.2) and the leak localization is performed for a fixed time window of two consecutive hours, resulting in $\tau = 24$.

For every timestep t_i inside the time window T_W, the $r(t_i)$ and the $FSM(t_i)$ are calculated (Equation 2.10 and Equation 2.12). Calculating Pearson's correlation coefficient of every node results in the following stacked vector of Pearson's correlation coefficients:

$$\rho_{r,FSM}(t_i) = \begin{bmatrix} \rho_{r,FSM_1}(t_i) \\ \vdots \\ \rho_{r,FSM_N}(t_i) \end{bmatrix} \in \mathbb{R}^N \tag{2.15}$$

Extending this for every timestep results in the matrix of all calculated Pearson's correlations per node and through time, defined as correlation matrix C:

$$C = \begin{bmatrix} \rho_{r,FSM}(t_1) & \cdots & \rho_{r,FSM}(t_\tau) \end{bmatrix} = \begin{bmatrix} \rho_{r,FSM_1}(t_1) & \cdots & \rho_{r,FSM_1}(t_\tau) \\ \vdots & \ddots & \vdots \\ \rho_{r,FSM_N}(t_1) & \cdots & \rho_{r,FSM_N}(t_\tau) \end{bmatrix} \in \mathbb{R}^{N \times \tau} \tag{2.16}$$

To achieve one correlation value $\theta_j \in \mathbb{R}$ per node j, all correlation values per time-step are summed for each node, hence the sum is taken for every row in matrix C:

$$s_j = \sum_{t=t_1}^{t_\tau} \rho_{r,FSM_j}(t) = \rho_{r,FSM_j}(t_1) + \cdots + \rho_{r,FSM_j}(t_\tau) \tag{2.17}$$

The correlation value θ_j per node j is then defined as follows:

$$\theta_j = \frac{s_j - \min_{\forall j=1,...,N}(s_j)}{\max_{\forall j=1,...,N}(s_j)} \in [0,1] \tag{2.18}$$

Due to this definition, the range of all correlation values lie between 0 and 1. The location of the leak in the simulation with the highest correlation value is theoretically most likely to be near the real leak ($\max_j \theta_j$).

However, there can be more simulations with high correlation values that do not differ significantly from each other such that there is an obvious winner. The correlation values of all nodes are therefore sorted in descending order, yielding in a list of nodes from most to least probable leak locations. The results are visualized by plotting the nodes of the network with a color relating to its correlation value θ_j. An example is shown in Figure 2.5, a node with a blue color refers to a high correlation value θ_j, hence a high likeliness that the leak can be found near that node.

2.4.2 Performance evaluation

In this study, simulations are run in which a leak with a fixed discharge is placed at a certain node $l \in \mathbb{N}$ ($1 \leq l \leq N$). It is implicitly assumed that a leak is situated at one of the nodes instead of somewhere along a pipe in the network. Its location is referred to as the 'actual leak' and during the leak localization, it is considered to be unknown. By performing the leak localization it is tried to trace back this leak location.

The visualized results on itself as shown in Figure 2.5 lack a quantification of how well the leak localization has performed. To quantify its performance, three different evaluation parameters are calculated from the result:

1. D_T: The topological distance between the leak found and the actual leak.
2. FP_r: The false positive rate.
3. MS: The maximum span of the false positives.

The first evaluation parameter D_T is defined as the topological distance between the node with the maximum correlation value and the actual leak node l. To calculate this distance, the skeleton of the WDN is transformed in an non-directed weighted graph (weighted by length) on which Dijkstra's shortest path algorithm (Dijkstra et al. 1959) is applied.

The second evaluation parameter FP_r is defined as the percentage of nodes with a higher correlation value than the actual leak, and calculated as follows:

$$FP = \{j \in \{1, 2, ..., N\} : \theta_j > \theta_l\} \tag{2.19}$$

$$FP_r = |FP|/N \cdot 100 \tag{2.20}$$

The third parameter MS is defined as the maximum span of all false positives. It is the maximum topological distance between all false positive nodes, calculated as follows:

$$MS = \max_{i,j}(D_T(i,j)) \qquad \forall i,j \in FP \tag{2.21}$$

These three evaluation parameters will be stated in the legend of every leak localization figure, as is shown in Figure 2.5.
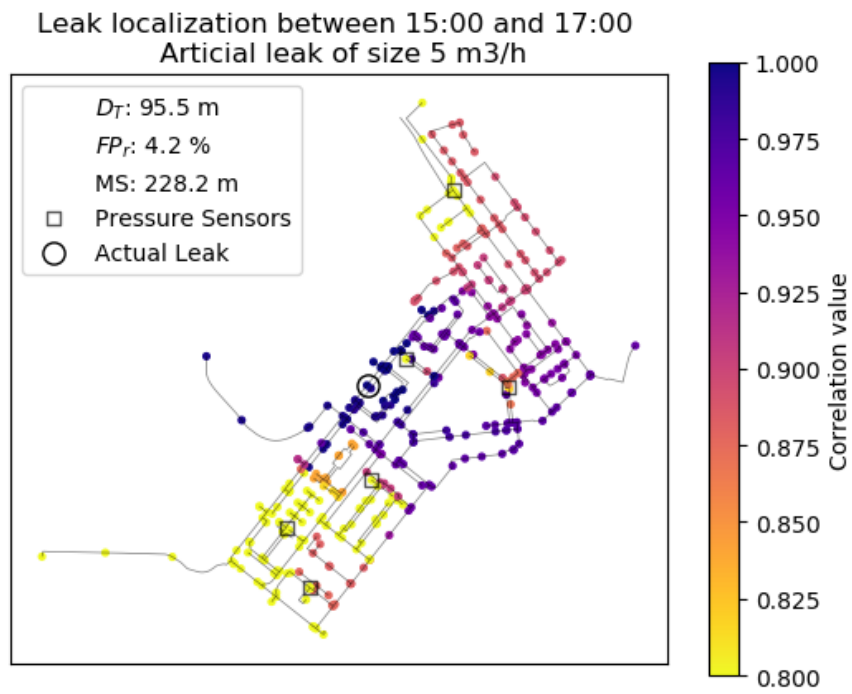
Figure 2.5: Example of leak localization result

3. Results and discussion

In this chapter, the results of conducting the methods of Chapter 2 are discussed. Stochastic demand is implemented into the hydraulic model and the simulated inflow and pressures are compared with the actual observed inflow and pressures in the first section. Subsequently, leaks are simulated to assess the robustness of the leak detection and localization method under the influence of stochastic demand. Twenty-seven leak scenarios are created to test the performance. The results of the leak detection are discussed in the second section, including a false alarm analysis. The results of the leak localization are discussed in the third section.

3.1 Simulated and observed inflow and pressures

The calibrated hydraulic model of case study area Duindorp is used. More information about the case study area can be found in Appendix B, the time series analysis of the measurements in the network are discussed in Appendix C, and an extensive explanation of the calibration of the hydraulic model with the measurements is described in Appendix D. With the implementation of stochastic demand into the hydraulic model, inflow and pressure levels at sensor locations are simulated.

Statistics regarding the case study area are shown in Table 3.1, as retrieved from CBS 2019 (see Section 2.2.3). Stochastic demand simulations are performed with these area-specific statistics. Daily stochastic demand patterns are then used as demand inputs in the hydraulic model. Daily sensor patterns are constructed from the output of the hydraulic model. Subsequently, these daily sensor patterns are compared with the measurement data. Comparison is done for two types of stochastic demand simulations. The first type is stochastic demand created from the default settings in the demand simulator, which is based on average Dutch statistics. The second type is stochastic demand resulting from modified demand simulator settings in which local information for SIMDEUM parameters are used.

Table 3.1: Areal statistics Duindorp implemented into demand simulator

Age distribution of 5875 residents		Household type distribution of 2825 households	
Age	**Distribution**	**Household type**	**Distribution**
0-15	19%	1-Person	42%
15-24	9%	2-P (no kids)	22%
25-64	57%	2-P (with kids)	36%
65+	15%		

3.1.1 Default settings demand simulator

The default settings of the stochastic demand simulator are based on average Dutch household statistics and are shown in Tables 2.1 and 2.2. They are fixed in this subsection. Subsequently, stochastic demand simulations are performed with the area-specific statistics.

With the implementation of stochastic demand into the hydraulic model, the inflow and

pressure levels at the sensors are simulated. By running a multitude of hydraulic simulations and computing the resulting simulated inflow and pressures, the median and 95% confidence interval of the simulated inflow and simulated pressure at the sensors is computed. The results of the computation of hydraulic simulations for 200 days ($N_{sim} = 200$) are shown in Figures 3.1 and 3.2. Furthermore, these figures show the median and confidence intervals of the measurements.
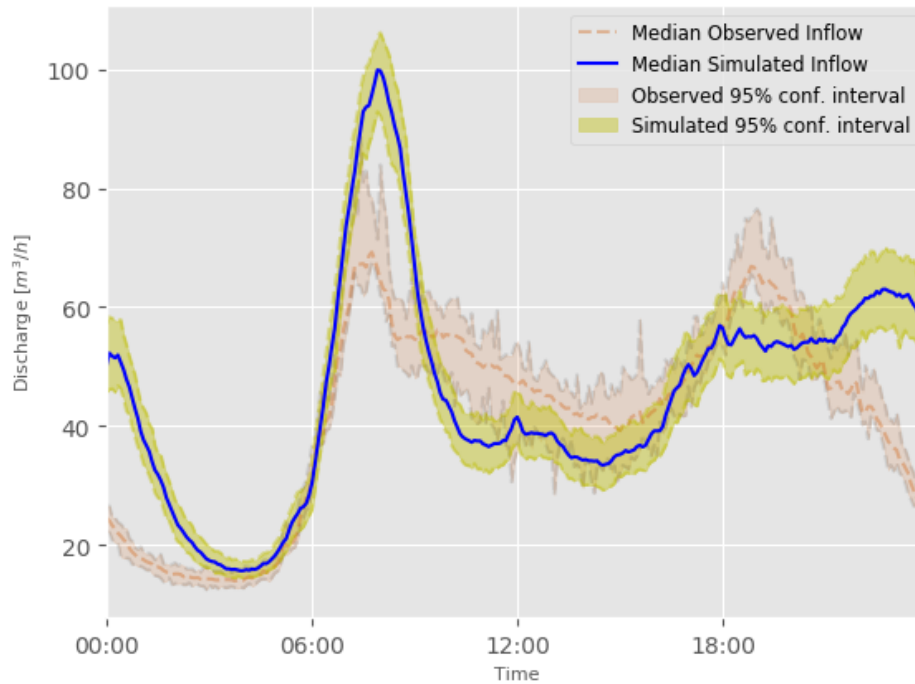
Figure 3.1: Observed and simulated inflow with default simulator settings
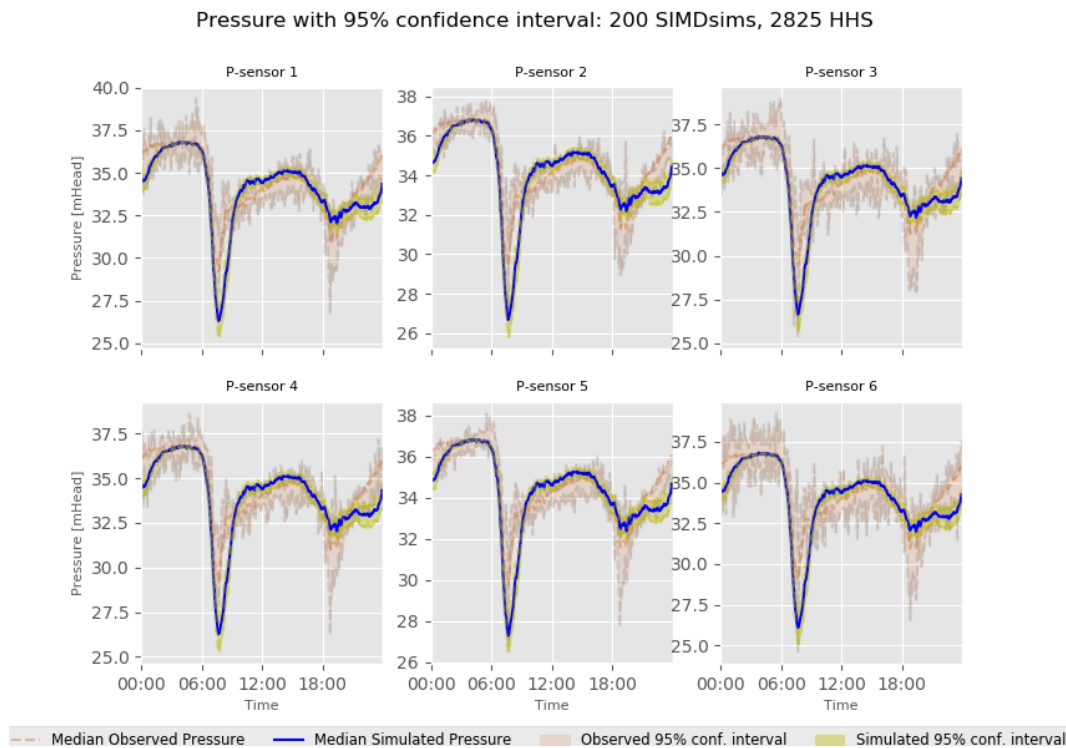
Figure 3.2: Observed and simulated pressures with default simulator settings

Five observations are made from the results:

1. Comparison of the areas under the observed and simulated inflow show that the total observed inflow over the day is smaller than the simulated inflow.

2. The simulated morning peak is too large compared to the observed morning peak. During the afternoon, the simulated inflow is generally lower than the observed inflow. Hence, the simulated total water use is overestimated in the morning, and generally underestimated in the afternoon.

3. Simulated inflow early in the night is higher than observed (see the nocturnal inflow in Figure 3.1).

4. Since pressures at the sensors are correlated to the inflow, an overestimation of the inflow leads to an underestimation of the pressures in the system (see the morning peak in Figure 3.2).

5. The confidence intervals are smaller in the simulations than in reality. Moreover, this difference becomes larger for the pressures. Hence, the overall variability of the simulations do not represent the variability of the measurements.

In an effort to achieve a better fit of the simulations to the observed inflow and pressures, SIMDEUM parameters are adapted (see Section 3.1.2).

3.1.2 Modified settings demand simulator

In an effort to overcome the former mentioned issues, parameters within SIMDEUM are adapted. The parameters that are adapted are the daily domestic water demand, employment rate and the diurnal patterns of the residents. The process of adapting parameters within SIMDEUM and checking whether it yields in simulated inflow and pressures that correspond better to the observations consists of four steps. First, the parameters are adapted to new values estimated by the modeler to improve the simulations. Second, domestic demand patterns are simulated with the new parameter set. Third, the demand patterns are implemented into the hydraulic model and 10 hydraulic simulations are conducted.

Fourth, the resulting simulated average inflow and pressures of all hydraulic simulations are compared with the observations. If the newly simulated patterns are better than all previous simulations, the new parameter set is accepted. This process is repeated until no more significant improvement is found.

To address the first bullet point on page 29, the total daily water use estimated by the demand simulator needed to be decreased. The simulated average inflow is 1114 m^3, based on $N_{sim} = 200$ simulations as retrieved from Figure 3.1. The observed average inflow is 995 m^3. To decrease the water consumption, outside water uses are neglected in the simulations. Observations of Duindorp support this argument, since it is mostly paved and the majority does not have a garden (pictures are shown in Appendix F). Neglecting the outside water uses in the simulations yields in an average decrease in daily water inflow to 1032 m^3. This results in a mismatch of 1.5 m^3/h. Since no other well founded arguments can be made to reduce the water consumption further without changing the water use behaviour of the residents significantly, this small error is acceptable.

To address the second bullet point on page 29, the morning peak has to be decreased while the afternoon consumption has to increase. This can be achieved by adapting the fraction of residents that leave their houses for work. This group wakes up between 6 and 8 and are on average 9.5 hours away from home. Investigations of the wake up times lead to the assumption that half of the residents wake up between 8 and 10. To account for this difference in wake up time, the unemployment parameter was raised to 49% such that more residents are staying at home during the day. It is assumed that a large fraction of this group are not without a job, but are either working from home or have different working schedules. The new household settings per household type are illustrated in Figure 3.3. Moreover, the diurnal patterns of the residents are slightly modified to flatten the simulated morning peak. Seniors and adults that are not working away from home are set to get up at 9:30, and are assumed to be away from home for 7 hours instead of 10 hours. The adults that go to work away from home are set to get up at half an hour earlier. The modified diurnal patterns of the residents are shown in Table 3.2. By adapting SIMDEUM according to these arguments the morning peak flattens and the water use during the afternoon increases since more people are staying at home during the day.
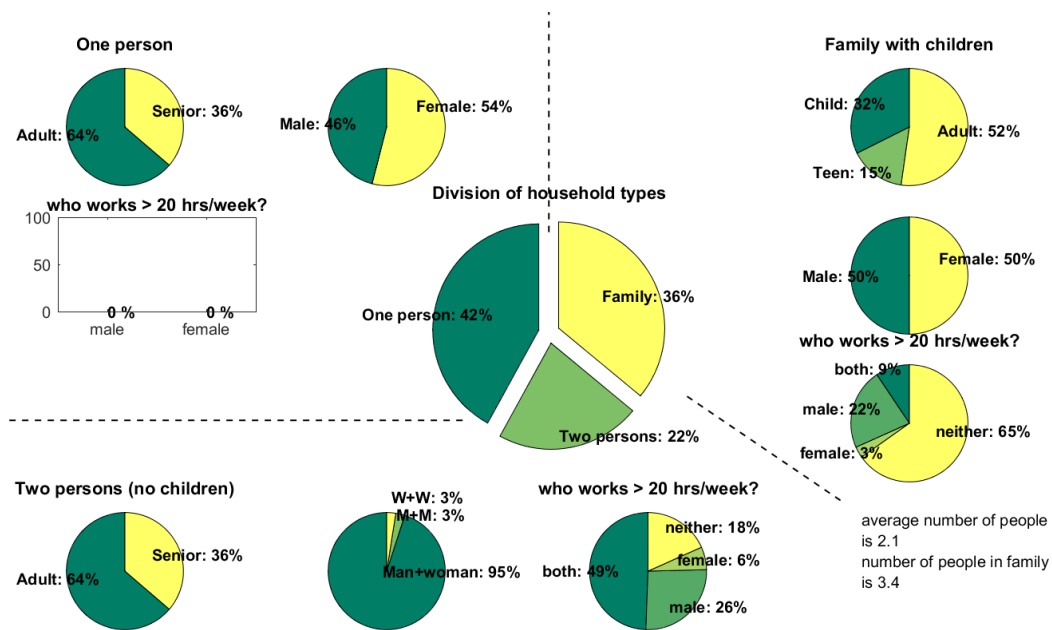
Figure 3.3: Modified composition households settings (original settings in Table 2.1)

Table 3.2: Modified diurnal patterns residents (original patterns in Table 2.2)

		child	teen	work ad	home ad	senior	total
up	mu	7:00	7:00	6:30	9:30	9:30	7:00
	sigma	1:00	1:00	1:00	1:00	1:00	1:00
go	mu	8:30	8:15	8:00	13:00	13:00	8:00
	sigma	0:30	0:30	0:45	3:00	3:00	1:00
away	mu	7:00	8:00	9:30	7:00	7:00	8:30
	sigma	2:00	2:00	3:15	4:30	4:30	1:00
sleep	mu	13:30	12:30	10:30	11:30	11:30	8:00
	sigma	1:15	1:15	1:15	1:15	1:15	1:00

To address the third bullet point on page 29, the water use early in the night estimated by the demand simulator needs to be allocated to different parts of the day. This could only be done by modifying the nocturnal patterns of the residents. The newly created diurnal and nocturnal patterns of the residents are shown in Table 3.2.

To sum up, the new parameter settings within SIMDEUM yield in simulated inflow and pressure patterns that represent the observed inflow and pressure patterns more accurately. The modified SIMDEUM parameters are shown in Figure 3.3 and Table 3.2. By using this local information for SIMDEUM parameters, new stochastic demand simulations are performed. Daily stochastic demand patterns are then used as demand inputs in the hydraulic model. Since they will be used in the next section, the computation is raised to hydraulic simulations for $N_{sim} = 1000$ days. The results are shown in Figures 3.4 and 3.5, plotted with the corresponding median and variability per sensor.
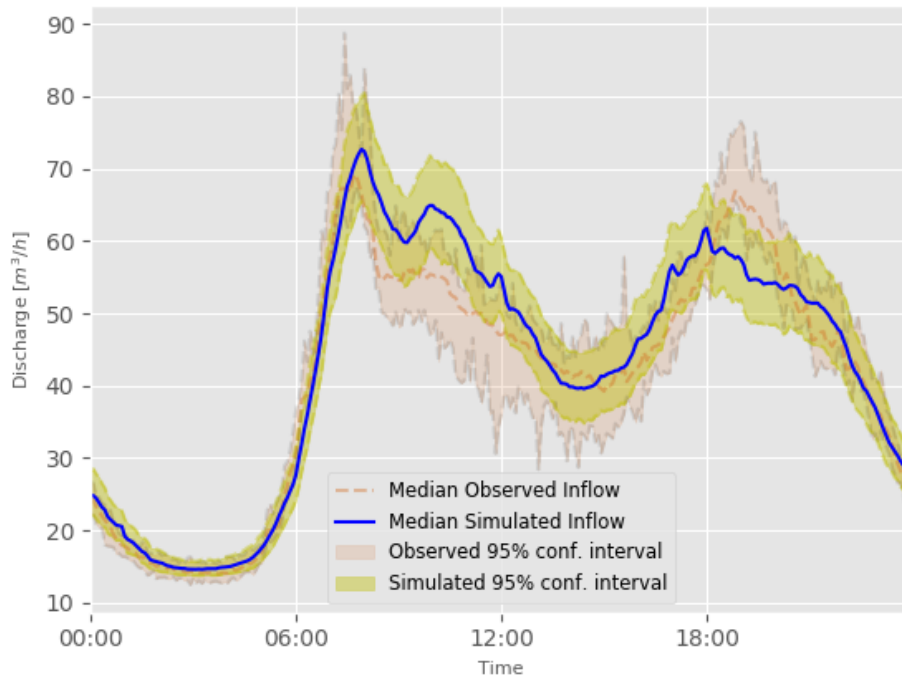
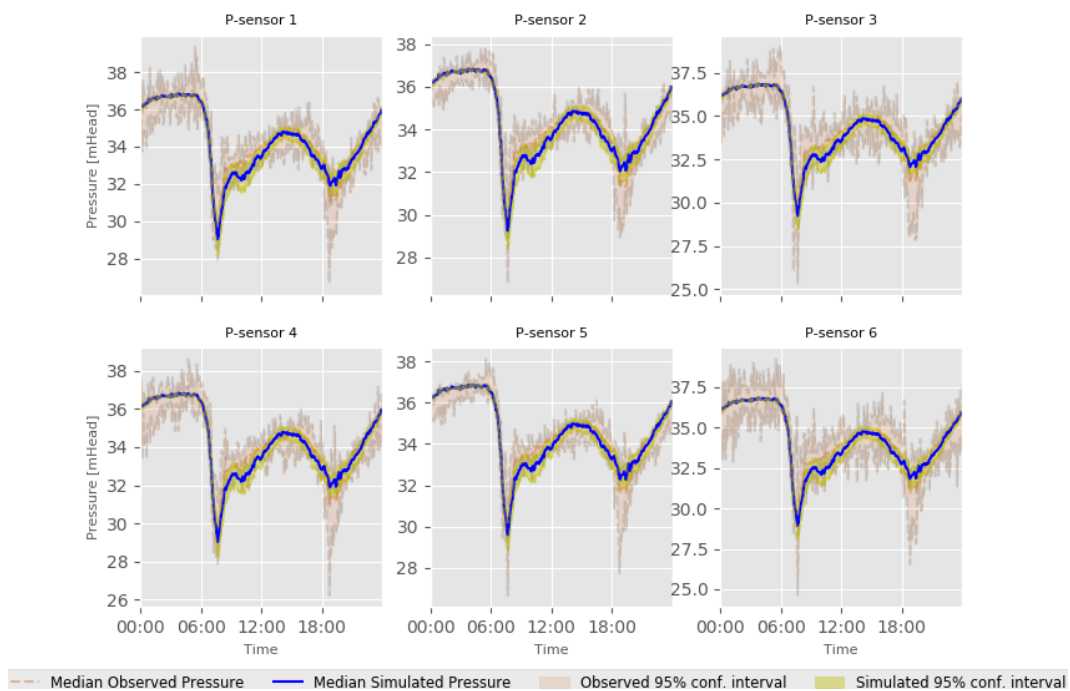Figure 3.4: Observed and modelled inflow with modified simulator settings

Figure 3.5: Observed and modelled pressures with modified simulator settings

Two observations are made from the results:
1. When local information for SIMDEUM parameters is used, the simulated sensor values lie closer to the observations than if the default parameter settings in the simulator are used (as was shown in Figures 3.1 and 3.2). However, a perfect fit is not achieved. Significant difference occurs late in the morning and during the evening peak.
2. The confidence intervals from the simulations are smaller than the observed intervals. Moreover, the difference becomes larger for the pressure sensors. The same was observed in Figures 3.1 and 3.2. Consequently, the variability of observations is not entirely covered by the simulations, regardless of whether the default SIMDEUM parameters or local information for these parameters are used. Hence, adapting the parameters of SIMDEUM does not influence the simulated variability at the sensors significantly.

As the first item above states, adapting the parameters in the simulator yields in better fits with respect to the measurements. Using the local information for the simulator parameters is therefore more applicable than using average Dutch household statistics.

Since the model with the demand loading conditions based on local information was found to be as realistic as possible, it will be used in the leak detection and localization. This means that the simulated sensor data as shown in Figures 3.4 and 3.5 are used in the leak detection and leak localization. Artificial measurements are then created by running a single hydraulic simulation with the model.

Furthermore, a normality analysis is conducted on the simulated sensor data, discussed in Appendix G. The results from the normality analysis reveal that the sensor data does not follow a normal distribution during the same time of the day, for a multitude of days. This means that only non-parametric statistical methods should be applied on the sensor data. Hence, the leak detection and leak localization method used in this study are non-parametric statistical methods.

3.2 Leak detection results

To assess the robustness of the leak detection and the leak localization methods with respect to stochastic demand, different leak scenarios are constructed.

Three different leak locations, leak sizes and leak starting times are chosen to create $3^3 = 27$ differing leak scenarios. See Figure 3.6 for the locations and Table 3.3 for details. The choice for these scenarios followed from a preliminary analysis. The leak starting times have been chosen to assess the influence of different demand conditions that occur during the day. Low demand and low stochastic variability during the night, highest demand and highest variability during the morning peak and average conditions during the afternoon. The leak locations are approximately evenly spread over the network. In detail, location A is placed near two pressure sensors, hence likely to be easily detected and localized. Location B is placed near only one pressure sensor, hence likely to be slightly more difficult to find. Location C is placed relatively far from the pressure sensors, hence likely to be hardest to detect and to localize.

Before applying the leak detection method on the different created scenarios, a false alarm analysis is conducted to determine the optimal time threshold value.

Table 3.3: Leak scenarios used in the leak detection and localization

27 different leak scenarios		
Starting time leak	Locations	Leak size (m^3/h)
03:00 [Night]	A	2.5
07:00 [Morning]	B	5
15:00 [Afternoon]	C	7.5

Figure 3.6: Simulated leak (alphabetical letters) and sensor locations (numbered)

3.2.1 False alarm analysis

As discussed in section 2.3, a detection alarm is raised if the confidence interval is exceeded for a certain time threshold. To determine this time threshold, a trade-off needs to be made between sensitivity of the method and an acceptable false alarm rate. A high sensitivity leads to a high amount of false alarms. A too high false alarm rate is unwanted from a controllers point of view, since it can result in negligence of the controller to these alarms. A low sensitivity yields in a low amount of false alarms, but the more insensitive the method is, the more insensitive it becomes to small leaks.

To determine the optimal threshold, a false detection alarm analysis is conducted. The false detection alarm analysis comprises of performing the leak detection method on a certain number of hydraulic simulations (with no leak included) and determining for each sensor how many false detection alarms are triggered. By repeating this process for different leak detection time thresholds in the leak detection method, the false alarm percentage for each sensor and for each used time threshold is determined.

$N_{sim} = 1000$ hydraulic day simulations are performed, each with different stochastic demand loading conditions. Then, sensor signals and confidence intervals are retrieved from the 1000 simulations and the threshold value is varied. TS_{Alarm} is defined to be the minimum amount of consecutive time steps in which the data needs to fall outside the confidence

interval for the leak detection to trigger an alarm. This threshold value is determined to vary from 1 to 6 consecutive time steps or 5 to 30 minutes, respectively. The results are shown in Table 3.4.

Table 3.4: False detection alarm analysis for different time thresholds

False detection alarm percentage of $N_{sim} = 1000$						
TS_{Alarm}	1	2	3	4	5	6
Q	100	88.0	33.4	7.8	1.4	0.2
P1	100	89.6	37.4	8.0	1.3	0.1
P2	100	89.8	36.6	7.9	1.2	0.3
P3	100	91.0	39.9	9.1	2.2	0.5
P4	100	90.4	36.6	7.6	1.2	0.2
P5	100	89.9	37.1	8.3	1.3	0.2
P6	100	90.5	36.8	7.8	1.5	0.2
Average	100	89.9	36.4	8.1	1.4	0.2

From Table 3.4 it follows that for every sensor and for every day simulation, the confidence interval gets exceeded for at least one time step, simply due to stochastic variability of the demand. This is logically explained by calculating the chance of a simulation falling inside the confidence interval of 95% for the 288 (five-minute) time steps in a day: $0.95^{288} \approx 3.84 \cdot 10^{-7}$. Hence, the chance of running a 1000 simulations and not one yielding in a false alarm: $(1 - 0.95^{288})^{1000} \cdot 100 \approx 99.96\%$.

If an alarm is raised only if at least 6 consecutive time steps fall outside the confidence interval, the percentage of false alarms drops down to an average of 0.2%. However, such a high time threshold can lead to insensitivity to small leaks.

From the results shown in Table 3.4, the optimal time threshold is chosen to be 5 time steps, in which the false alarm rate lies between 1.3 and 2.2%. Over a year, this would result in 4 to 7 false alarms. This is considered to be acceptable from a controllers point of view.

3.2.2 Scenario results

For each scenario, the leak detection is performed on a multitude of hydraulic simulations, each with different stochastic demand loading conditions. The Leak Detection Time (LDT) is calculated per sensor and per simulation and is defined as the time between the start of the leak and the time at which the first detection alarm is triggered at that sensor. All LDTs for each sensor are calculated and the average and standard deviation of the LDTs can be computed.

To illustrate the effect of increasing the amount of simulations on the average and standard deviation of the LDT, their development for a specific scenario is plotted in Figure 3.7, in which the amount of simulations increases to a maximum of $N_{sim} = 500$. A leak of discharge 5 m^3/h at location B with starting time 15:00 is added to each simulation in this figure.

The uncertainty of the average value is the standard deviation of the mean, also known as the standard error. The standard error depends on the amount of measurements and is always smaller than the standard deviation. It is given by:

$$\sigma_{\overline{LDT}} = \frac{s}{\sqrt{N}} \tag{3.1}$$

where $\overline{LDT}$ is the average leak detection time of N simulations and s is the standard deviation.

By calculating the average LDT with its standard error;

$$\overline{LDT} \pm \sigma_{\overline{LDT}} \tag{3.2}$$

the accuracy of the average leak detection time is determined. It is plotted in Figure 3.7 as the filled color surfaces around the average LDT per sensor.
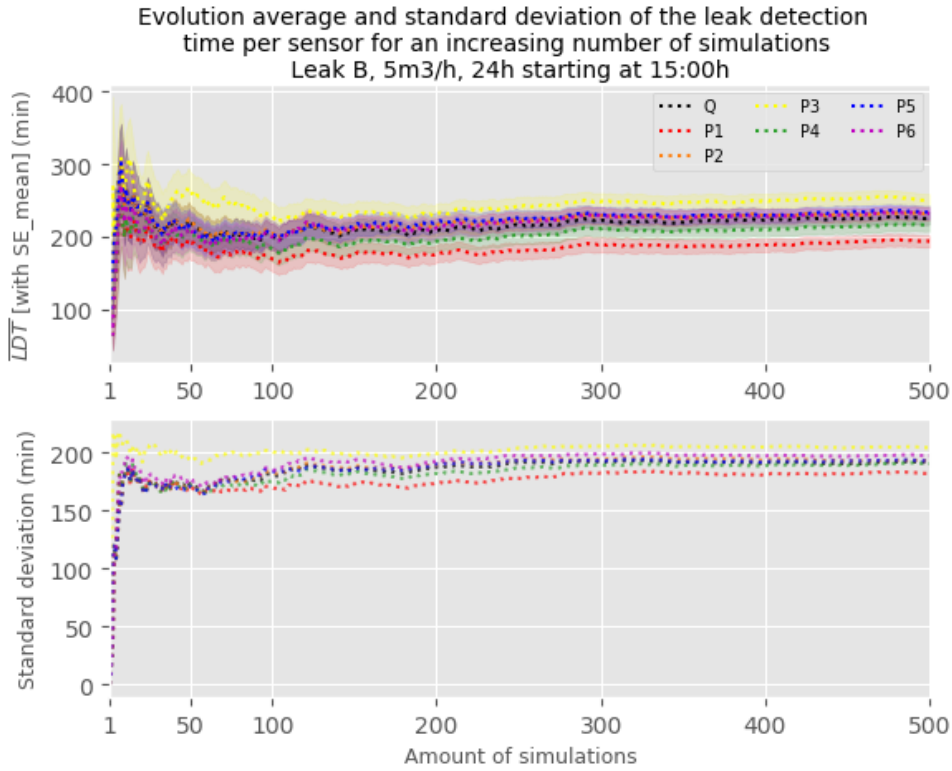

Figure 3.7: Evolution average and standard deviation LDT per sensor

It can be seen from Figure 3.7 that the average and the standard deviation of the LDT converge to a constant value for each sensor if the amount of simulations increase. Hence, the standard error converges to 0. The standard error for 500 simulations is approximately 9 minutes for all sensors.

To compare the leak detection for the different scenarios from Table 3.3, the average and standard deviation of the LDT per sensor are calculated for each scenario. The standard error needs to be smaller than the differences in LDTs between the sensors. Hence, $N_{sim} = 500$ simulations are performed in which it is assumed that the standard error of the average drops down to an acceptable small value for all scenarios, parallel to the results shown in Figure 3.7. The resulting average and standard deviation of the LDT for all scenarios with leak location A, leak location B and leak location C are shown in Figures 3.8 and 3.9, Figures 3.10 and 3.11 and Figures 3.12 and 3.13, consecutively.
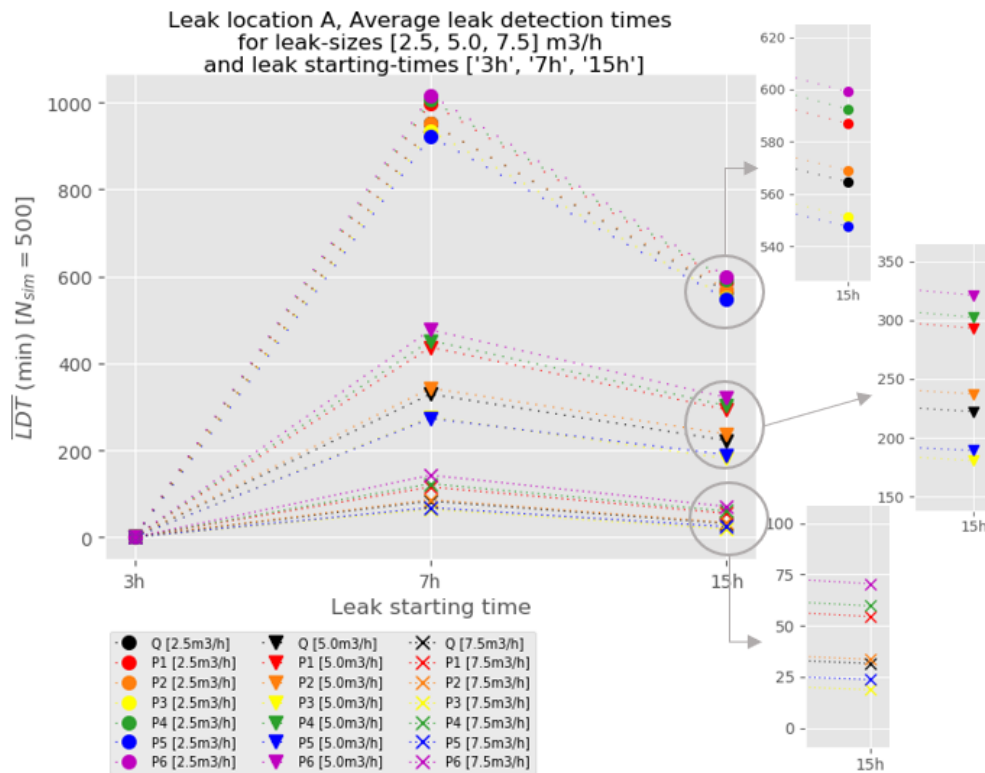
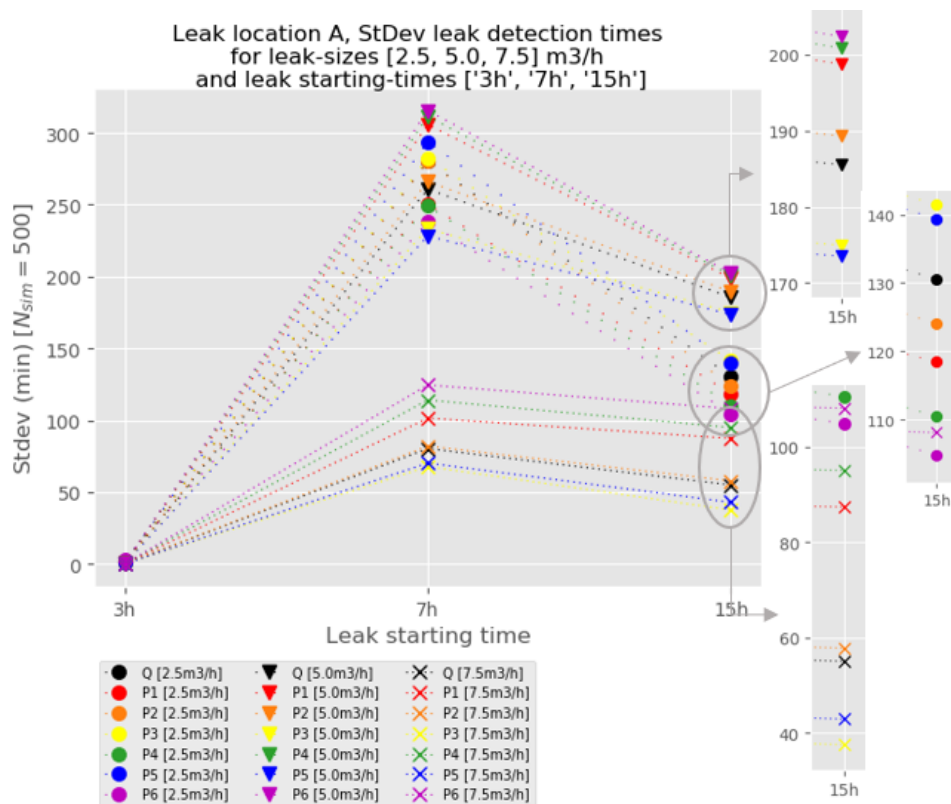Figure 3.8: Average LDT results for all scenarios with leak location A

Figure 3.9: Standard deviation LDT results for all scenarios with leak location A
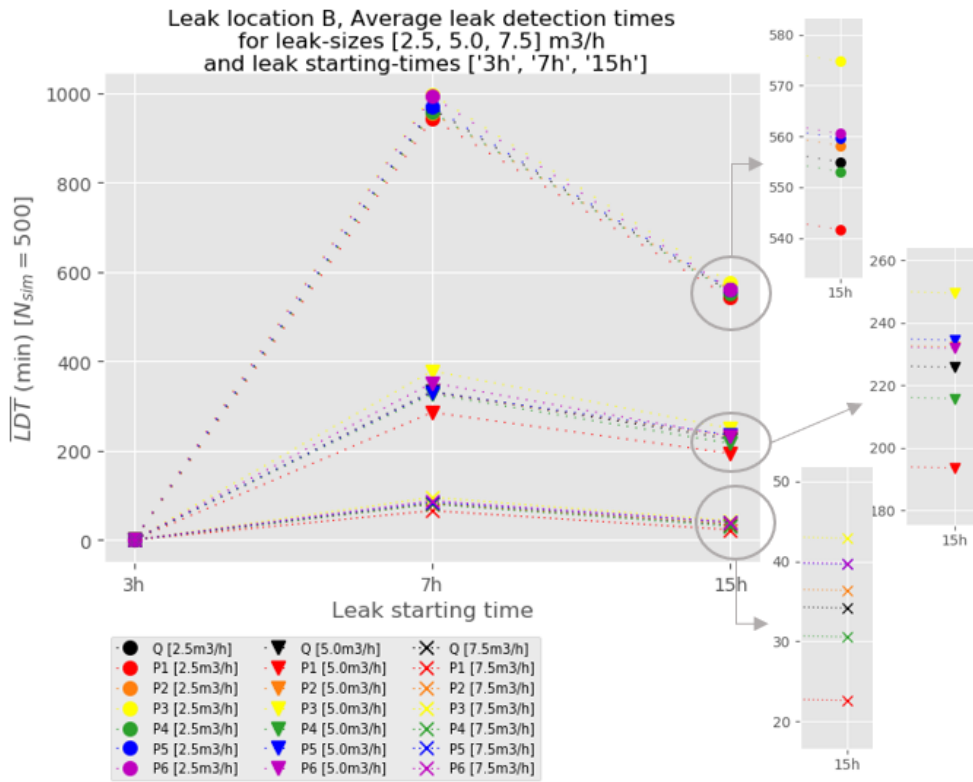
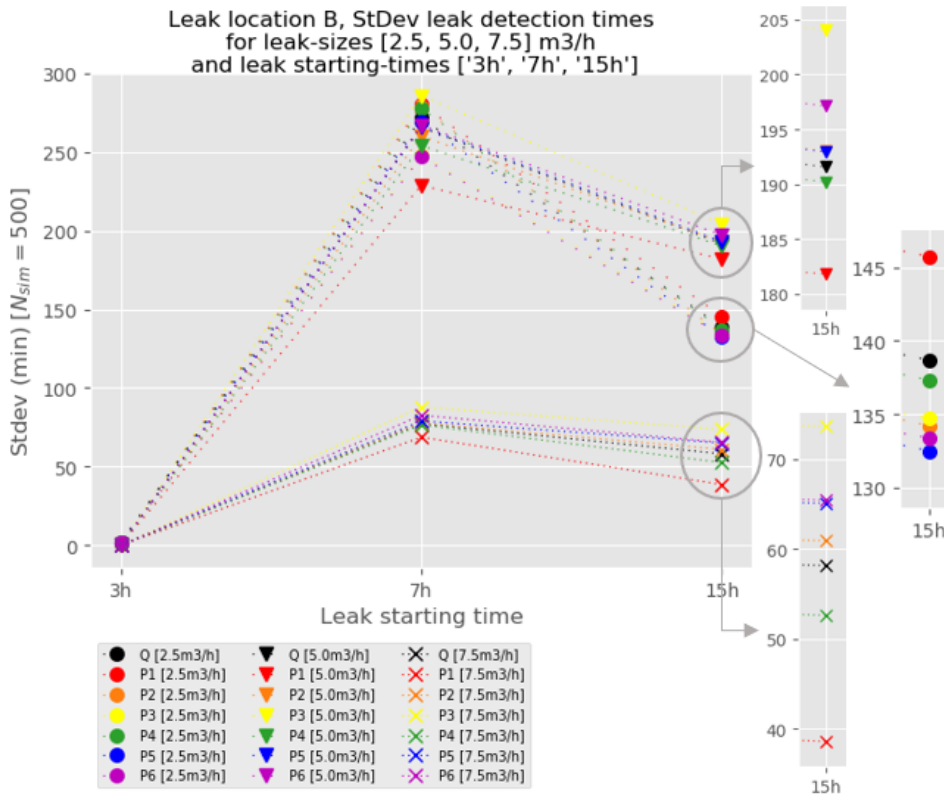Figure 3.10: Average LDT results for all scenarios with leak location B

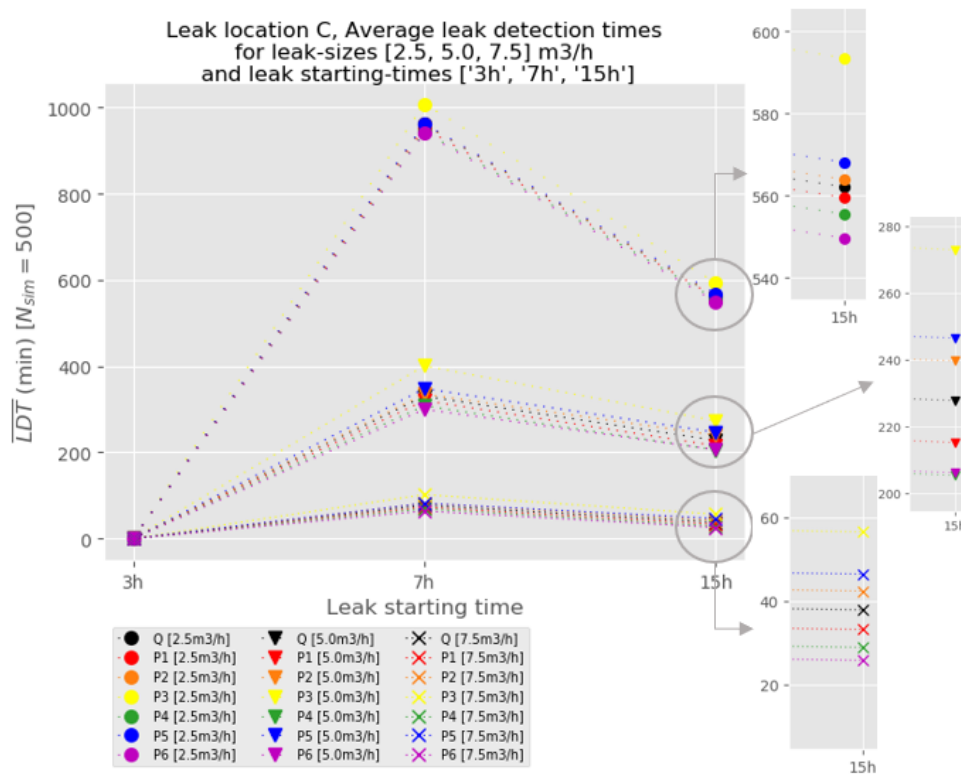Figure 3.11: Standard deviation LDT results for all scenarios with leak location B

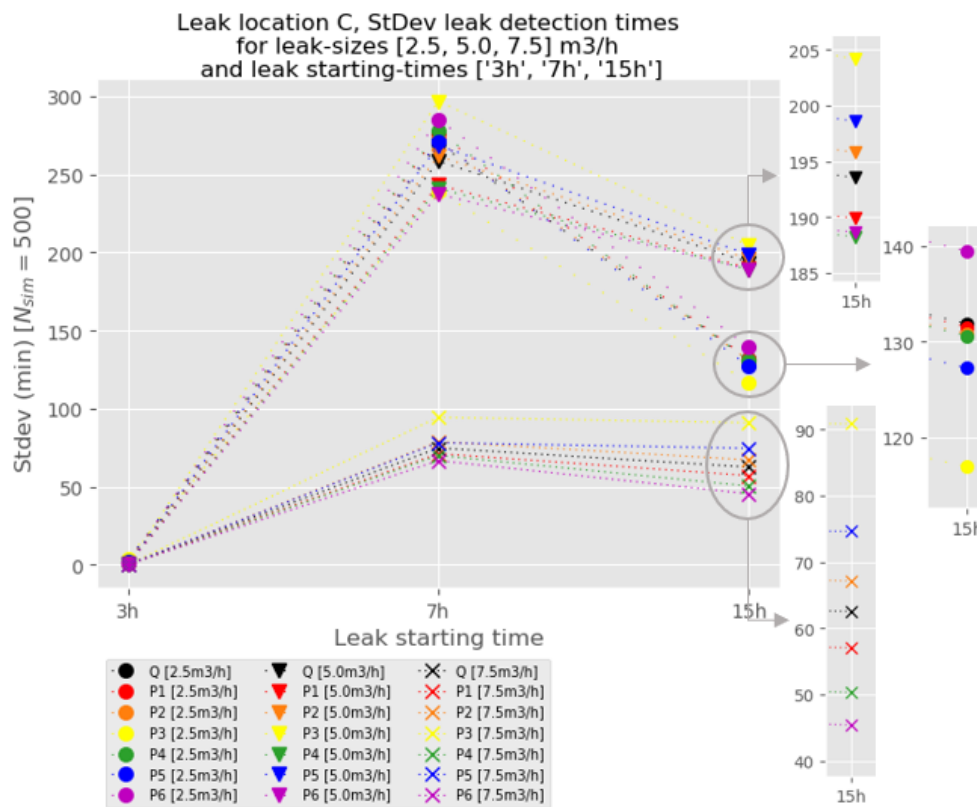Figure 3.12: Average LDT results for all scenarios with leak location C

Figure 3.13: Standard deviation LDT results for all scenarios with leak location C

Five general observations are made from the results:

1. A larger leak yields in a faster leak detection time. This holds for all sensors in all tested scenarios.
2. A leak happening during the night yields in a faster leak detection time than during the day. Furthermore, a leak happening in the afternoon is faster detected than a leak happening in the morning.
3. Some sensors are more sensitive to certain leak positions than others, fastest detection times generally occurred for sensors closest to the leak, in terms of topological distance. Although topological distance seems to play a role in sensor sensitivity, the sensitivity is not solely related to topological distance. Since the sensitivity depends largely on how the water flows in the network, other factors that can play a role are for example whether the sensor lies upstream or downstream or how looped the system is.
4. Lowest standard deviation in LDT is observed during the night, and highest standard deviation in LDT is observed during the day. This is the result of nocturnal demand fluctuations being smaller than diurnal demand fluctuations.
5. Although the leak scenarios with leak size 7.5 m^3/h generally lead to the smallest standard deviation in LDTs for most tested scenarios, a larger leak does not generally yield in a smaller standard deviation in LDT in all cases. This can be seen in the afternoon, where the standard deviation in LDT is highest for the scenarios with leak size 5.0 m^3/h. An hypothesis for this result is elucidated in the discussion.

3.3 Leak localization results

To assess the robustness of the leak localization method under the influence of stochastic demand, the same scenarios as discussed in Table 3.3 are used. Different stochastic demand characteristics are linked to different times during the day, hence, the leak localization is performed for a fixed 2 hours.

$N_{sim} = 250$ hydraulic simulations per scenario are computed to determine the influence of stochastic water demand on the performance of the leak localization method. To conduct the method, the measured pressures at the sensors ($p(t)$) and the simulated pressures at the sensors in a leak-free scenario ($\hat{p}_0(t)$) are needed. Each simulation uses different stochastic demand loading conditions, resulting in $p(t)$, at the sensors. The simulated pressures at the sensors in a leak-free scenario, $\hat{p}_0(t)$, is determined from averaging a 1000 simulations with different stochastic demand loading conditions. Hence, $\hat{p}_0(t)$ is kept fixed for all hydraulic simulations conducted in the leak localization.

By performing 250 hydraulic simulations per scenario, 250 correlation coefficients per node are computed. Statistics of the performance parameters (topological distance (D_T), the false positive rate (FP_r) and the maximum span (MS)) over all simulations are calculated to quantify the performance of leak localization over the different scenarios. A more extensive overview of the leak localization results is discussed in Appendix H.

3.3.1 Scenario plots

On the next six pages, a schematized overview of the twenty-seven leak localization scenario results are shown. They are shown in pairs of two pages. For each of the pairs, the first page shows the average correlation coefficients throughout the network, including the resulting averaged evaluation parameters. On the consecutive page, the standard deviation of the correlation coefficients throughout the network are illustrated.

Figure 3.14: Average leak localization results for all scenarios with leak location A
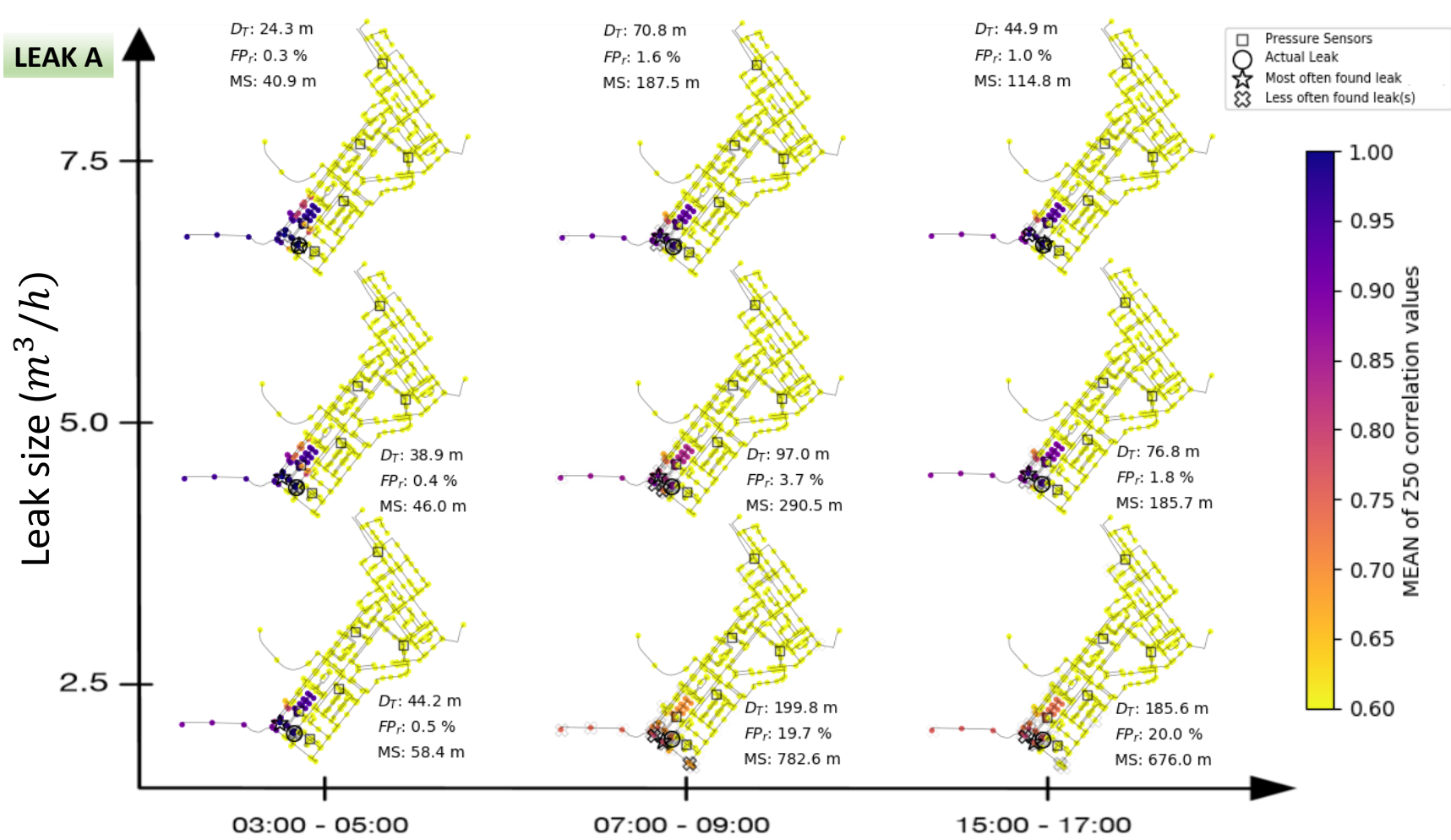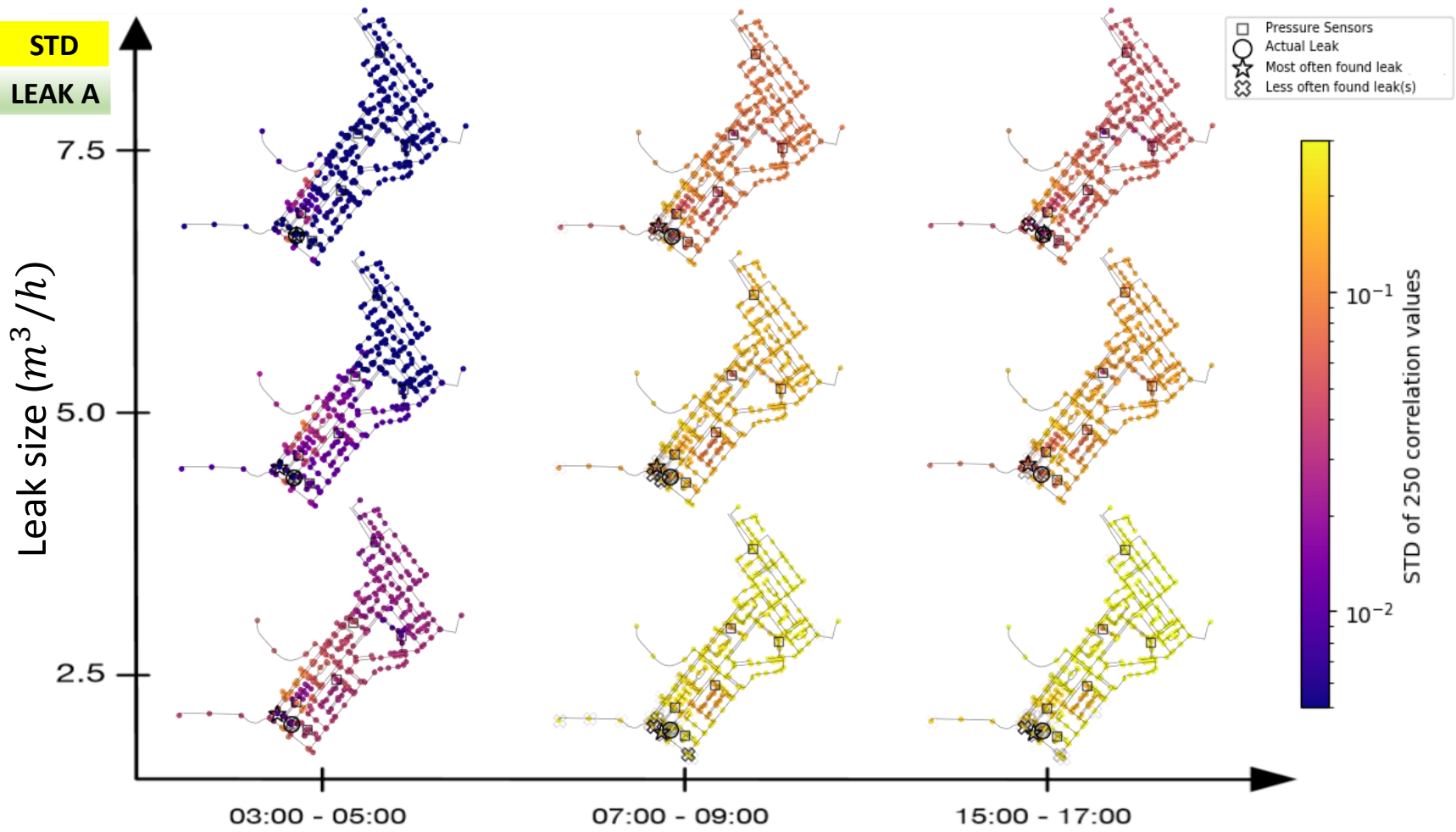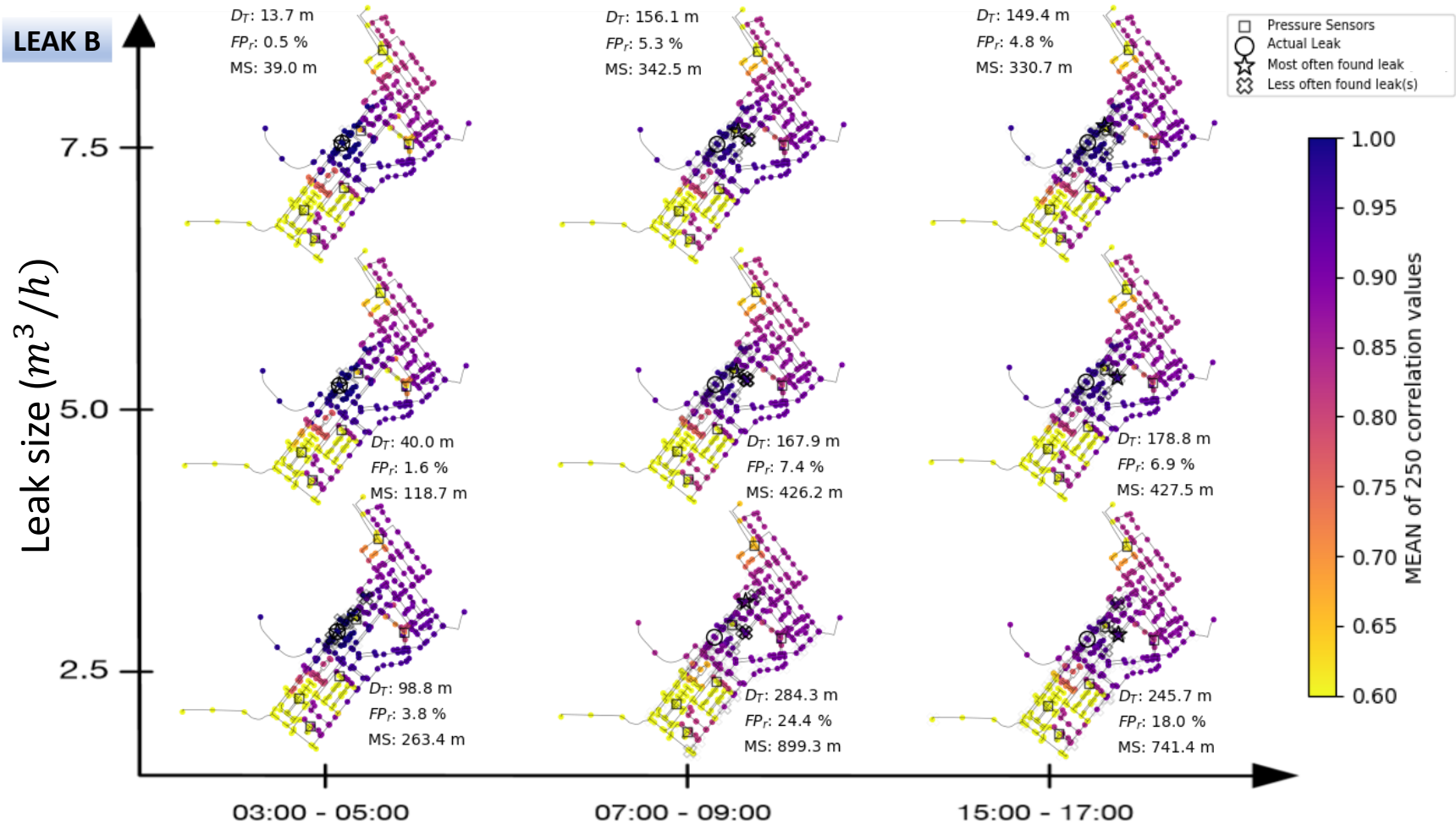
Figure 3.15: Standard deviation leak localization results for scenarios with leak location A

Figure 3.16: Average leak localization results for all scenarios with leak location B
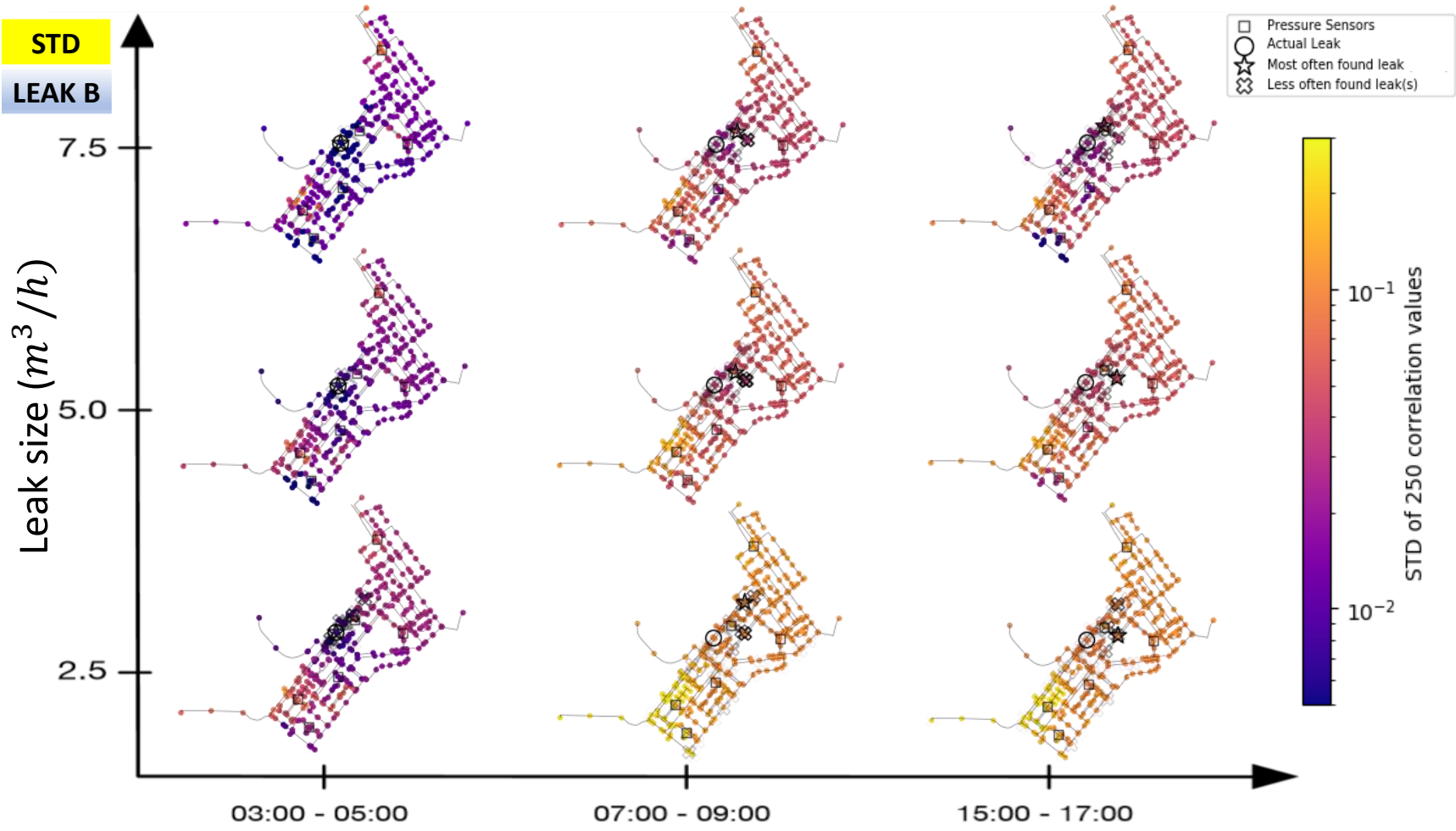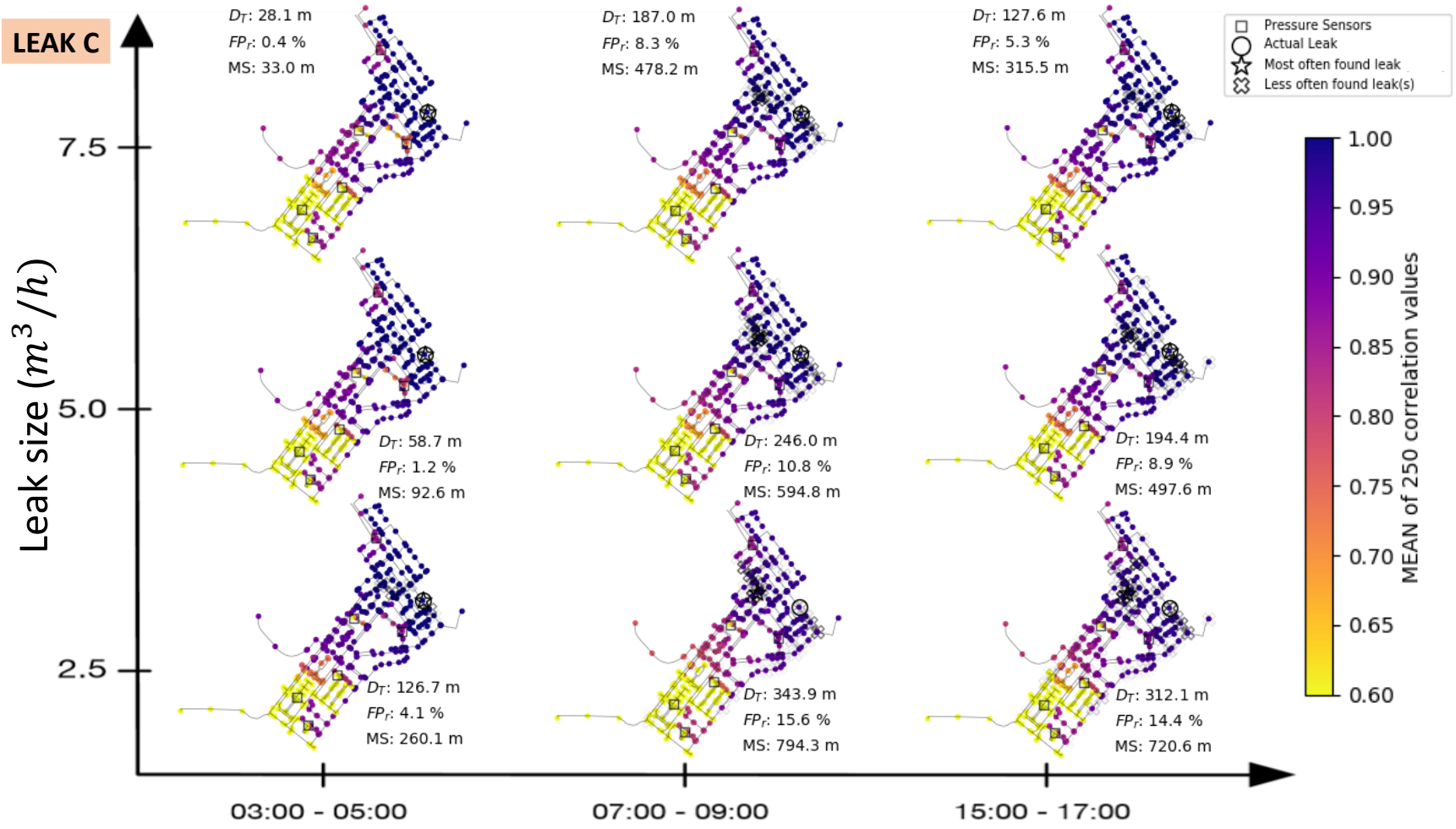
Figure 3.17: Standard deviation leak localization results for scenarios with leak location B

Figure 3.18: Average leak localization results for all scenarios with leak location C
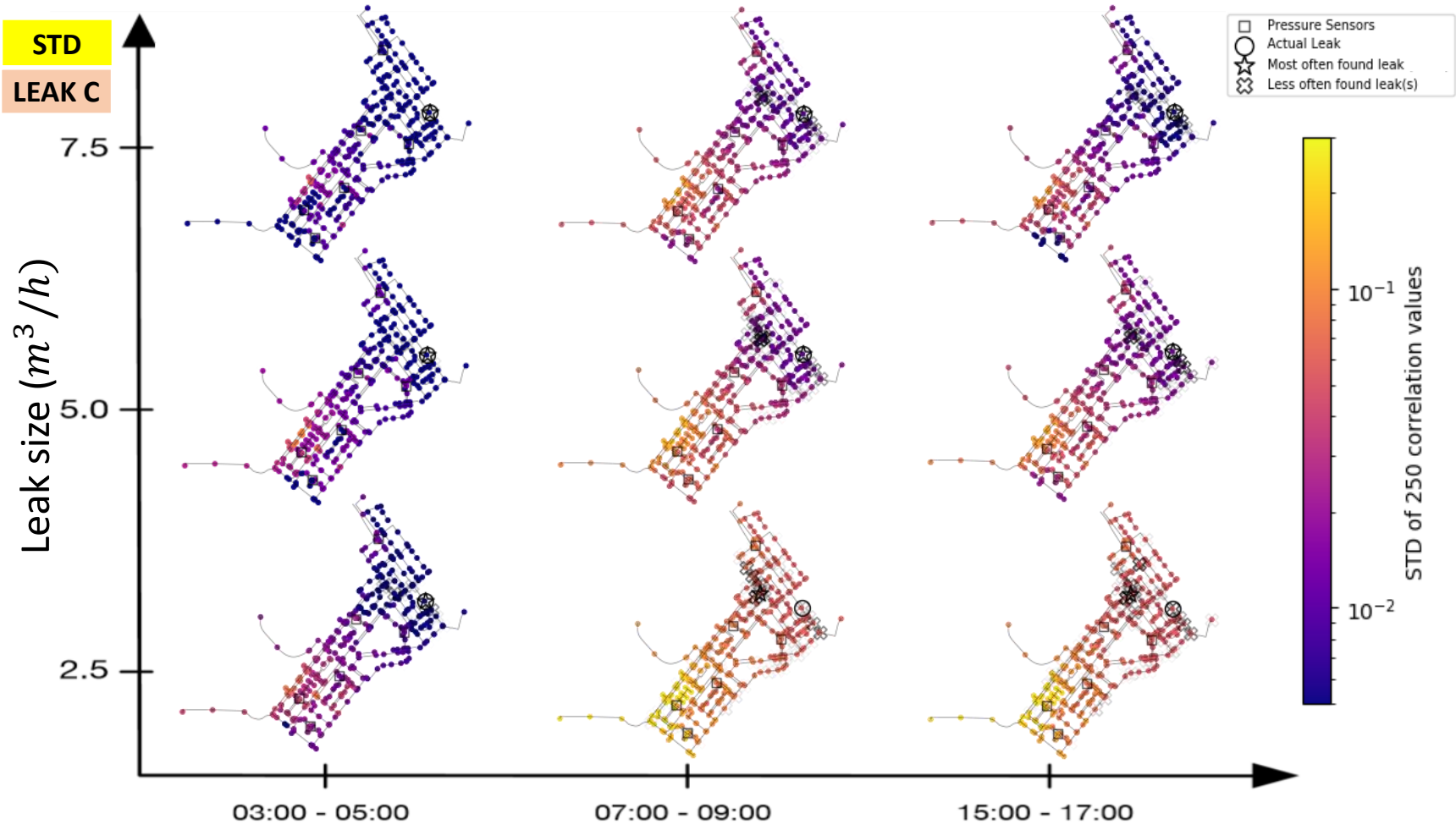
Figure 3.19: Standard deviation leak localization results for scenarios with leak location C

3.3.2 Result analysis

To represent a general overview of the influence of stochastic demand on the performance of the leak localization method, four parameters are extracted from the figures and Appendix H. The first one is the percentage of simulations that found the actual leak node in each scenario. The results are shown in Figure 3.20, in which the percentage of 250 simulations that found the actual leak node per scenario is illustrated. Furthermore, the center of gravity of the coordinates of all leak nodes found by the simulations is determined and compared with the coordinates of the actual leak node. The distance between these two points is defined to be the distance to gravity center, and is shown for all scenarios in Figure 3.21. These two parameters are a measure of the leak localization method's accuracy.

The second parameter is the topological distance between the leaknode found by the algorithm and the actual leaknode (D_T). The third is the percentage of nodes that have a higher correlation value than the actual leaknode (FP_r). The average and standard deviation of both these parameters are calculated and plotted in Figures 3.22 to 3.25. While the averages of both two parameters are a measure of the leak localization method's accuracy, the standard deviations are a measure of the leak localization method's precision. The difference between accuracy and precision is shown in Figure 3.26.
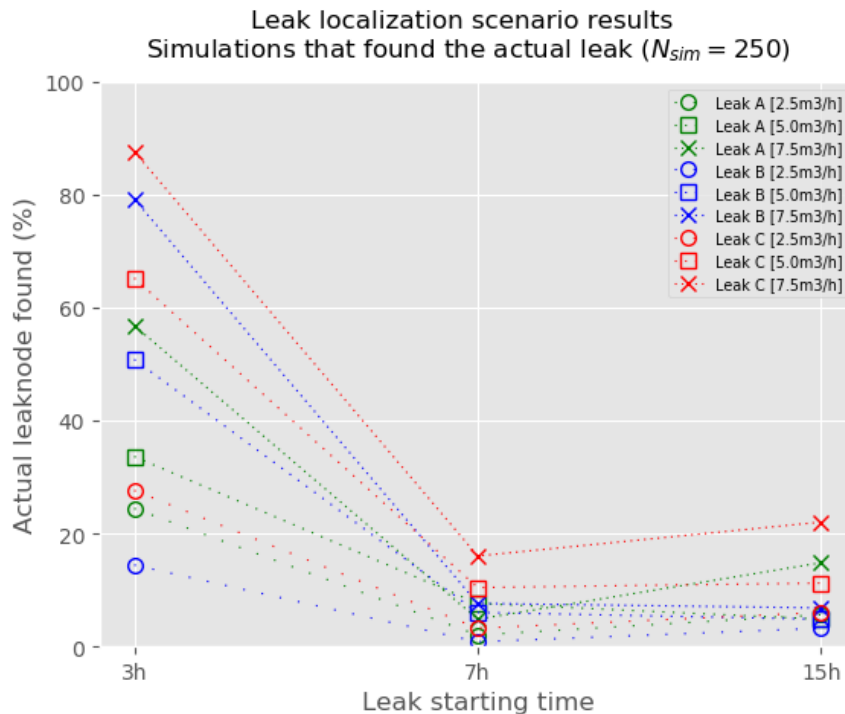

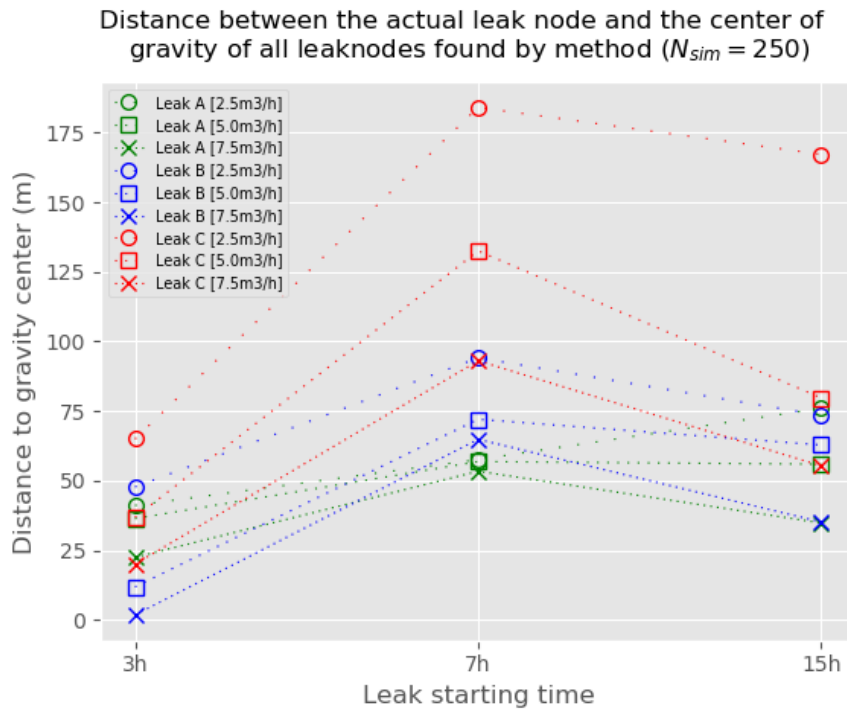Figure 3.20: Percentage of 250 simulations that found the actual leaknode

Figure 3.21: Distance to gravity center (gravity center determined from 250 simulations)
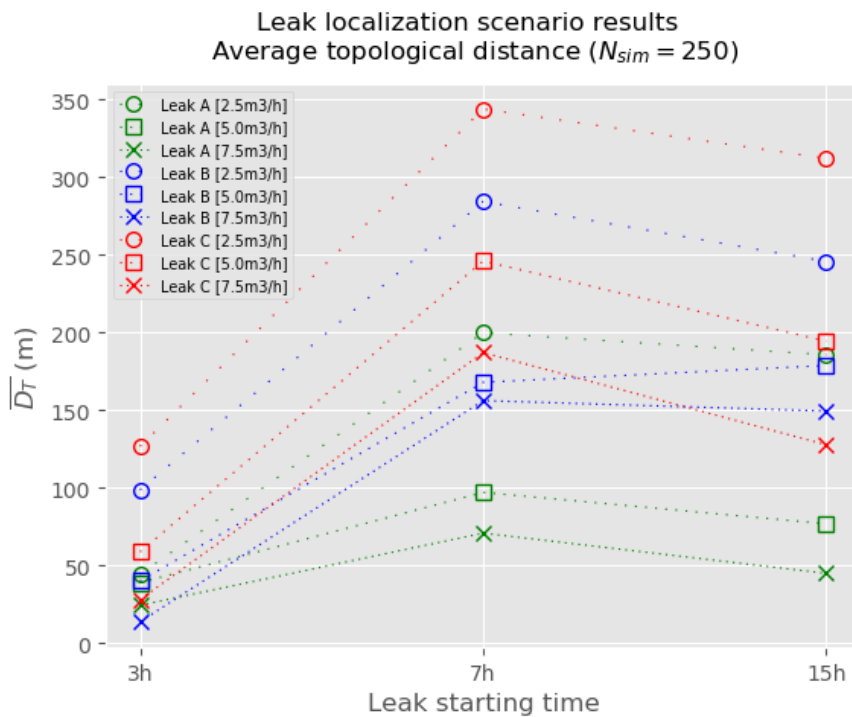

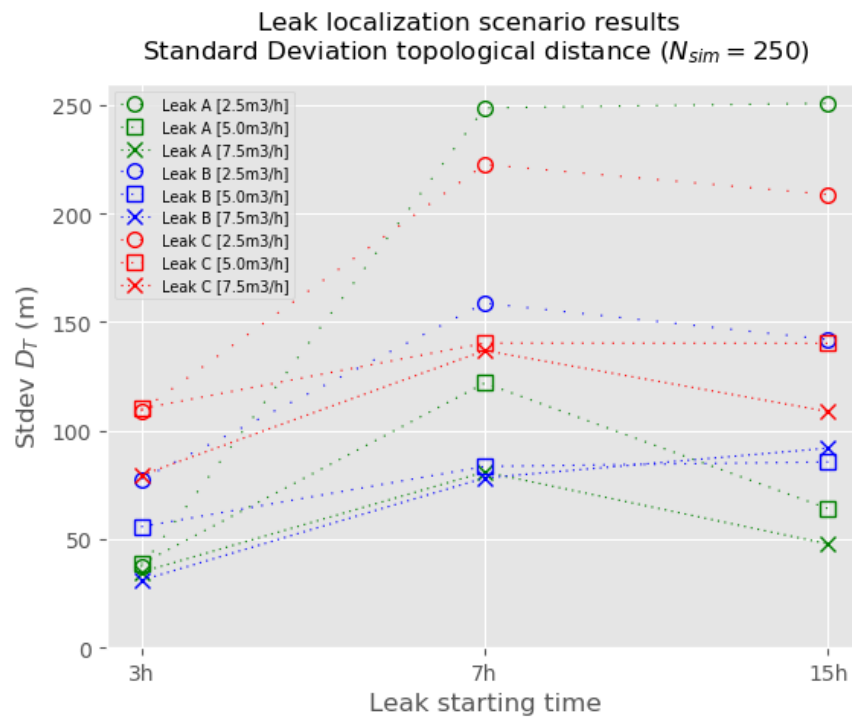Figure 3.22: Average topological distance per scenario

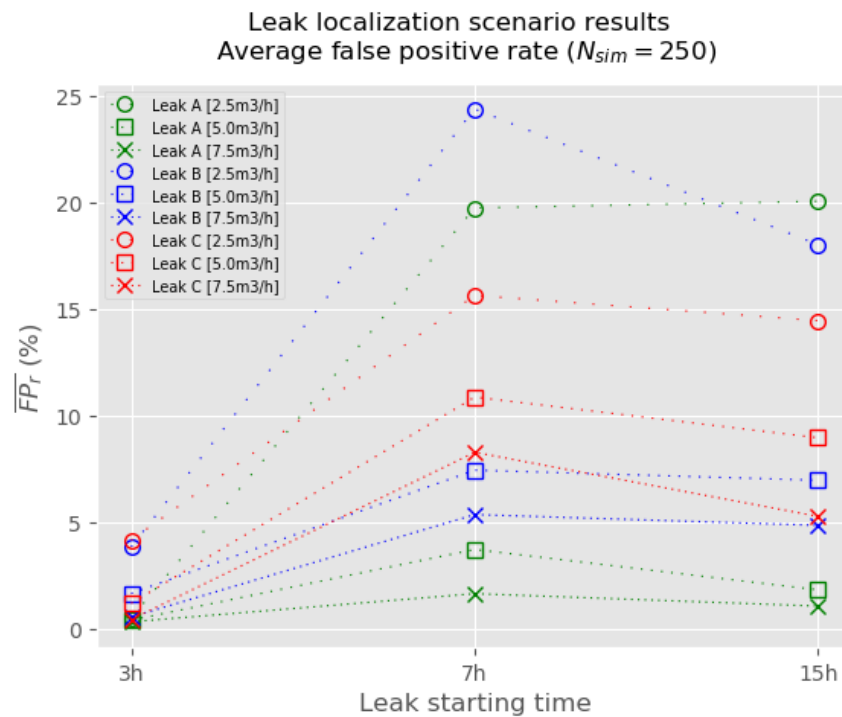Figure 3.23: Standard deviation topological distance per scenario

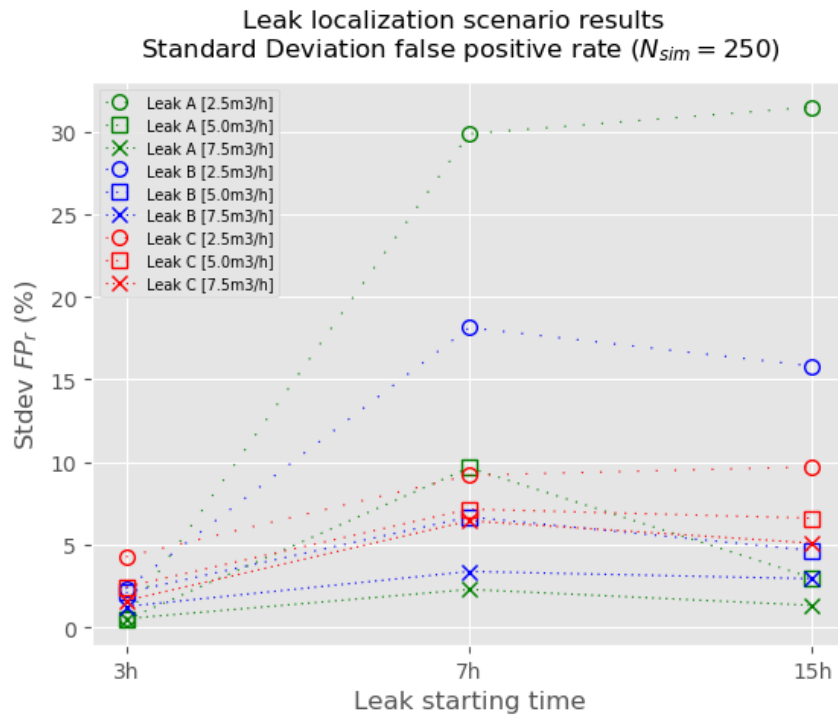Figure 3.24: Average false positive rate per scenario

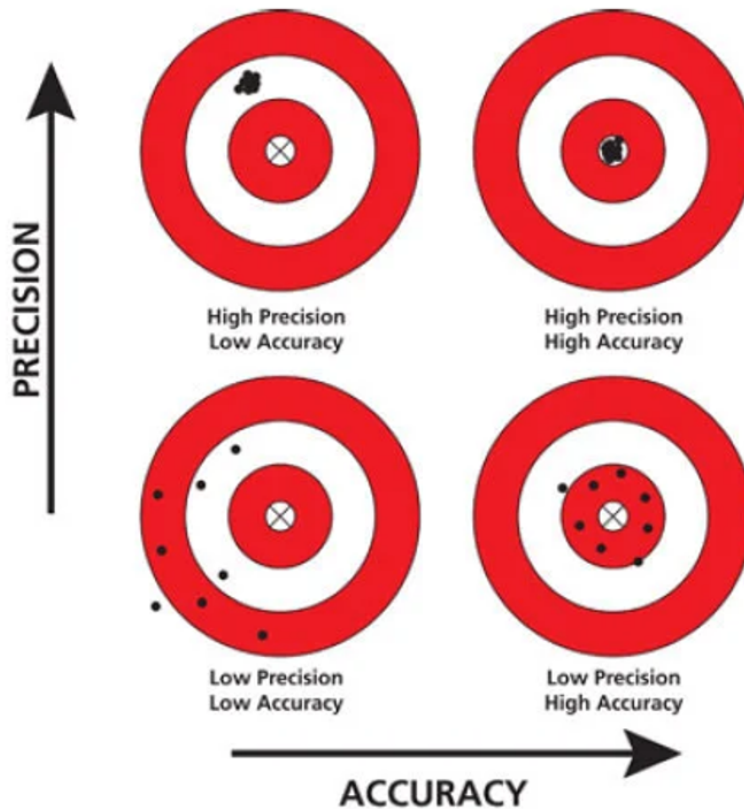Figure 3.25: Standard deviation false positive rate per scenario

Figure 3.26: Difference accuracy and precision, image adopted from Edvotek 2020

Three general observations are made from the leak localization results:

1. A larger leak yields in a higher probability of the actual leak to be found by the method and decreases the distance between actual leak node and the center of gravity. Furthermore, it raises the average topological distance between the actual leak and the found leak and lowers the average false positive rate. Hence, the accuracy of the leak localization improves. Moreover, a larger leak lowers the variance (or standard deviation) of the topological distance and the false positive rate. Hence, the precision of the leak localization improves.

2. A leak happening during the night leads to better leak localization results (lower topological distances, distances to the gravity center and FP_r). Hence, the accuracy of the leak localization improves. Furthermore, it decreases the variance of the results. This is because stochastic demand fluctuations are low.

3. There is a difference in performance between the morning and the afternoon. A leak happening during the morning yields in slightly worse leak localization results (higher topological distances, distances to the gravity center and FP_r) than compared to the afternoon. Furthermore, it generally increases the variance of the results slightly. This is because stochastic demand fluctuations are highest during the morning peak.

3.4 Discussion

By conducting hydraulic simulations with stochastic demand loading conditions, fluctuations in flow and pressure in the system are simulated and investigated. The SIMDEUM software (Blokker 2006) is used to simulate stochastic water demand. Using this software with average Dutch household statistics does not yield in simulated inflow and pressures that fit the measurements of the case study area. The large mismatch that appears between the simulated and observed inflow is unexpected since SIMDEUM has been validated on single households, an aggregation of up to 45 households and for several streets with demand measurements (Blokker et al. 2017). A large number of households (2825) are simulated in this study, hence, it is expected that using the average Dutch household statistics would describe the measurements more accurately.

Because of this mismatch between the observations and simulations, it is assumed that the household statistics in this area deviate from the average Dutch household statistics. In an effort to achieve a better fit of the simulations to the observations, the SIMDEUM software is modified in accordance with local statistics of the case study area. This results in simulations that match the measurements in the area more realistically. However, the average and variance of the simulated inflow and pressures at the sensor locations still show large differences with the observations during certain parts of the day.

Applying the SIMDEUM software with either average Dutch household statistics or local statistics of the case study area does not yield in inflow and pressure patterns that match the observations perfectly. On one hand, this is a limitation of SIMDEUM. It is unable to adjust parameters in the stochastic demand simulator such that the resulting demand loading conditions yield in simulations that represent the measurements in the network accurately. On the other hand, it could be the result of the uniqueness of the used case study. When observing the average observed water inflow, the morning peak is nearly as high as the evening peak, as is shown in Figure 3.4, an uncommon observation for DMAs in the Netherlands. Hence, water use behaviour of the residents in this case study could be too different than can be described by SIMDEUM's parameters. A potential reason is the fact that the case study directly borders the sea, yielding in more people going to the beach and showering at uncommon times during the day, resulting in unusual water use behaviour.

Beside the minor limitations, the model with the new demand loading conditions (from

the SIMDEUM software with local statistics) is considered to represent a reliable picture of the network. By conducting Monte Carlo simulations, the effect of stochastic water demand on the performance of leak detection and localization is quantified.

Artificial leak scenarios are created by simulating leaks with different leak positions, sizes and at different times. The results of the leak detection and leak localization confirm and invalidate some of the expectations.

From the leak detection results, it logically follows that if the leak is larger, the average Leak Detection Time (LDT) drops, for all sensors and in all tested scenarios. However, the results of the standard deviation of the LDT is less trivial. An hypothesis is set up to explain these results. A certain unknown threshold leak discharge is defined. If a leak size is larger than this threshold, the headloss this leak creates is so large that it is rarely regarded as noise anymore. Hence, the standard deviation of the LDT drops. If a leak size is smaller than this threshold, the headloss this leak creates is so small that it is only rarely distinguished from noise. Hence, not only does the average LDT drops, but it also yields in a lower standard deviation of the LDT.

Therefore, highest standard deviation in LDT is reached when the leak size is at its threshold. An extra dimension to this complex problem is given by the fact that the discussed leak size threshold can differ throughout the day due to the noise that varies throughout the day. Hence, the discussed leak size threshold differs for the different leak scenarios in which the time is varied. This explains for the 15:00 scenarios that the highest standard deviation of the LDT is reached when the leak size is 5 m^3/h, which appears to be closer to the discussed threshold value for this time than the other leak sizes. For the 07:00 scenarios, the 2.5 m^3/h and 5 m^3/h scenarios yield in approximately the same standard deviations in LDT. Hence, they both must be as close to the discussed threshold value for this time, meaning that the leak discharge threshold value must be somewhere between 2.5 m^3/h and 5 m^3/h.

From both the leak detection and localization, some similar results are found. Both methods confirm that a larger leak yields in improved performance. This is expected since a larger leak results in more flow in a pipe and therefore a larger pressure drop. Hence, larger leaks cause a larger hydraulic impact and are therefore more likely to be earlier detected (Bakker et al. 2014a) and better localized (Sophocleous et al. 2019).

Beside the size of the leak, the time of the leak influences the performance of both methods. The results show that the best performance is achieved during the night due to low nocturnal demand fluctuations, and worst performance is achieved during the morning peak when diurnal demand fluctuations are highest. This result confirms as well as contradicts other findings in the literature. It supports the argument of Perez et al. 2014 and Farley et al. 2008, stating that performance improves during the night when there is less demand and, hence, less noise. However, it contradicts one of the conclusions stated by Moors et al. 2018, who applied the same leak localization method on a different case study with real measurements but using a factorized deterministic demand model. They found that best performance in leak localization was achieved during the morning peak, arguing that when the flow is large, the pressure drop caused by a leak is also large, hence making it easier for the leak localization to localize a leak in the morning.

Hence, two contradictory effects are explained in the literature regarding the times during the day at which leaks are faster detected and better localized. It depends on one hand on the pressure drop as a result of the leak, influencing the sensitivity of the sensors. On the other hand it depends on the amount of noise present in the system. Leakages during maximum demand yield in larger pressure drops because of the larger flow and the non-linear relationship between flow and pressure. However, it also contains a lot of noise. Leakages during minimum demand means smaller flow is present, hence yield in smaller pressure

drops but they also contain little noise. The latter effect is dominant in this study, yielding in a better performance during the night than during the morning peak.

From the leak localization results specifically, it is found that stochastic demand fluctuations influence the precision of the results. The precision of the leak localization performance generally improves during the night when low demand fluctuations are present, and declines during the day when demand fluctuations are higher.

The leak localization method of Quevedo et al. 2011 is used in this study. By using fully stochastic demand loading conditions, the robustness of this method under the influence of realistic demand fluctuations is assessed. The leak localization method applied in this study is deterministic because the simulated pressures at the sensors in the leak-free scenario ($\hat{p}_0(t)$) are fixed. For the method to become fully stochastic, $\hat{p}_0(t)$ needs to be dependent on stochastics as well. Hence, for every hydraulic simulation that is conducted in the leak localization, a random simulation with implemented stochastic demand can be used for determining $\hat{p}_0(t)$.

The problem with making the leak localization fully stochastic is that by reformulating $\hat{p}_0(t)$ for every simulation, the Fault Signature Matrix (FSM) needs to be computed for every simulation. In this study, the leak localization method is kept deterministic such that $\hat{p}_0(t)$ and thus the FSM is fixed for every leak scenario. Hence, the FSM just needs to be computed once for every scenario. Since the computation of the FSM is a slow and time-inefficient process, computing it for every simulation takes a long time.

A solution to circumvent this obstacle could be to use another leak localization method that is not bounded by the computation of the FSM. A computationally much faster method is proposed by Cheng and He 2011, in which a matrix analysis has been carried out to set up the sensitivity matrix for a water distribution network. This matrix relates changes in demand to changes in head in the system. The computation of the sensitivity matrix with some improvement is elucidated in Sanz 2016. Applying this method would only need one simulation for each leak scenario, hence, a full stochastic approach would become feasible.

4. Conclusions and recommendations

With this study, a tool is created to assess the robustness of leak detection and localization techniques under the influence of realistic stochastic demand variations. With this tool, the influence of uncertain water demand fluctuations on the performance of leak detection and localization can be quantified.

The applied case study is a residential area in the Netherlands consisting of a water distribution network with an inflow and pressure sensors. The corresponding hydraulic model uses stochastic demand loading conditions as inputs. These inputs are simulated with the stochastic demand modelling software SIMDEUM (Blokker 2006), and is applied with average Dutch household statistics and local statistics of the applied case study area. Using the latter as demand loading conditions for the hydraulic model yields in inflow and pressure simulations that match the observations more accurately, with some minor limitations.

The main limitation that appears to be independent from changing the statistics in SIMDEUM is that simulated variances stay larger than the observed variances (for the inflow and pressures). On one hand, an extra tool could be created in the stochastic demand model to let the average daily consumption vary between certain boundaries. In this way, the variance of the daily consumption can be controlled, influencing the variance of the simulated inflow and pressure levels. Hence, the necessary boundaries the average daily consumption needs to match the observed variances at the sensors can be derived. On the other hand, the observed variance derived by applying Seasonal and Trend decomposition using LOESS (STL) could be the issue. More sophisticated time series analysis could be applied.

Within the current parameterization of SIMDEUM, it is a hassle to find the input statistics the stochastic demand model needs to fit the resulting simulations to the observations. This is done in this study with a trail-and-error method, a laborious and time-consuming task. It is recommended to change the parameterization of SIMDEUM, such that this process becomes much easier. A tool can be created that shows how the adaptation of certain parameters in SIMDEUM will influence the daily consumption outcome.

It is shown that with the implementation of stochastic water demand, the expected variability in pressure throughout the network as a result of the variability of water demand can be determined. Hence, it can be determined at what spots in the network the variability in pressure is small as a result of low variability in water demand. This is valuable information for optimal sensor placement algorithms and further investigations might lead to more robust measurement locations in the future.

The SIMDEUM software with the local statistics is used to create stochastic demand loading conditions as inputs for the hydraulic model. This model is used in assessing the performance of the leak detection and localization. Since real leak measurements in the system are absent, the leak detection and localization are applied with leak simulations. Different artificial leak scenarios are set up in which the leak position, leak size and leak time is varied. For each scenario, Monte Carlo simulations are conducted and the leak detection and leak localization methods are applied. Hence, the robustness of both methods is assessed.

The results of the leak detection indicates that detection time drops during the night, when water demand and its fluctuations are low. The detection time is highest during the morning peak, when water demand and its fluctuations are highest. Both results hold for

all sensors and all tested scenarios. Furthermore, since the sensors sensitivity to a leak depends on how the water flows in the network, it is clearly but not solely dependent on the topological distance between the sensor and the leak. Other potential factors are whether the sensor lies upstream or downstream of the leak or how looped or branched the network is.

The results of the leak localization indicates that demand fluctuations are also strongly linked to the performance of the leak localization. It is found that for all tested scenarios, high accuracy and precision in localization is found during the night, when nocturnal demand fluctuations are lowest. Low accuracy and precision in localization is found during the morning peak, when diurnal demand fluctuations are highest.

Only single-leak scenarios are considered in this method. Scenarios in which multiple leaks exist at the same time are not considered. Further investigations into the influence of multiple leaks on the leak detection and localization performance could lead to more robust algorithms.

The applied leak localization method is deterministic with stochastic demand loading conditions. It is not conducted in a full stochastic manner because the sensitivity matrix needed to be computed for every simulation of a leak localization. Since calculating the sensitivity matrix within this method is computationally very slow, calculating the matrix for every simulation takes too much time. It is recommended to apply the method proposed by Cheng and He 2011, in which the computation of the sensitivity matrix is done a lot more efficient. Applying this method would make it easy to assess the robustness of the leak localization under full stochastic conditions.

Hence, it is recommended to apply stochastic demand in more leak detection and localization techniques. Furthermore, future studies on networks with available smart meter data that measure the water demand in the network might be valuable to further validate the use of stochastic demand. Moreover, the availability of real leak measurement data can be valuable in the robustness assessment of detection and localization algorithms.

List of acronyms

CDF   Cumulative Distribution Function.

DD   Demand Driven.
DE   Differential Evolution.
DMA   District Metered Area.
DW   Darcy-Weisbach.

FSM   Fault Signature Matrix.

HW   Hazen-Williams.

IQR   Inter Quartile Range.
IWA   International Water Association.

KDE   Kernel Density Estimation.

LDT   Leak Detection Time.

MNF   Minimum Night Flow.
MSE   Mean Squared Error.

NRW   Non-Revenue Water.

PDD   Pressure Dependent Demand.

SI   International System of Units.
STL   Seasonal and Trend decomposition using LOESS.

WDN   Water Distribution Network.
WNTR   Water Network Tool for Resilience.

Bibliography

Bakker, M, D Jung, J Vreeburg, M Van de Roer, K Lansey, and L Rierveld (2014a). "Detecting pipe bursts using Heuristic and CUSUM methods". In: *Procedia Engineering, 70, 2014; CCWI 2013: 12th International Conference on Computing and Control for the Water Industry*. Elsevier.

Bakker, M, JHG Vreeburg, M Van de Roer, and LC Rietveld (2014b). "Heuristic burst detection method using flow and pressure measurements". In: *Hydroinformatics Journal* 16.5, pp. 1194–1209.

Bakker, M, JHG Vreeburg, KM Van Schagen, and LC Rietveld (2013). "A fully adaptive forecasting model for short-term drinking water demand". In: *Environmental Modelling & Software* 48, pp. 141–151.

Bakker, Martijn (2014). "Optimised control and pipe burst detection by water demand forecasting". In:

Bao, Yixing and Larry W Mays (1990). "Model for water distribution system reliability". In: *Journal of Hydraulic Engineering* 116.9, pp. 1119–1137.

Blokker, EJM (2006). "Modeling water demand patterns; description and evaluation of simulation model SIMDEUM". In: *Kiwa NV, Nieuwegein, The Netherlands (in Dutch)*.

Blokker, EJM, JHG Vreeburg, and JC Van Dijk (2009). "Simulating residential water demand with a stochastic end-use model". In: *Journal of Water Resources Planning and Management* 136.1, pp. 19–26.

Blokker, Elisabeth Johanna Maria (2010). "Stochastic water demand modelling for a better understanding of hydraulics in water distribution networks". PhD thesis. Delft University of Technology.

Blokker, Mirjam, Claudia Agudelo-Vera, and George Mesman (2018). "Drinking Water Demand under Stressed Conditions; Quantification with SIMDEUM". In: *WDSA/CCWI Joint Conference Proceedings*. Vol. 1.

Blokker, Mirjam, Claudia Agudelo-Vera, Andreas Moerman, Peter van Thienen, and Ilse Pieterse-Quirijns (2017). "Review of applications for SIMDEUM, a stochastic drinking water demand model with a small temporal and spatial scale". In: *Drinking Water Engineering and Science* 10.1, pp. 1–12.

CBS (2019). *Kerncijfers wijken en buurten 2019*. URL: https://www.cbs.nl/nl-nl/maatwerk/2019/31/kerncijfers-wijken-en-buurten-2019 (visited on 02/19/2020).

Cheng, Li, Du Kun, Tu Jia-peng, and Dong Wei-xin (2017). "Optimal placement of pressure sensors in water distribution system based on clustering analysis of pressure sensitive matrix". In: *Procedia Engineering* 186, pp. 405–411.

Cheng, Weiping and Zhiguo He (2011). "Calibration of nodal demand in water distribution systems". In: *Journal of Water Resources Planning and Management* 137.1, pp. 31–40.

Cleveland, Robert B, William S Cleveland, Jean E McRae, and Irma Terpenning (1990). "STL: A seasonal-trend decomposition". In: *Journal of official statistics* 6.1, pp. 3–73.

Cochran, Josh (2020). *Water main in a city, New York Times*. URL: https://viewing.nyc/new-york-times-explores-how-new-york-gets-its-water-in-new-new-york-101-column/ (visited on 06/01/2020).

Colombo, Andrew F, Pedro Lee, and Bryan W Karney (2009). "A selective literature review of transient-based leak detection methods". In: *Journal of hydro-environment research* 2.4, pp. 212–227.

Crowl, Daniel A and Joseph F Louvar (2001). *Chemical process safety: fundamentals with applications*. Pearson Education.

Cugueró-Escofet, Miquel À, Vicenç Puig, and Joseba Quevedo (2017). "Optimal pressure sensor placement and assessment for leak location using a relaxed isolation index: Application to the Barcelona water network". In: *Control Engineering Practice* 63, pp. 1–12.

D'Agostino, Ralph and Egon S Pearson (1973). "Tests for departure from normality. Empirical results for the distributions of b2 and sqrt(b)". In: *Biometrika* 60.3, pp. 613–622.

Dijkstra, Edsger W et al. (1959). "A note on two problems in connexion with graphs". In: *Numerische mathematik* 1.1, pp. 269–271.

Donkor, Emmanuel A, Thomas A Mazzuchi, Refik Soyer, and J Alan Roberson (2014). "Urban water demand forecasting: review of methods and models". In: *Journal of Water Resources Planning and Management* 140.2, pp. 146–159.

Edvotek (2020). *Micropipeting Basics*. URL: https://www.edvotek.com/site/pdf/Pipet_Guide.pdf (visited on 07/16/2020).

EPA, US (2005). *Water distribution system analysis: Field studies modeling and management. A reference guide for utilities*.

EurEau (2017). *Europe's water in figures: An overview of the European drinking water and waste water sectors*.

Farley, B, JB Boxall, and SR Mounce (2008). "Optimal locations of pressure meters for burst detection". In: *Water Distribution Systems Analysis 2008*, pp. 1–11.

Farley, Malcolm and Stuart Trow (2003). *Losses in water distribution networks*. IWA publishing.

Farley, Malcolm, Sanitation Water, Water Supply, Sanitation Collaborative Council, the World Health Organization, et al. (2001). *Leakage management and control: a best practice training manual*. Tech. rep. World Health Organization.

Gargano, Rudy, Federico Di Palma, Giovanni de Marinis, Francesco Granata, and Roberto Greco (2016). "A stochastic approach for the water demand of residential end users". In: *Urban Water Journal* 13.6, pp. 569–582.

Hyndman, Rob J and George Athanasopoulos (2018). *Forecasting: principles and practice*. OTexts.

Jarque, Carlos M and Anil K Bera (1980). "Efficient tests for normality, homoscedasticity and serial independence of regression residuals". In: *Economics letters* 6.3, pp. 255–259.

Kapelan, Zoran (2002). "Calibration water distribution system hydraulic models". PhD thesis. University of Exeter.

Klise, Katherine A, Regan Murray, and Terra Haxton (2018). *An Overview of the Water Network Tool for Resilience (WNTR).* Tech. rep. Sandia National Lab.(SNL-NM), Albuquerque, NM (United States).

Lambert, Allan and Wolfram Hirner (2000). *Losses from Water Supply Systems: Astandard Terminology and Recommended Performance Measures.* IWA.

Liou, Chyr Pyng (1998). "Limitations and proper use of the Hazen-Williams equation". In: *Journal of Hydraulic Engineering* 124.9, pp. 951–954.

Lippacher, Jakim (2018). "Methoden der Kalibrierung von Trinkwasserverteilnetzen und deren Einfluss auf die modellbasierte Leckage Lokalisierung." Graz University of Technology.

Lutz, Mark (2001). *Programming python.* " O'Reilly Media, Inc."

Mallick, Keshaw N, Iftekhar Ahmed, Kevin S Tickle, and Kevin E Lansey (2002). "Determining pipe groupings for water distribution networks". In: *Journal of Water Resources Planning and Management* 128.2, pp. 130–139.

Mameren, Harry van and François Clemens (1997). "Guidelines for hydrodynamic calculations on urban drainage in the Netherlands: overview and principles". In: *Water Science and Technology* 36.8-9, pp. 247–252.

Meseguer, Jordi, Josep M Mirats-Tur, Gabriela Cembrano, and Vicenç Puig (2015). "Model based monitoring techniques for leakage localization in distribution water networks". In: *Procedia Engineering* 119, pp. 1399–1408.

Meseguer, Jordi, Josep M Mirats-Tur, Gabriela Cembrano, Vicenç Puig, Joseba Quevedo, Ramón Pérez, Gerard Sanz, and David Ibarra (2014). "A decision support system for on-line leakage localization". In: *Environmental modelling & software* 60, pp. 331–345.

Mirats-Tur, Josep Maria, P-A Jarrige, J Meseguer, and G Cembrano (2014). "Leak detection and localization using models: field results". In: *Procedia Engineer* 70, pp. 1157–1165.

Moors, Janneke, Jurjen den Besten, and Peter Mense (2016). "Eerste resultaat met DMA behaald: verborgen lekkage efficiënt opgespoord". In: *H2O online*.

Moors, Janneke, L Scholten, JP van der Hoek, and J den Besten (2018). "Automated leak localization performance without detailed demand distribution data". In: *Urban Water Journal* 15.2, pp. 116–123.

Mullender, K Sjoerd (1995). *X Python Reference Manual.* Centrum voor Wiskunde en Informatica.

Niazkar, M, N Talebbeydokhti, and SH Afzali (2017). "Relationship between Hazen-William coefficient and Colebrook-White friction factor: Application in water network analysis". In: *European Water* 58, pp. 513–520.

Ostfeld, Avi, Elad Salomons, Lindell Ormsbee, James G Uber, Christopher M Bros, Paul Kalungi, Richard Burd, Boguslawa Zazula-Coetzee, Teddy Belrain, Doosun Kang, et al.

(2012). "Battle of the water calibration networks". In: *Journal of Water Resources Planning and Management* 138.5, pp. 523–532.

Perez, Ramon, Gerard Sanz, Vicenc Puig, Joseba Quevedo, Miquel Angel Cuguero Escofet, Fatiha Nejjari, Jordi Meseguer, Gabriela Cembrano, Josep M Mirats Tur, and Ramon Sarrate (2014). "Leak localization in water networks: a model-based methodology using pressure sensors applied to a real network in Barcelona [applications of control]". In: *IEEE control systems magazine* 34.4, pp. 24–36.

Pudar, Ranko S and James A Liggett (1992). "Leaks in pipe networks". In: *Journal of Hydraulic Engineering* 118.7, pp. 1031–1046.

Puust, R, Z Kapelan, DA Savic, and T Koppel (2010). "A review of methods for leakage management in pipe networks". In: *Urban Water Journal* 7.1, pp. 25–45.

Quevedo, Casin, Joseba Jokin, Miquel Àngel Cugueró Escofet, Ramon Pérez Magrané, Fatiha Nejjari Akhi-Elarab, Vicenç Puig Cayuela, Josep Maria Mirats Tur, et al. (2011). "Leakage location in water distribution networks based on correlation measurement of pressure sensors". In: *IWA Symposium on System Analysis and Integrated Assessment*, pp. 290–297.

Rossman, Lewis A et al. (2000). "EPANET 2: Users Manual". In: *Water Supply and Water Resources Division, National Risk Management Research Laboratory*.

Sanz, Estapé Gerard (2016). "Demand modeling for water networks calibration and leak localization". PhD thesis. Universitat Politècnica de Catalunya (UPC).

Savic, Dragan A, Zoran S Kapelan, and Philip MR Jonkergouw (2009). "Quo vadis water distribution model calibration?" In: *Urban Water Journal* 6.1, pp. 3–22.

Scan (2020). *Water distribution network sketch*. URL: `https://www.s-can.at/applications/drinking-water` (visited on 07/17/2020).

Shapiro, Samuel Sanford and Martin B Wilk (1965). "An analysis of variance test for normality (complete samples)". In: *Biometrika* 52.3/4, pp. 591–611.

Sophocleous, Sophocles, Dragan Savić, and Zoran Kapelan (2019). "Leak localization in a real water distribution network based on search-space reduction". In: *Journal of Water Resources Planning and Management* 145.7, p. 04019024.

Steffelbauer, DB (2018). "Model-Based Leak Localization in Water Distribution Systems". PhD thesis. Technical University Graz.

Wagner, Janet M, Uri Shamir, and David H Marks (1988). "Water distribution reliability: simulation methods". In: *Journal of water resources planning and management* 114.3, pp. 276–294.

Weisstein, Eric W (2002). "Normal distribution". In: *https://mathworld. wolfram. com/*.

Appendices

A. Software materials

A.1 EPANET

The hydraulic model of DMA Duindorp that is retrieved from the water utility company is given in EPANET, a public domain software application that is used globally to model water distribution systems (EPA 2005). A hydraulic model in EPANET can perform steady and quasi-steady simulations (Rossman et al. 2000) and consists of pipes, nodes (pipe junctions), storage tanks, reservoirs, pumps and valves. For a quasi-steady model in EPANET (the type this study will focus on), the water levels in tanks have to be updated at each time-step according to the water that enters or leaves the network. Variation of nodal demand and heads at reservoirs is given in the form of patterns through time.

The version of EPANET that will be used throughout this study is 2.0. This version of EPANET is able to perform demand-driven simulations. An updated version of EPANET (2.2) is also able to perform pressure-driven demand simulations, but is not used in this study.

A.2 Python and WNTR

In this study, the main programming language that will be used is Python version 3.7 (Mullender 1995) and Spyder version 3.3.6. Python is an interpreted high-level open source programming language which has become increasingly popular the last thirty years (Lutz 2001). Spyder is an integrated development environment for scientific programming in Python, written in Python and for Python.

Python is able to communicate with EPANET via the WNTR package. The WNTR (Klise et al. 2018) is an EPANET compatible Python package designed to simulate and analyze resilience of water distribution networks. This tool will be used in this study to communicate with EPANET efficiently and to perform hydraulic simulations. There are two simulators in WNTR able to perform hydraulic simulations, the Epanet-Simulator which uses the programmers toolkit of EPANET 2.0, and the WNTR-Simulator consisting of a pure Python hydraulics simulation engine which is based on the same equations as EPANET. The latter is chosen to run hydraulic simulations in this study because the WNTR-Simulator is able to run Pressure Dependent Demand (PDD) driven simulations. The Epanet-Simulator is unable to run these kind of simulations because it uses EPANET version 2.0, a version that does not include PDD simulations.

A.3 SIMDEUM

As already discussed before in this study, SIMDEUM is an end-use model that can simulate stochastic demand. Since SIMDEUM is not written in Python but in Matlab, this model cannot be easily connected to the hydraulic model such that the simulated demands are implemented directly. To bridge this gap, the model is first run in Matlab and the generated demand patterns are saved to a separate file. By loading these demand patterns from this file into Python, they are implemented into the hydraulic model.

B. Case study area: Duindorp

This chapter describes the case study area Duindorp and the corresponding hydraulic model that is used in this study. The original hydraulic model and some minor updates that are conducted are explained in the first section. The measurement devices and the available sensor data are explained in the second section. A detailed analysis of the available sensor data is described in Appendix C, after which the hydraulic model is calibrated in Appendix D.

Duindorp is an urban domestic area located in the city district Scheveningen, part of the city Den Haag, situated in the province of Zuid-Holland in the Netherlands. It comprises of 91 hectares ($0.91 km^2$), is mainly residence area and mostly paved. It can be seen as a coastal village since it directly borders the dunes and the sea. Pictures are shown in Appendix F. The DMA Duindorp is under surveillance of the water utility company Dunea, and it covers solely the area of Duindorp. Hence, statistics of Duindorp are directly applicable to the DMA Duindorp.

The following statistics of Duindorp are publicly available and retrieved from CBS 2019, the date at which the statics are fixed is October 23, 2019. There are 5875 registered citizens in Duindorp, of which 19% is younger than the age of 15, 9% between age 15-24, 57% between age 25-64, 15% of age 65+. There are 2825 households present in Duindorp, of which 1195 one-person households (42%), 625 households without kids (22%) and 1015 households with kids (36%). The average amount of people per households is 2.08. The amount of households in Duindorp is verified by summing all the unique addresses in the billing information retrieved from Dunea.

B.1 Hydraulic model DMA Duindorp

The configuration of the pipe network, including structural and geometrical data of the DMA Duindorp is available as a hydraulic model in EPANET. This model is retrieved from Dunea and was last updated in 2016. It comprises the network including the different pipe diameters, pipe lengths and deduced Darcy-Weisbach (DW) roughness coefficients. A visualisation of the network can be seen in Figure B.1, in which the pipe diameters are shown in different colors, the small black dots representing connections of the different mains and the enumerated pressure sensors are illustrated as white dots.

Because the model is relatively old, some figures are retrieved from the water utility DUNEA in the year 2020 concerning the last-updated diameters and pipe materials that are present in the network. The two illustrations that were retrieved are shown in Figure B.2 and Figure B.3. They show some minor updates concerning the pipes (pipe diameters, pipe materials and thus roughness coefficients) compared with the old model shown in Figure B.1. This is simply due to the fact that over the years some pipes were replaced. Hence, the hydraulic model is modified to incorporate these changes. This included some adaptions related to some pipe diameters and Darcy-Weisbach (DW) pipe roughness coefficients (according to its pipe material).

All the different materials of the pipes that are present in the network, visualized in Figure B.2, consist of PVC(A), Cast Iron, Asbestos Cement (H)PE, (Ductile) Cast Iron or Copper. The total pipe-length of the network is approximately 13.9 km of which 64% is PVC or PE. They are incorporated into the EPANET model in which the Darcy-Weisbach

coefficients are modified accordingly. An analysis of the network regarding the diameters and the DW coefficients after the incorporated changes is shown in Table B.1.
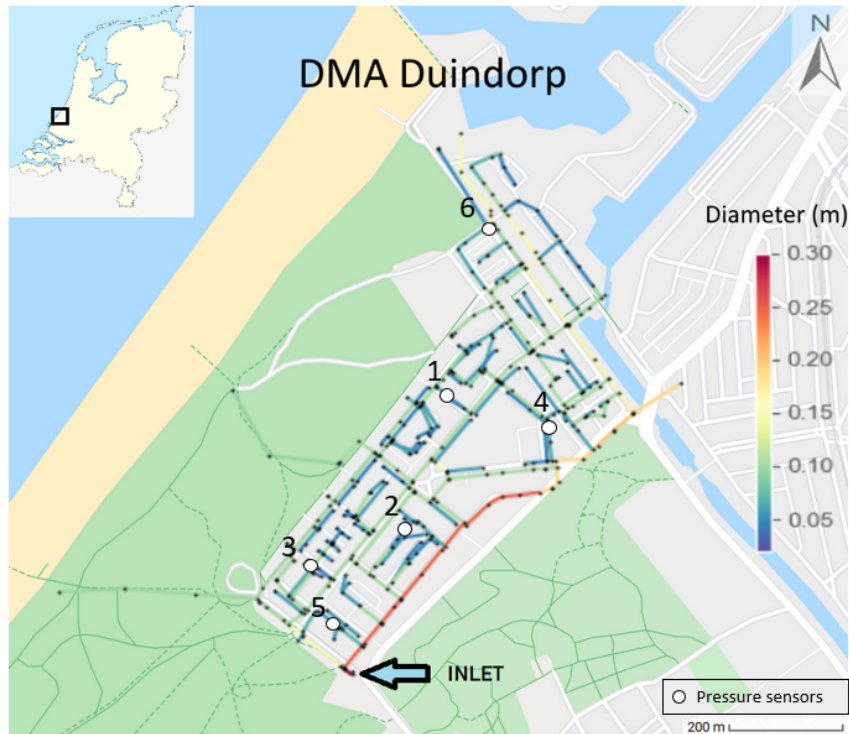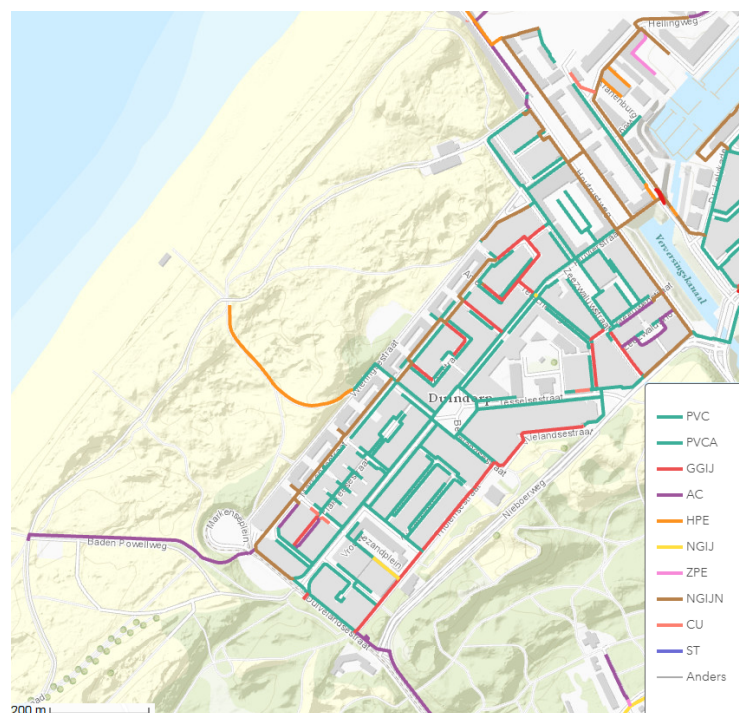

Figure B.1: Network DMA Duindorp

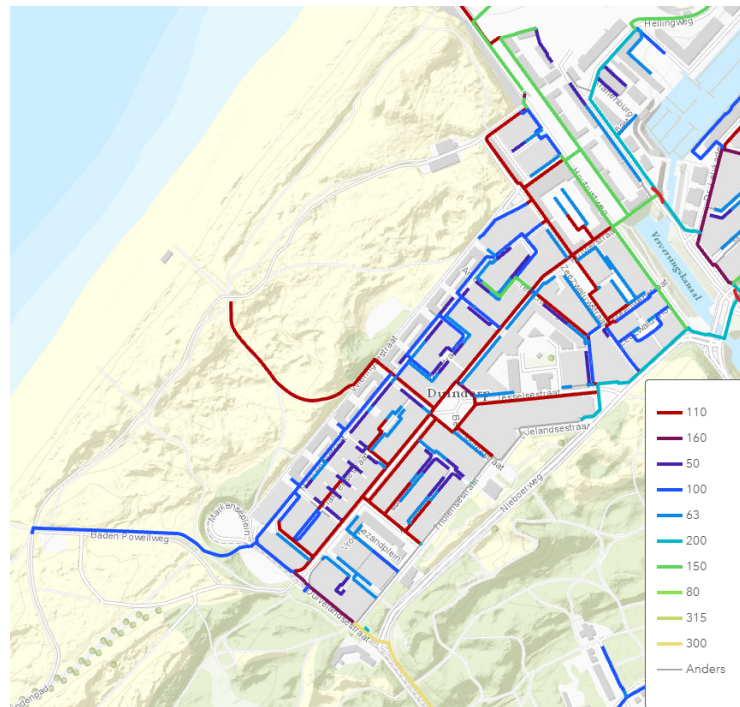Figure B.2: Updated pipe materials in the network

Figure B.3: Updated pipe diameter sizes in the network

Table B.1: Pipe network information

DMA Duindorp			
D-W coeff. (mm)	Pipes	Unique diameter groups	Diameter range (mm)
0.05	279	13	[46,200]
0.1	3	3	[20, 49]
0.2	95	4	[100, 250]
1.0	2	1	[96]
2.0	70	5	[52, 250]

In the original hydraulic model, the DW headloss formula is used. However, the WNTR-Simulator can only coop with the Hazen-Williams (HW) headloss formula from EPANET (Rossman et al. 2000) if pressure-dependent demand simulations are performed. And since this study will focus on performing such simulations, the headloss formula and the corresponding roughness coefficients need to be converted from DW to HW. The HW headloss formula is defined in Section 1.3.3 (Equation 1.1).

The WNTR-Simulator solves for pressures and flows throughout the network as a set of linear equations. The flow rate in a pipe is positive if the water is flowing from the starting node to the ending node and negative the other way around. However, if the flow through a pipe is negative, Equation 1.1 is not valid. Hence the WNTR-Simulator reformulates the equation so that it can be used for flow in either direction:

$$h_L = \begin{cases} -10.667C^{-1.852}d^{-4.871}L|q|^{1.852}, & q < 0 \\ 10.667C^{-1.852}d^{-4.871}L|q|^{1.852}, & q \geq 0 \end{cases} \tag{B.1}$$

Changing the headloss formula in the hydraulic model is easily done. However, the corresponding pipe roughness coefficients do not automatically change because they are

inherently different depending on which headloss formula is used. Hence the original roughness coefficients used in the DW equation need to be converted somehow to roughness coeffcients that can be used in the HW equation. Niazkar et al. 2017 describe a relation between the two coefficients that is used in this study:

$$C_{HW} = -348.15C_{DW}^6 + 1436.1C_{DW}^5 - 2132C_{DW}^4 + 1315.9C_{DW}^3$$
$$- 224C_{DW}^2 - 85.538C_{DW} + 149.32 \tag{B.2}$$

where C_{HW} and C_{DW} are the Hazen-Williams and Darcy-Weisbach roughness coefficients.

However, this relation is only valid for $0.0015mm < C_{DW} < 1.5200mm$, hence it cannot be applied to the group of the highest DW value (2 millimeters) shown in Table B.1. A HW coefficient of 110 is assumed for this group since it solely consists of cast-iron pipes and the pipe age of this group is estimated to be 20 years or older (Liou 1998). The results of the roughness coefficient conversion for the different DW values in the network are shown in the table below (Table B.2):

Table B.2: Pipe roughness coefficient conversions

Roughness coefficient conversion	
DW coeff. (mm)	HW coeff. (-)
0.05	144.6
0.1	139.6
0.2	130.8
1.0	111.6
2.0	110

Other information that is implemented in the hydraulic model are the base demands. The nodal base demand is retrieved from the yearly billing information per household. It is assumed that the billing information is from the years 2015-2016, since the model is last updated in 2016. With the billing information, the amount of water consumption per household for one year is known. Hence by clustering the households to their nearest node, a yearly water consumption per node is calculated. This yearly nodal water consumption can be scaled back to average day, hour or even second consumption. This average nodal consumption per time-unit is known as the base demand, only the units have to be set.

Like the rest of the flow units in this study, the base demand units are fixed at cubic meters per hour. Hence, the nodal base demand is given in units of m^3/h. To account for the variability of consumption throughout the day, it is multiplied with a certain daily pattern. This daily consumption pattern is determined from the average daily inflow, discussed in subsection D.1.1.

B.2 Measurement devices and available data

Various measurement devices are installed in DMA Duindorp by the responsible water utility company Dunea, see Figure B.4. There are six different pressure sensors present in the DMA, shown as red dots with their names (or streets) on the map. Each sensor is numbered for convenience such that they can be easily referred to later in this study. A pump is located at the inlet of the DMA, hence in this study the inlet will be referred to as the pump. Its location is illustrated as a yellow triangle on the map. Pictures of the pump can be seen in Appendix F. The discharge and the pressure are logged at the pump.

The log frequency and the amount of data present is not the same for each sensor. The frequencies and time-frames of all available measurement devices are shown in Table B.3.

The available data from the pressure sensors are in units meter head. A distinction is made between three types of data: the discharge data at the pump (Q-data), the pressure data at the pump (PH-data), and the pressure data from the six different pressure sensors (P-data). The time period column in this table does not necessarily mean that there is a continuous amount of data present in that period, there can still be small gaps in which the data is missing.

Figure B.4: Network with sensor locations

Table B.3: Available measurement data

Name	Sensor	Data	Freq. (min)	Timeperiod of data
Pump	Pump	Q (m^3/s)	1	[2018-10-12, 2019-07-16]
Pump	Pump	P (mHead)	5	[2019-03-09, 2019-07-16]
Schiermonninkoogstr.	#1	P (mHead)	2	[2018-11-06, 2019-03-11]
Bruinbankstr.	#2	P (mHead)	1	[2018-11-06, 2019-07-15]
Walchersestr.	#3	P (mHead)	5	[2018-11-06, 2019-07-15]
Terschellingsestr.	#4	P (mHead)	2	[2018-11-06, 2019-07-15]
Doggersbankstr.	#5	P (mHead)	1	[2018-11-06, 2019-07-15]
Zeezwaluwstr.	#6	P (mHead)	5	[2018-11-06, 2019-07-15]

The measurements of the pressure sensors are snapshots, hence a frequency resolution of 2 minutes means that one snapshot measurement is taken per 2 minutes. All the available data will be re-sampled to a 5 minute resolution, the lowest possible common frequency. This means that the sensors with higher resolution (sensor 2 and 5) will contain less noise than the sensors with lower resolution (sensor 3 and 6) because some sensors use only one snapshot measurement and others take the mean of multiple snapshot measurements. This will become apparent in Appendix C.

The specifications of the different pressure sensors in the DMA are elucidated in Appendix E. The six installed pressure sensors throughout the area are LACROIX Sofrel CNPR sensors (see Figure E.1). They have a range of 0-16 bar and an accuracy of 0.35% FSO (full scale output). Hence, the accuracy is $16 \cdot 10 \cdot 0.35/100 = 0.56$ meter head. At the pump, a VEGA Vegabar-52 pressure sensor is present (see Figure E.2). This model has an range of -1 to 72 bar, with a maximum deviation of 0.075%. Hence the accuracy of this sensor is $0.075/100 \cdot 73 \cdot 10 = 0.55$ meter head. Therefore, all the pressure sensors have a rounded accuracy of 0.6m head.

The rounded accuracy of the inflow meter is known to be 0.48 m^3/h. No further specifications are available about the pump. A picture of the pump is shown in Appendix F.

As table B.3 shows, there is no long time period available in which data is present of all measurement devices, in which the main issue is the minor overlap of the pressure data from the pump and from sensor 1 of only two days. The period [2018-11-21 : 2019-02-20] is chosen to be analyzed. Choosing a longer period would mean including incoherent data which are probably the result of different settings of sensors. Furthermore, the data is observed to be most stable and the seasonal influence minimal in this time-period. However, there is no data present of the pump pressure in the chosen period. Hence for the pressure of the pump, the data of the later period [2019-03-09 : 2019-04-16] is analyzed, in which later in this study the created average week and weekend daily patterns in this period is implicitly assumed to be similar to the period [2018-11-21 : 2019-02-20]. The data analysis is conducted and described in Appendix C.

C. Timeseries analysis

A timeseries is a series of data points which are indexed in time order. Timeseries analysis comprises methods that analyse timeseries data to extract meaningful statistics. This Appendix comprises of an extensive timeseries analysis of the sensor data of the case study Duindorp. The period of analysis is defined to be in the period [2018-11-21 : 2019-04-16], in which a distinction is made between [2018-11-21 : 2019-02-20] and [2019-03-09 : 2019-04-16] depending on the sensor data as concluded in Appendix B. In the first two sections, two methods that are applied on the data are explained. In the third and fourth section these methods are applied and a further data analysis is conducted on the sensor data in which characteristic week and weekend patterns are created for all sensors.

In this study, solely the characteristic working-day (excluding the weekend) patterns of the sensors will be used to calibrate the hydraulic model. Therefore, the characteristic weekend pattern will be noted in this chapter, but is further neglected in the rest of this study. The focus is set on working-days because the stochastic demand simulator is able to produce more accurate working-day water demands in comparison with predicting weekend consumption.

C.1 Interquartile range (IQR) method

The Inter Quartile Range (IQR) method, also known as the Tukey fence test, is a measure of statistical dispersion. This method is based on dividing a data set into different quartiles and can be used to identify outliers. Suppose a one-dimensional data set q, the Inter Quartile Range (IQR) of this data set is then calculated as follows:

$$\Delta q = q_3 - q_1 \tag{C.1}$$

in which q_i is the i-th quartile of the dataset. Once the quartile values and IQR are calculated, a data range is set up as follows:

$$[q_1 - k\Delta q, q_3 + k\Delta q] \tag{C.2}$$

If a datapoint lies outside of this range given by Equation C.2, it is defined as an outlier. The boundaries for normal outliers is given by $k = 1.5$, and for far outliers $k = 3.0$. Outliers can have a large impact on the dataset's average or variability, hence it is sometimes wanted to exclude them from the data. If outliers are present and excluded, the quartiles and the interquartile range of the updated data set change as well, hence new outliers can appear which were previously not identified as such. Hence, the IQR test can be run iteratively until no more outliers are found.

The IQR method identifies outliers which can then easily be filtered out, if wanted. This method will be used in this study for determining unusual demand during Minimum Night Flow (MNF) hours, further discussed in section C.3.

C.2 Decomposition method (STL)

Timeseries data can exhibit multiple patterns at the same time, hence it can be useful to deconstruct the time series into several components, each representing an underlying pattern

category. The decomposition that will be used in this study is based on rate of change, in which three components are distinguished reflecting different rates of changes. The three components are defined as follows: the trend-cycle component reflecting long-term progression of a series, the seasonal component reflecting a pattern over a known and fixed period (e.g. a day, week, month or year) and the remainder component (or noise) describing random and irregular behaviour.

These components can either be combined additive or multiplicative, in which the different components are simply summed or multiplied to construct the time series. The multiplicative decomposition is appropriate if the variation in the seasonal pattern or the variation around the trend-cycle appears to be proportional to the level of the time series (Hyndman and Athanasopoulos 2018). If this is not the case, the additive model is most appropriate. Since it appeared not to be the case in this study, the additive model is used in this study, hence, the data is assumed to be an aggregate of the three components, shown in Equation C.3:

$$y_t = S_t + T_t + R_t \qquad\qquad\qquad (C.3)$$

in which y_t is the data, S_t is the seasonal component, T_t is the trend-cycle component and R_t is the remainder, all at time t.

There are various Python modules that can decompose time series automatically, though caution and healthy skepticism is needed when using the results from automated decomposition methods. In this study, the Seasonal and Trend decomposition using LOESS (STL), developed by Cleveland et al. 1990 will be used, in which LOESS is a method for estimating non-linear relationships and stands for 'locally estimated scatterplot smoothing'. The STL is an additive model and considered to be versatile and robust for the decomposition of time series (Cleveland et al. 1990).

STL has two main advantages over other decomposition methods, which is that it will handle any type of seasonality (e.g. not only monthly) and it can be robust to outliers if the robust decomposition setting is used. This robust setting allows the model to tolerate larger errors that are visible in the residuals plot. The main parameter that should be chosen when applying STL is the period window of the seasonal cycle (or a certain frequency could be given). The period window of the seasonal cycle is the length of the consecutive observations used to estimate the seasonal cycle. A seasonal smoother and a trend smoother can be given optionally.

STLs decomposition method is chosen in this study to decompose the trend, seasonality and residuals from a time series that includes some weekly pattern and some daily pattern, applied and discussed in section C.4.

C.3 Minimum night flow (MNF) analysis

The Minimum Night Flow (MNF) analysis is performed by calculating the average nightflow between 3:15AM - 4:30AM. This specific time-window is chosen because the discharge is observed to be generally lowest for every day in the week within timeframe (week and weekend nights). To determine which days show an unusual demand during Minimum Night Flow (MNF) hours, the IQR method (elucidated in section C.1) is applied iteratively.

Plotting the results for the chosen period ['2018-11-21','2019-02-20'] reveals that there is one far outlier on Tuesday the 1st of January 2019 and one normal outlier on Friday the 15th of February 2019, see Figure C.1. Outliers can significantly influence the mean and variability of the average pattern. If one would create an average Tuesday pattern from this dataset, including new year's day would influence the average a lot. Since new year's day is not an average Tuesday, it should be excluded from the dataset. This is done for all the
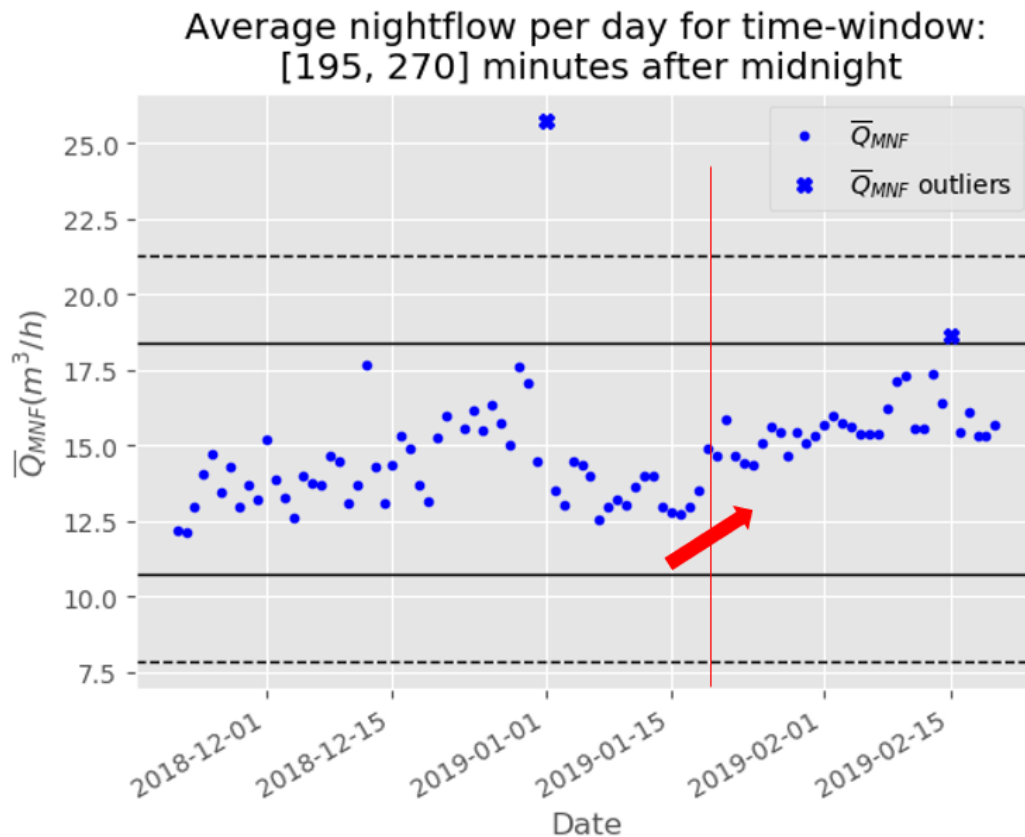
Figure C.1: MNF analysis

outliers. Hence, the abnormal days associated to these outliers are excluded to create a more representative characteristic daily pattern, discussed further in section C.4.

Furthermore, it can be observed from Figure C.1 that the average MNF seems to increase from the 19th of January onwards, with a change in discharge of about $2.5 m^3/h$. The change is highlighted in the figure with a vertical red line and an arrow. This could be the result of a change in the system settings of the pump or the result of the appearance of a leak.

C.4 Characteristic day patterns

Water demand changes every day. However, patterns can be clearly distinguished when analysing the sensor data. This is due to the fact that human water-use behaviour is repetitive and in essence based on habits. They go to work and go to sleep usually around the same times they always do, depending on the day of the week. A general distinction is made between working- and weekend-days, in which the data is defined to be part of the weekend, starting from Friday 17:00 until Sunday 17:00, and otherwise part of the working-week. The reason for this choice becomes apparent in the analysis of the inflow data. By making this classification, grouping all the data in groups of working- and weekend-days, excluding the obvious abnormal days, characteristic working-day and weekend patterns are constructed by taking the average.

These two characteristic patterns are constructed for the different sensor data available: the inflow data (Q-data), the pressure sensor data (P-data) and the pump pressure data (PH-data). As stated before, the period of analysis is set to be [2018-11-21 : 2019-02-20], except for the pump pressure data it is [2019-03-09 : 2019-04-16]. The holidays and other abnormal days (e.g. drainage testing days or 'spuidagen' by the water utility) are excluded.

The two constructed characteristic patterns reveal what would be observed for an average working-week day or weekend day for that sensor. However, this does not include the variance for the characteristic patterns.

To include the variance for the characteristic patterns, the STL decomposition method is used to retrieve the residuals from the raw data. By using this method, the trend, seasonality and residuals are decomposed from a time series that includes some weekly pattern and some daily pattern. Using a period window of an amount of observations in one day (making the seasonality repetitive over one day), would yield in a noisy trend pattern that would account for the weekly pattern. Taking a period window of a week (making the seasonality repetitive over one week) would yield in larger seasonality but a much smoother trend pattern. This is illustrated for the Q-data (in m^3/s) in Figure C.2.
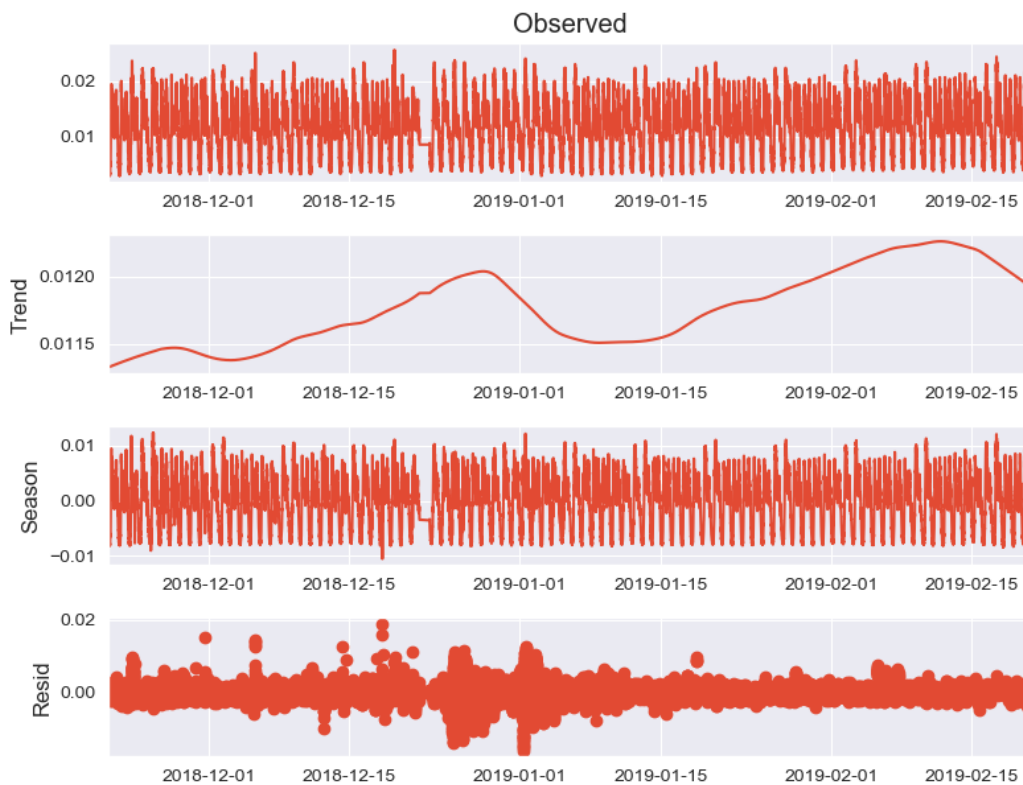
Figure C.2: Decomposition method STL of the raw inflow data

By applying STL on the inflow data, the trend and seasonality information extracted from the series seem reasonable. The residuals are also interesting, showing periods of high variability in 2018 compared to 2019. The residuals are grouped in working-week and weekend groups, the abnormal days are excluded and the average is taken per group to retrieve the variance of the characteristic curves. The same process is applied in determining the variance of the characteristic curves of the other types of data (P-data, PH-data).

C.4.1 Observed inflow pattern

The average observed inflow can be plotted per day of the week, and is shown in Figure C.3. Two trajectories can be easily distinguished from the figure, the working-week days and the weekend days. Because of this similarity, it is chosen to group the data into two groups: the working-week day group and the weekend day group. However, it can be seen that the Fridays after 17:00 has a higher similarity with the weekend days (which makes sense since people see it as the beginning of the weekend). The same holds for Sundays after 17:00 which looks more similar to an average working-week day, people are perhaps preparing for another week of work and go to sleep earlier. It is therefore chosen to define the working-week group from Sunday 17:00 until Friday 17:00, and the weekend group from Friday 17:00 until Sunday 17:00.

Taking the average of these grouped days shown in Figure C.3 yields in a characteristic working-week and weekend pattern. However, it can be seen that an average Tuesday is slightly different from an average Friday, and the same holds for Saturdays and Sundays. Because there is a structural difference in average between certain days in the same group, simply taking the variance of all these days would yield in a higher variance than what is expected for a single day. To exclude this structural difference, the 'seasonality' is excluded by applying the STL decomposition method. This results in the average and variance of the characteristic week and weekend pattern Figure C.4.

In this study, the average weekend pattern is not part of the analysis and is neglected in the rest of this study. The focus is set on working-days because the stochastic demand simulator is able to produce accurate working-day water demands, and is less accurate in predicting weekend consumption. The focus is therefore set on the creation of characteristic working-week day patterns for all sensors. The created characteristic working-day inflow pattern shown in Figure C.4, will be used and compared with the summed stochastic demand of all the households in the area, and will also be used in Appendix D for the calibration of the hydraulic model on background leaks.
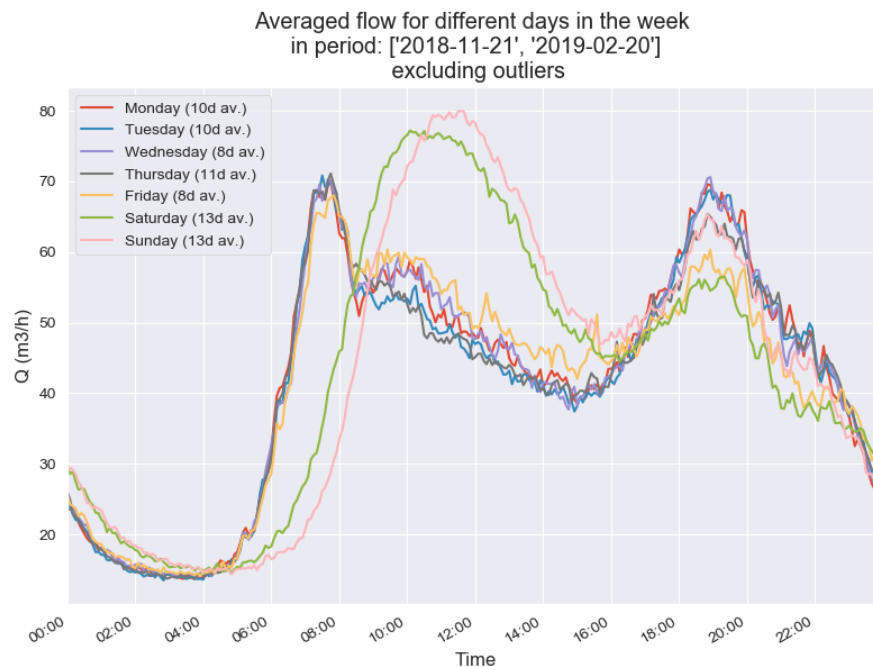

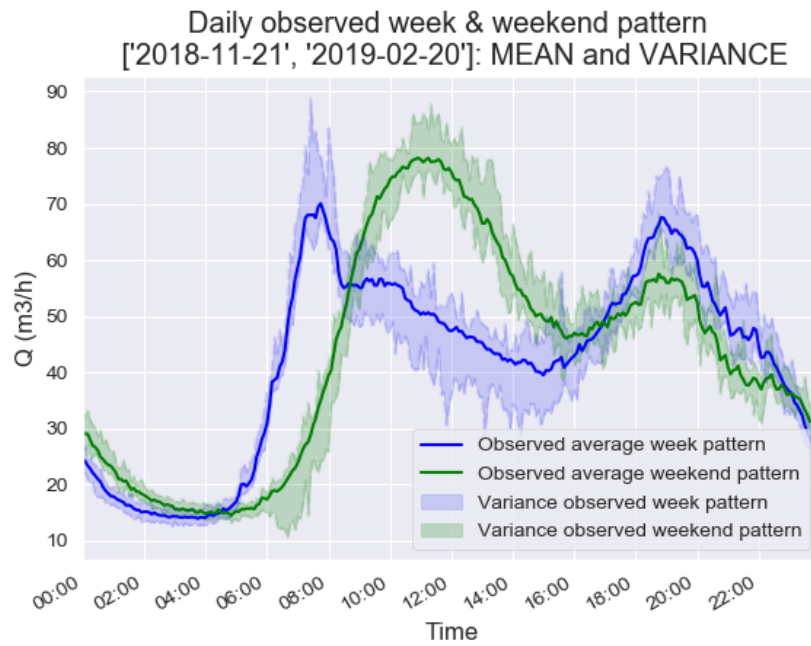Figure C.3: Average inflow patterns per day of the week

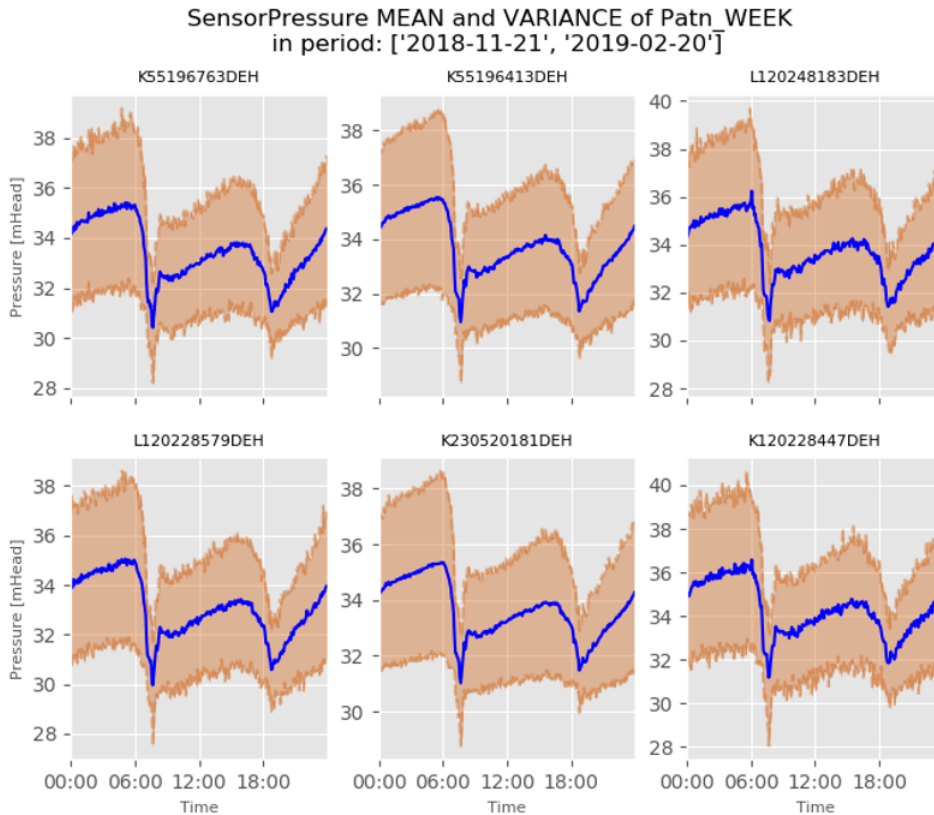Figure C.4: Characteristic inflow curve for working-week/weekend day

Figure C.5: Characteristic pressure working-day curves for sensors 1,2,3 (top) and 4,5,6 (bottom) for time window [2019-01-19 : 2019-02-20] resulting in high variances.

C.4.2 Observed pressure patterns

When performing the same process for the observed pressures, unrealistic high values for the variances of up to 6 meters head at all the pressure sensors are observed, shown in Figure C.5, in which pressure sensors 1,2,3 are shown in the top and 4,5,6 in the bottom. Only the characteristic working-week day patterns are illustrated. After analysis of individual sensors by plotting all the daily measured data in one plot for every sensor (as is done for sensor 2 in Figure C.6), different clusters of pressure patterns are observed which yield in the very high variances observed in Figure C.5. This is probably due to different settings of the system, since it observed at all the sensors. Therefore, a clustering is chosen based on time period only. Hence, a smaller interval [2019-01-19 : 2019-02-20] for the pressure sensors is chosen to be analysed, which is the top group of daily pressure patterns shown in Figure C.6. This is done to only account for one group of pressure patterns (hence one set of settings). This yields in much lower and more realistic values for the variances of the pressure sensors, as is shown in Figure C.7.

Figure C.6: All daily observed pressures of sensor 2 in period [2018-11-21 : 2019-02-20].

These characteristic (working-day) observed pressure patterns per sensor will be used in Appendix D for the calibration of the hydraulic model on roughness coefficients. A curious observation following from Figure C.7 is that all the pressures at the sensors seem to generally increase throughout the night. One would expect a more constant pressure in the network during the night due to minimal consumption. The water utility was not entirely sure what caused this effect, but it is expected that the pumping control of the booster was incorrectly set which caused the pressures to systematically increase throughout the night.

Another observation that can be made from Figure C.7 is that the observed noise in the average and variance of the pressure sensor data is generally larger for the sensors 1,3,4 and 6. This corresponds with what is expected from Table B.3, which shows that the frequency of (snapshot-)measurements is higher for sensor 2 and 5, hence the mean is taken over multiple data points, yielding in less noise.
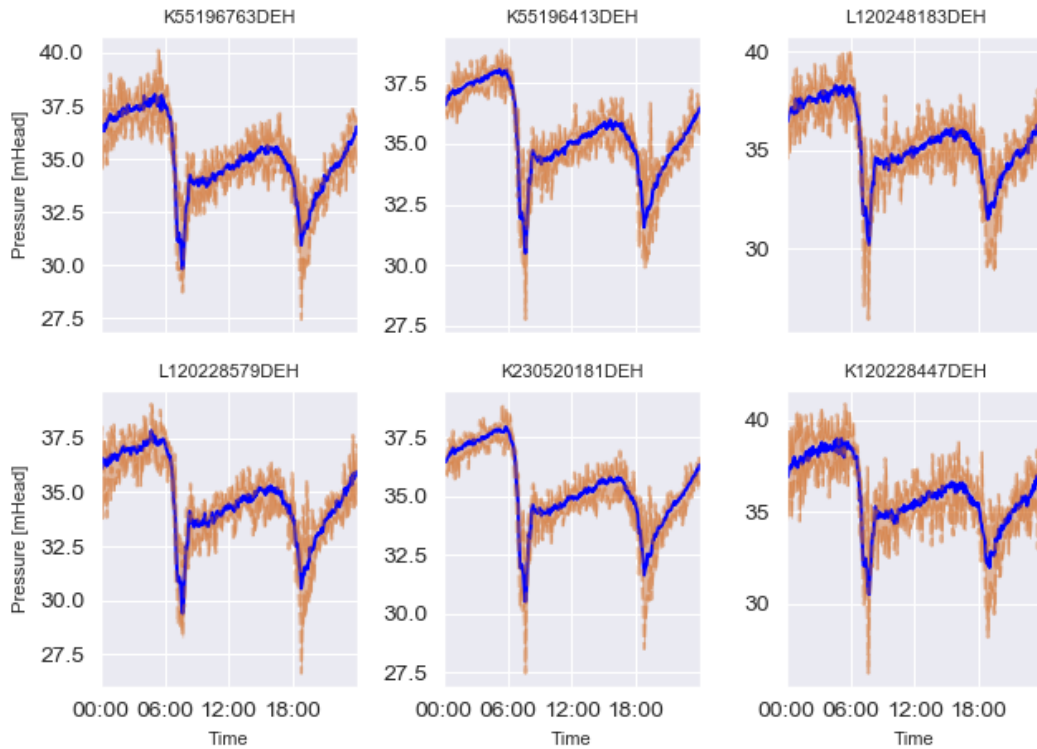
Figure C.7: Characteristic pressure working-day curves for sensors 1,2,3 (top) and 4,5,6 (bottom) for time window [2019-01-19 : 2019-02-20].

C.4.3   Pump pressure data patterns

The same process is also done for the pump pressure data, however for a different period since no pump pressure data is available for the previously used period. The time window for the pump pressure that is used is [2019-03-09 : 2019-04-16]. Plotting the average pump head patterns per day of the week results in Figure C.8. It can be seen again that a general distinction can be made between a working-day and weekend-day. However, the weekend days seem to show a higher discrepancy between themselves compared to the working days. This yields in a higher variance of the average weekend day pattern, but as stated before, only the characteristic working-day patterns are used in this study.

Again, the apparent abnormal days are excluded from the data, the STL decomposition method is performed and the data is grouped into working-week and weekend days. The resulting characteristic pump head curve for working-week and weekend days is shown in Figure C.9. The characteristic pump head curve will be implemented into the hydraulic model to account for changes in pressure unrelated to the area.

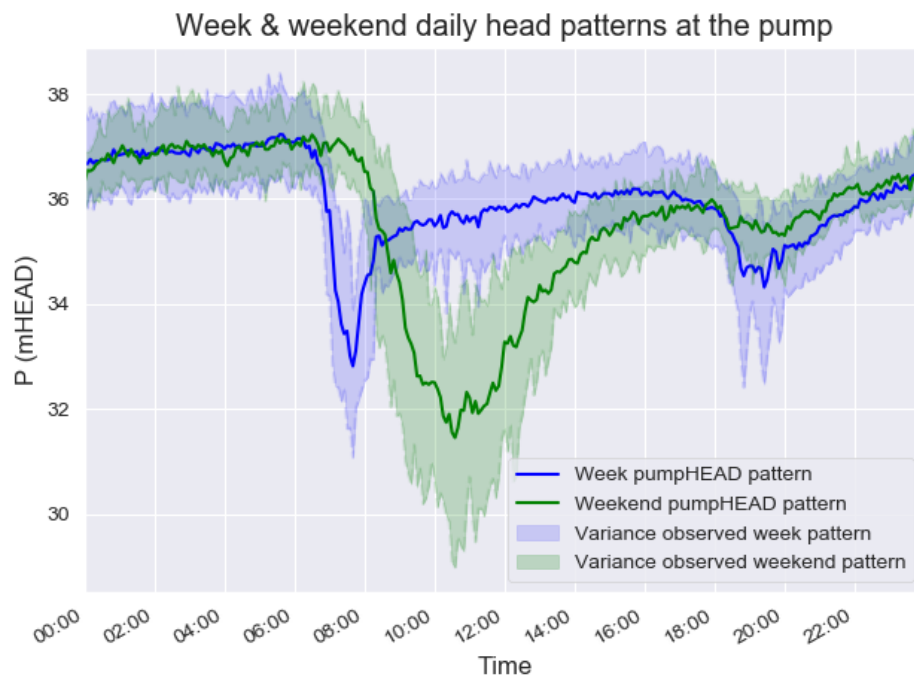Figure C.8: Average pump head patterns per day of the week

Figure C.9: Characteristic pump head working-day and weekend-day curves

D. Hydraulic model calibration

One of the essentials in performing model-based leak detection and localization is a calibrated hydraulic model. It needs to be calibrated such that the model can reliably simulate the network. As stated in Section 1.3.3, it is emphasized that the process of calibration is neither unique nor straight-forward and its success is partly based on the modelers experience and intuition (Ostfeld et al. 2012).

Flow and pressure measurements in the network are needed for the calibration. During the calibration of the model, observed and simulated flows as well as observed and simulated pressures are compared. An optimization method minimizes the difference between the two by adjusting the model parameters (Mameren and Clemens 1997). In this study, the calibration consists of adjusting the emitters (representing background leaks) and the Hazen-Williams roughness coefficients as model parameters, in which differential evolution is used as optimization method.

The calibration is performed in two consecutive steps. The background leaks are added first such that the modelled inflow pattern is calibrated to the observed inflow. Afterwards, the pipe roughness coefficients in the network are modified such that the modelled pressure patterns at the sensors are calibrated to the observed pressure patterns, as derived from Appendix C.4.2.

D.1 Calibration background leaks

The first step in the calibration of the hydraulic model is adding background leaks to the model. Before this can be done, the actual consumption of the customers in the area needs to be derived from the observed inflow into the network. Furthermore, the nodal demands (or consumption) have to be implemented accordingly. This is done in the first subsection. In the second subsection, the difference in inflow and total consumption is assumed to be solely the result of background leaks. Background leaks are then homogeneously allocated to the hydraulic model in the form of nodal emitters, and their discharge coefficients are calibrated.

D.1.1 Daily consumption pattern

The inflow to the DMA is measured, so it is known how much water the area uses throughout the day. However, this usage consists of consumption and potential background leaks, in which consumption is defined here as water that reaches the customers. To estimate the consumption in the area, it is assumed that the stochastic demand simulator SIMDEUM used in this study is able to accurately predict the MNF consumption of the area (by using the statistics of the case study area Duindorp). The consumption throughout the day for the entire area is then estimated with the following equation:

$$Q_{csmp}(t) = Q_{inflow}(t) - \overline{Q}_{MNF} + \overline{Q}_{SIMD_{NC}} \qquad \text{(D.1)}$$

where $Q_{csmp}(t)$ is the consumption of the area throughout the day, $Q_{inflow}(t)$ is the observed inflow throughout the day, $\overline{Q}_{MNF}$ is the average minimum night flow of the area determined in Appendix C.3 and $\overline{Q}_{SIMD_{NC}}$ is the average night consumption (excluding the background leaks) determined from multiple runs of SIMDEUM with the known details of this area (amount of households, inhabitants statistics etc.).

Hence, the daily consumption pattern of the entire network can be estimated. By using the observed average working-day and weekend-day inflow patterns as derived in Appendix C.4.1 in Equation D.1, average working-day and weekend-day consumption patterns are set up. The result is illustrated in Figure D.1.
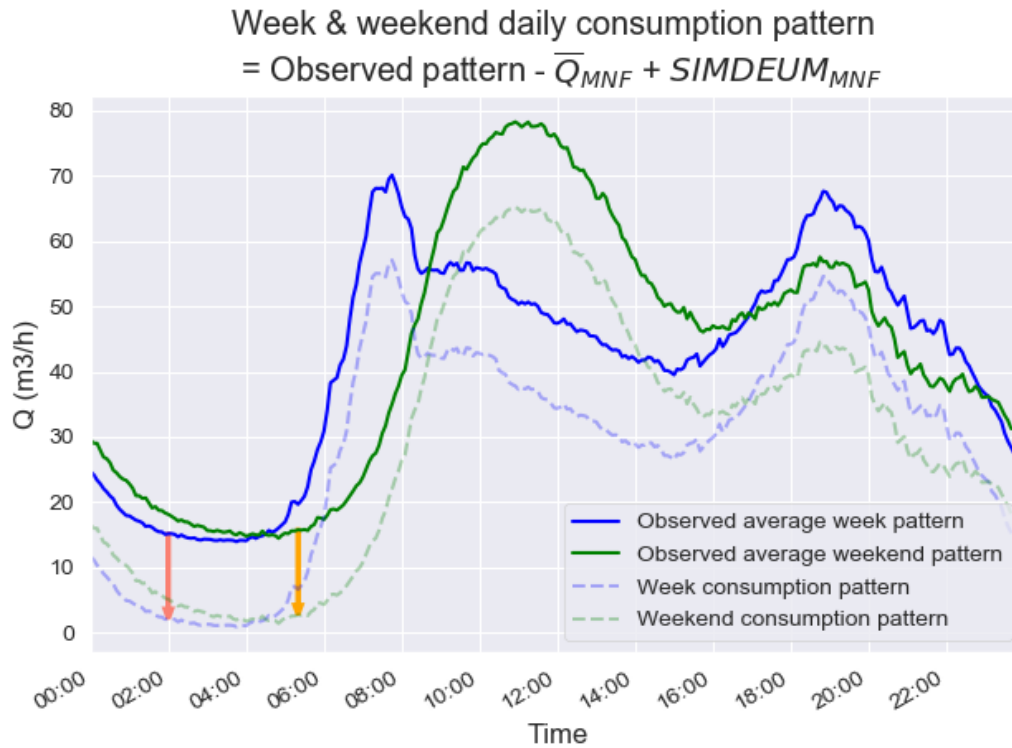

Figure D.1: Deriving working-day and weekend-day consumption patterns

The focus in this study is set on the average working-day, hence the working-day consumption pattern is used and implemented in the calculation of the nodal demand. The nodal base demands are already implemented into the model, as discussed in Appendix B.1. To make sure that the summed nodal consumption in the area is equivalent to the total consumption, the nodal consumption pattern is defined as follows:

$$P_{n_i}(t) \equiv \frac{B_{n_i}}{\sum\limits_{i} B_{n_i}} \cdot Q_{csmp}(t) \tag{D.2}$$

where B_{n_i} is the base demand factor for node i, $P_{n_i}(t)$ is the consumption pattern throughout the day for node i and $Q_{csmp}(t)$ is the total consumption throughout the day for the entire area.

D.1.2 Implementation emitters

After the implementation of the nodal demands, the mismatch between the observed inflow and the total consumption (shown in Figure D.1) is compensated by adding background leaks to the hydraulic model. Background leaks are added to the model in the form of adding emitters. Because pressure dependent demand simulations are performed in this study (elucidated in Section 2.2.2), the discharge of a leak depends on the pressure and is described

with Equation (2.4), noted here again:

$$d_{leak} = C_d \cdot A \cdot p^\alpha \sqrt{\frac{2}{\rho}} \tag{D.3}$$

where d_{leak} (m^3/s) is the leak demand, C_d is the unitless discharge coefficient, A (m^2) is the area of the hole of the leak, p (Pa) is the gauge pressure inside the pipe, α is the emitter exponent and ρ is the density of the fluid.

In this study some of these parameters of Equation D.3 are set. The default emitter exponent is $\alpha = 0.5$. This default value cannot be modified when using the WNTR-Simulator to run pressure driven demand simulations, hence it is fixed. The density of water is fixed at $\rho = 1000$ kg/m^3.

The background leaks are modelled such that every node has a certain background leak described by Equation D.3. However, since no information is available about the distribution of potential background leaks in the case study area, it is safest to assume that the background leaks are homogeneously distributed over the network; every meter pipe-length has the same background leakage. Therefore, it is necessary to determine how much pipe length is connected to one node. This is calculated by running a simple script that sums up all the pipe length connected to each node and divide it by two. This will be defined as the node length l_{n_i} for node i.

To determine the total background leakage in the area, the inflow is simply subtracted with the consumption:

$$Q_{BGleaks}(t) = Q_{inflow}(t) - Q_{csmp}(t) \tag{D.4}$$

where $Q_{inflow}(t)$ is the observed inflow throughout the day, $Q_{csmp}(t)$ is the consumption of the area throughout the day, $Q_{BGleaks}(t)$ is the total background leak discharge throughout the day. This total background leak discharge is distributed over all the nodes via calibration. Hence, it is aimed to reach the following equality using optimization:

$$Q_{BGleaks}(t) = \sum_i d_{n_i}(t) \tag{D.5}$$

where $d_{n_i}(t)$ is defined to be the background leak throughout the day for node i. The background leak for node i is described as follows:

$$d_{n_i}(t) = C_{n_i} \cdot A \cdot p_{n_i}^\alpha(t) \sqrt{\frac{2}{\rho}} = \frac{l_{n_i}}{\sum_i l_{n_i}} C \cdot A \cdot p_{n_i}^\alpha(t) \sqrt{\frac{2}{\rho}} \tag{D.6}$$

in which l_{n_i} is the node length for node i and C_{n_i} is the unitless discharge coefficient for node i, in which the fraction of its length divided by the total network length is included. The variables in this equation that change throughout time are the pressure at node i throughout the day $p_{n_i}(t)$ and the nodal background leak discharge $d_{n_i}(t)$.

By solely modifying the defined general discharge coefficient C in Equation (D.6) (and set to be the same for all nodes), and keeping parameters like the hole of the leak A, the emitter exponent α and the density of the fluid ρ constant, all the nodal background leak discharges are influenced. Hence, this parameter can be optimized to retrieve the wanted total background leakage. However, C_{n_i} has to be calculated and implemented per node. The calibration can be done for a certain time window $T_W = \{t_1, t_2, ..., t_\tau\}$ in which $\tau \in \mathbb{N}$ stands for the amount of consecutive time steps. This results in the following optimization function in which the mean squared error is incorporated:

$$\min \frac{1}{|T_W|} \sum_{\forall t \in T_W} \left(Q_{BGleaks}(t) - \sum_i \left(\frac{l_{n_i}}{\sum_i l_{n_i}} C \cdot A \cdot p_{n_i}^{\alpha}(t) \sqrt{\frac{2}{\rho}} \right) \right)^2 \tag{D.7}$$

The optimization method that is used in this study to solve Equation (D.7) is differential evolution. By performing the background leak calibration during the minimum night flow, the consumption is lowest and pressures are highest, hence due to the pressure dependent background leak discharge, the background leak discharges are also highest. The MNF is determined to be between 02:30 and 04:30. The background leaks are homogeneously added to the network, and the result is shown in Figure D.2. However, as is observed from the figure, due to a change in pressure throughout the day, the total background discharge is slightly smaller in moments of low pressure (morning and evening peaks). Due to this decrease, the observed inflow pattern does not fit the summed consumption and background leaks perfectly anymore. This deficit (minor blue area in the figure) is therefore added as additional consumption to the consumption pattern at the nodes.
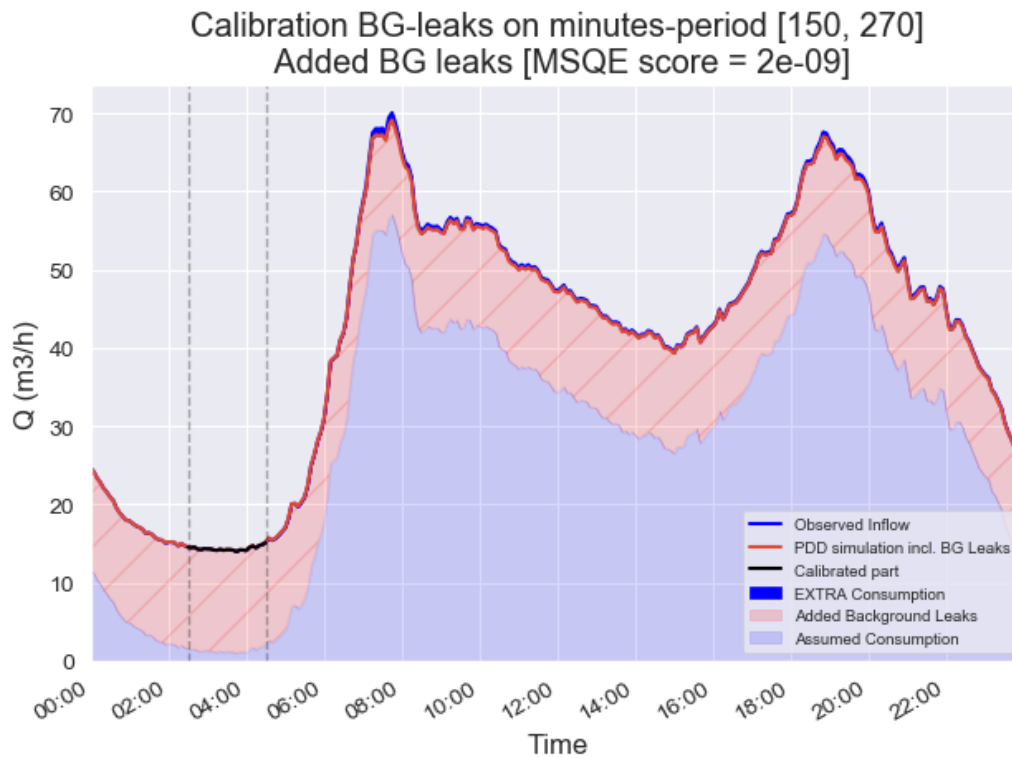
Figure D.2: Calibration of background leaks

D.2 Calibration pipe roughness coefficients

The inflow measurements are used to calibrate the background leaks, as is done in the previous calibration step. In this calibration step, pressure measurements are used to calibrate the pipe roughness coefficients in the network. Because the pressures in the network are now of importance, the pressure at the pump needs to be implemented first. If the pressure at the inflow (modeled as a reservoir) changes, the pressure in the entire system changes with it, hence influences the entire calibration. The characteristic working-day pump pressure from Appendix C.4.3 is implemented as pattern into the hydraulic model.

When the background leaks and the pump pressure pattern are implemented into the hydraulic model, the simulated pressures at the sensors can be compared with the pressure measurements. The observed (working-day) pressure patterns at the sensors are retrieved from Appendix C.4.2 and are plotted with the modeled pressures in Figure D.3. There is still a large discrepancy between the modeled and the observed values, illustrating the necessity of another calibration step to get a better fit.

Figure D.3: Observed and modelled pressures at sensors (before roughness calibration)

The elevation of the pressure sensors are unknown. To perform a reliable calibration of the pipe roughness values, it is essential to first correct the elevations of the pressure sensors. This is done in the first subsection. After the elevation correction is implemented, the roughness values are calibrated, elucidated in the second subsection.

D.2.1 Elevation pressure sensor correction

It is unknown at what elevations the pressure sensors are located, hence it is likely that this yields in a vertical mismatch (independently of time) between the simulated and observed pressures. To correct for this, the elevations are estimated by running the uncalibrated hydraulic model and looking at the minimum night consumption. During the night, flow is at its minimum and the influence of the roughness of the pipe is small. Therefore, the difference during this time in measured and simulated pressure during minimum consumption is considered to be the elevation of the pressure sensor. The minimum night flow (highest observed pressures) is considered to be between 04:00 and 06:00, as is observed from Figure D.3. Note that the curious increase in observed pressures during the night (as discussed in Appendix C.4.2) also influences the elevation correction and therefore the roughness calibration.

Since it is difficult to model elevations of pressure sensors in the hydraulic model, the calculated elevation corrections are applied to the measurements instead of the hydraulic

model. This is possible because it only contains a vertical translation independent of time. Hence, applying the correction transforms the observed pressure at the sensor into the pressure that would be measured in the corresponding pipe at that location. The result of the elevation pressure sensor correction is shown in Figure D.4.
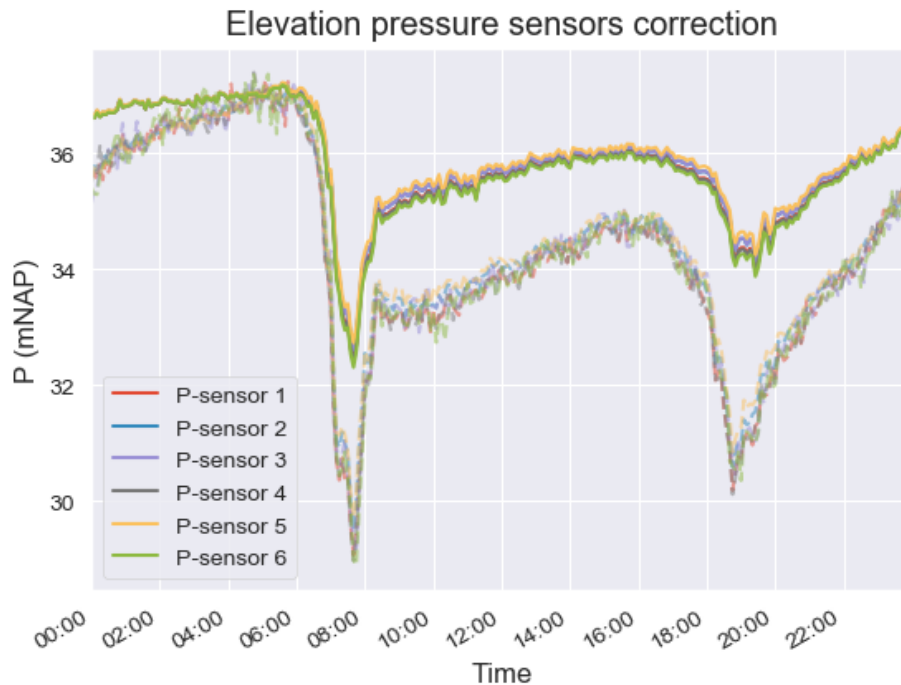

Figure D.4: Result elevation pressure sensor corrections. The calculated elevations for the six consecutive sensors are [0.78, 0.98, 1.1, 0.44, 0.79, 1.63] meter.

D.2.2 Modification pipe roughness values

After the elevation correction of the pressure sensors, the roughness values are modified. Two methods have been tried in this study. The first method proposes dividing all the pipes in a certain amount of groups, based on their Hazen-Williams (HW) roughness coefficient. If all pipes are clustered into one group, the calibration is conducted by multiplying all the roughness coefficients with the same factor. This factor is then optimized by comparing the observed pressures to the newly simulated pressures. The roughness coefficients can also be split up into more groups, hence the optimization is conducted with several factors. This generally improves the calibration results because a more detailed calibration in the network is allowed.

However, a different method yielded in far better results. This method divides the pipes into self-determined groups based on their spatial location. All the roughness coefficients in a group are then multiplied with a certain factor. Hence the factors (as many as there are groups) are optimized by comparing the observed pressures to the newly simulated pressures. Because it is observed from Figure D.4 that there exists a general mismatch in pressure sensor values and modelled values for all sensors, it is decided to give the inflow pipes into the system a specific group and let the roughness values in this group increase to unrealistic values. This was determined to be the only way to achieve acceptable calibration results with reliable roughness coefficients (except for the inflow pipes). The rest of the groups are

generally distinguished by how far they are from the pump. The groups that are created are shown with different colors in Figure D.5.
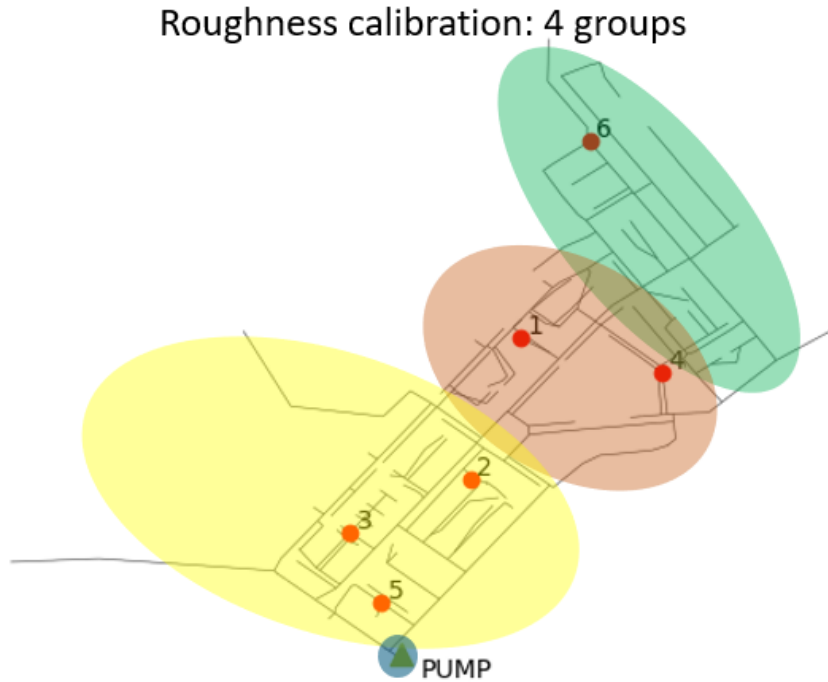

Figure D.5: Roughness calibration method, red dots are the locations of the pressure sensors.

To perform this calibration, the roughness values of the pipes are modified as discussed and the resulting pressures at the sensors are simulated and compared to the observed pressures. The mean squared error is taken between the modeled and observed pressures, hence the optimization function that is solved is as follows:

$$\min \frac{1}{|T_W|} \sum_{\forall t \in T_W} \sum_{i=1}^{6} (p_i(t) - \hat{p}_i(t))^2 \tag{D.8}$$

where T_W contains all the time steps throughout the day, $p_i(t)$ and $\hat{p}_i(t)$ are the observed and simulated pressure of sensor i at time step t. The optimization method that is used to perform the optimization is differential evolution.

The results of the calibration are shown in Figures D.6 and D.7, in which the optimized factors represent the factors for which the pipe roughness coefficients in the blue, yellow, red and green area are multiplied with. The minimized Mean Squared Error (MSE) follows from Equation D.8. This yields in reliable HW coefficients in the network of between 60 and 150, except as expected for the inflow pipes (the blue area) which have a HW coefficient value of around 9. These high values are also due to the fact that the inflow pipes have a short length, hence the roughness has to be very high to account for the dissipation of energy.
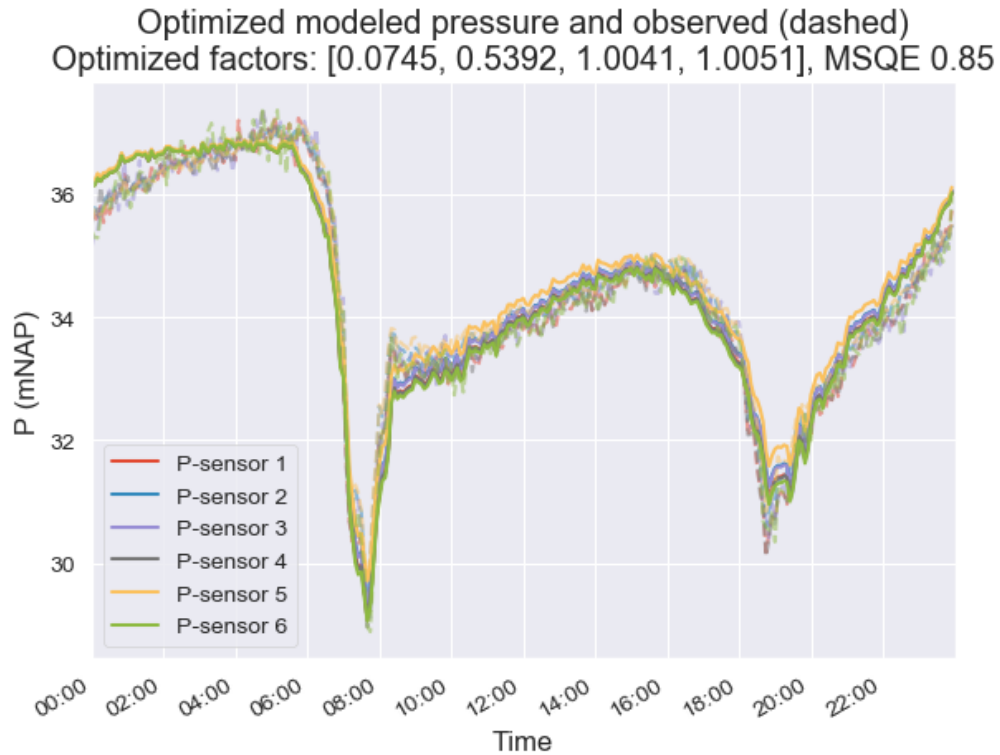
Figure D.6: Optimized simulated pressure and observed pressure
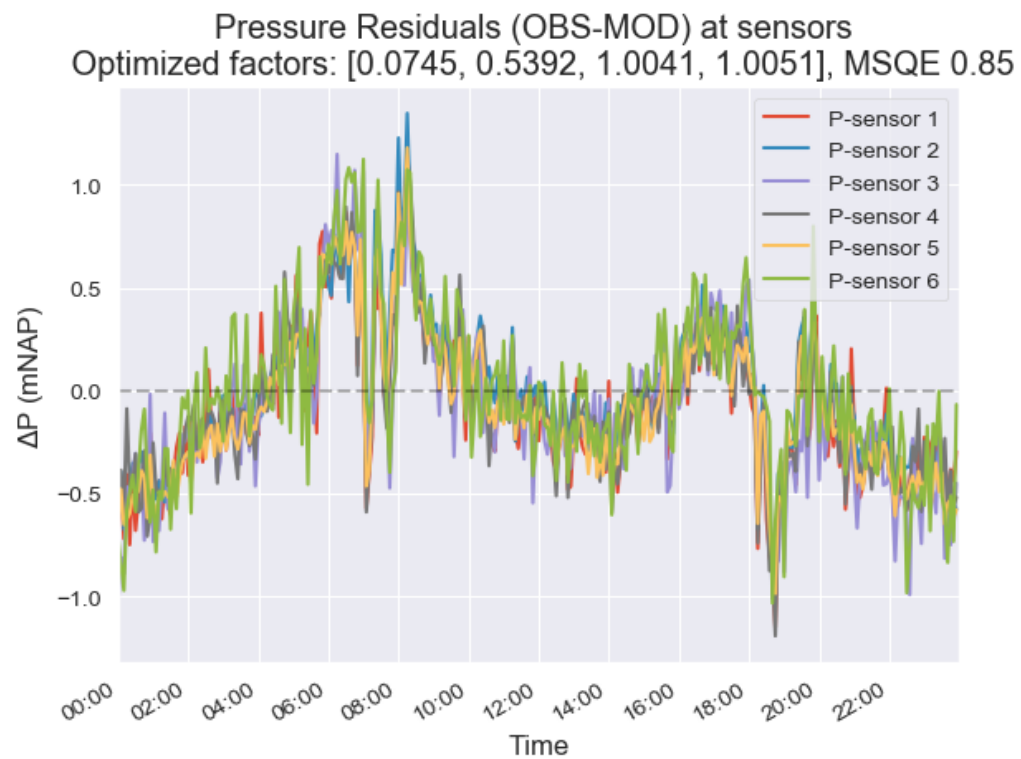

Figure D.7: Optimized sensor pressure residuals

E. Sensor specifications

Sofrel
LACROIX

March 17 – V 2.1 D

Sofrel Sensors CNPR/CPR, CNPI, CNPA
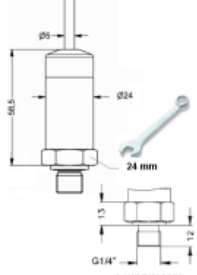**Level and pressure measurement**

1. Presentation
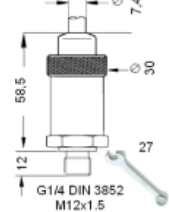
CNPR

Connectable: Measurement of drinking water pressure (pipes, etc.)
- CNPR range: 0 to 16 bar
- ¼ inch cylindrical gas connection DIN 3852 with watertight connector tightened using Ø 27mm key
- Measurement of clean water pressure
- Precision: +/- 0.35% FSO
- Inbuilt surge protection
- Watertightness: IP68
- Surge resistance: 60 bar
- Optimised power consumption: -30%

CPR

Connectable: Drinking water pressure measurement (pipes, etc.)
- CPR range: 10 or 20 bar
- ¼ inch cylindrical gas connection DIN 3852 with watertight connector tightened using Ø 24mm key
- Measurement accuracy: 0.5% FSO
- Inbuilt surge protection
- Watertightness: IP68
- Surge resistance: 60 bar
- Optimised power consumption: -30%

CNPI

Submersible: Measures level of clean water (reservoirs, drill holes, etc.)
- Stainless steel case
- Remotely powered 4-20 mA two-wire link
- Range: 6m, or 9m (or made to measure)
- Precision < +/-0.35% FSO
- Inbuilt surge protection
- ACS Certification
- Highly sensitive steel sensor: any contact with other objects or even your finger may cause damage. Do not under any circumstances remove the black cover.

CNPA

Submersible: Measures sewage levels
- Stainless steel case
- Remotely powered 4-20 mA two-wire link
- Range: 3m, or 6m (or made to measure)
- Precision < +/-0.35% FSO
- Inbuilt surge protection
- Suitable for wastewater or sewage (ceramic sensor, cleaning)
- Optimised power consumption
- The sensor is delivered with a black cover; when used with sewage, this cover must be removed before use.

Figure E.1: SOFREL pressure sensor specifications

Specification sheet

VEGA

VEGABAR 52
4 … 20 mA

Pressure transmitter with CERTEC® measuring cell

Technical data

Measuring ranges	-1 … +72 bar/-100 kPa … +7200 kPa (-14.5 … +1044 psig)
Smallest measuring range	+0.1 bar/+10 kPa (+1.45 psig)
Deviation	< 0.075 %, optionally up to < 0.05 %
Process fitting	Thread G½ (EN 837), thread from G1½ (DIN 3852-A), flanges from DN 25 or ANSI 1", fittings for the food processing and paper industry
Process temperature	-40 … +150 °C (-40 … +302 °F)
Ambient, storage and transport temperature	-40 … +80 °C (-40 … +176 °F)
Operating voltage	12 … 36 V DC
SIL rating	up to SIL2

Area of application

The VEGABAR 52 pressure transmitter can be used universally for measurement of gases, vapours and liquids. Also substances such as sand are not problem for the abrasion-resistant ceramic measuring cell. The VEGABAR 52 is an economical solution for a multitude of applications in all areas of industry.

Advantages

- High plant availability through maximum overload and vacuum resistance of the ceramic measuring cell
- Measurement down to the last drop through extremely small measuring ranges with high accuracy.
- Low costs for maintenance thanks to wear-free ceramic measuring cell

Function

The heart of the pressure transmitter is the pressure measuring cell that transforms pressure into an electrical signal. This pressure-dependent signal is converted into a standard output signal by the integrated electronics.
The sensor element is the CERTEC® measuring cell with excellent long-term stability and high overload resistance. The CERTEC® measuring cell is also equipped with a temperature sensor. The temperature value can be displayed via the indicating and adjustment module or processed via the signal output.

Materials

The wetted parts of the instrument are made of 316L, PVDF, Hastelloy, C4-plated or Sapphire-ceramic®. The process seal is available in FKM, FFKM as well as EPDM.
You will find a complete overview of the available materials and seals in the "configurator" on our homepage under www.vega.com/configurator.

Housing versions

The housings are available as single chamber or double chamber version in plastic, stainless steel or aluminium.
They are available in protection ratings up to IP 68 (25 bar) with external electronics.

Electronics versions

The instruments are available in different electronics versions. Apart from the two-wire electronics with 4 … 20 mA or 4 … 20 mA/HART, two purely digital versions with Profibus PA and Foundation Fieldbus are available.

Approvals

The instruments are suitable for use in hazardous areas and are approved e.g. according to ATEX and IEC. The instruments have also different ship approvals such as e.g. GL, LRS or ABS.
You can find detailed information on the existing approvals in the "*configurator*" on our homepage under www.vega.com/configurator.

Figure E.2: VEGA Vegabar 52 pressure sensor specifications

F. Pictures Duindorp

Figure F.1: Typical Duindorp street

Figure F.2: Typical Duindorp street

Figure F.3: Duindorp edge: dunes

Figure F.4: Duindorp edge: dunes

Figure F.5: Pump at inlet

Figure F.6: P-sensor location

Pictures by author: Jip van Steen

G. Normality analysis

Important within probability theory and statistics is checking if a data set can be drawn from a normal (or Gaussian) distribution. The normal distribution should not be confused with the standard normal distribution, in which the latter is a specific case of the former (Weisstein 2002). If the data is assumed to be drawn from a normal distribution or sufficiently normal-like, parametric statistical methods can be applied. If not, non-parametric statistical methods can be applied. If methods are used that assume a normal distribution, while it actually behaves like a different distribution, the results may be misleading. Hence, before determining a leak detection or localization method, it is of importance to analyse the model results (the simulated inflow and pressures at the sensors) on normality.

G.1 Methods

The *skewness* and *kurtosis* of a data set can be calculated. These are two important terms that describe the shape of a probability distribution of a random variable and they can give an indication of how similar the distribution looks to a normal distribution. Analyzing the skewness and kurtosis of a data set gives an indication of how the data set can be modelled by a normal distribution. Figure G.1 illustrates how these two terms influence the shape of a probability distribution, in comparison with a normal distribution.
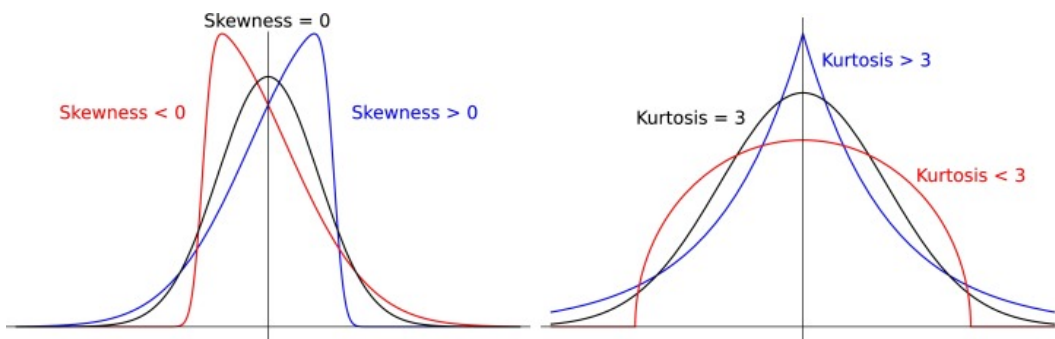

Figure G.1: Illustration probability distribution shape parameters: skewness and kurtosis

Skewness is a measure of asymmetry, in which a normal distribution has a skewness of zero and any symmetric data should have a skewness of near zero. A negative skewness indicates the data is generally skewed left, which means that the left tail is long relative to its right tail. A positive skewness logically indicates the opposite, that the data is skewed right. As a rule of thumb, a distribution with a skewness of between -0.5 and 0.5 is approximately symmetric. If the distribution has a skewness between -1 and -0.5 or between 0.5 and 1, the distribution is moderately skewed. A distribution with a skewness lower than -1 or greater than 1 is said to be highly skewed. Kurtosis is defined as the 'tail-heaviness' of a distribution. Data sets with a high kurtosis have heavy tails, or outliers. Data sets with a low kurtosis have light tails, or lack of outliers. The normal distribution has a kurtosis of 3. The equations that will be used in this study to calculate the skewness and kurtosis are adopted from Jarque and Bera 1980:

$$S = \frac{\frac{1}{n}\sum_{i=1}^{n}(x_i - \bar{x})^3}{(\frac{1}{n}\sum_{i=1}^{n}(x_i - \bar{x})^2)^{3/2}} \tag{G.1}$$

$$K = \frac{\frac{1}{n}\sum_{i=1}^{n}(x_i - \bar{x})^4}{(\frac{1}{n}\sum_{i=1}^{n}(x_i - \bar{x})^2)^2} \tag{G.2}$$

in which S is the skewness, K is the kurtosis and x is the data sample of n values and $\bar{x}$ is the sample mean.

To go further than solely an indication of normality that the skewness and kurtosis give, one can use normality tests to determine whether the data set follows a normal distribution. A normality test is used to determine how well a data set follows a normal distribution. It is a statistical test that starts with the null-hypothesis, which stands for the assumption that all values were sampled from a population that follows a normal distribution. A normality test reports a resulting P-value, which indicates the risk of concluding the data does not follow a normal distribution when it actually does. Hence it means that if the null-hypothesis were true, what is the chance of this sample to be the result of 'normal' randomness.

P-values are expressed in decimals, $p \in [0,1]$. A P-value of 0.03 means the results have a probability of 3% to just be a matter of 'normal' random chance if the data follows a normal distribution. Therefore, the smaller the p-value, the stronger the evidence that the null-hypothesis should be rejected and a normal distribution cannot be assumed.

To determine whether the null-hypothesis should be accepted or rejected, the resulting p-value has to be compared to a fixed significance level α. If $p > \alpha$, the null-hypothesis is accepted, hence it shows the data are not inconsistent with a normal distribution. Note that this does not prove the data were sampled from a normal distribution. If $p \leq \alpha$, the data is not consistent with a normal distribution and the null-hypothesis is rejected. The significance level is traditionally set at $\alpha = 0.05$, which will be adopted in this study.

There are multiple available normality tests described in the literature. While it is sometimes proposed that some tests are better than others, no test is best against all alternatives. It is therefore chosen in this study to compute the P-value results of three different normality tests: the Jarque-Bera test (Jarque and Bera 1980), the D'Agostino's and Pearson's test (D'Agostino and Pearson 1973), and the Shapiro-Wilk test (Shapiro and Wilk 1965). The resulting P-values of these three tests are compared, such that if all tests conclude a $p \leq 0.05$, it can be stated with 95% confidence that the data does not fit a normal distribution.

G.2   Performance on simulated sensor data

Once the stochastic demand is implemented into the hydraulic model, sensor data is simulated. Before describing a model-based leak detection method, it is of importance to first analyse the simulated sensor data on normality. If a leak detection method is used that assumes the sensor data behaves like a normal distribution, while it actually behaves like a different distribution, the results may be misleading. The resulting simulated inflow and pressure data at the sensors are therefore checked on normality in this section.

The simulated sensor results are based on $N_{sim} = 1000$ demand simulations. The time-span of the results is one day of 24 hours, and the frequency is 5 minutes, hence there are 288 time steps. This means that every 288 time steps consist of 1000 data points. Because the skewness, the kurtosis and the p-values in the normality tests can vary for every consecutive timestep, the mean average of 2 hours is calculated to determine what the overall trajectory of the scattered data points is.

The shape of the distribution (of the 1000 data points) can change throughout the day. Hence, the shape of the distribution in the morning can be very different from the shape of

the distribution in the evening. This is further discussed in the first subsection. The second subsection discusses the resulting normality tests, as described in the previous section. The resulting figures that are produced are shown in the third subsection.

G.2.1 Distribution shapes

Since every time step represents a distribution of $N_{sim} = 1000$ data points, the skewness and kurtosis can be calculated at each time step. Furthermore, Kernel Density Estimation (KDE) can be drawn at every time step. The Kernel Density Estimation (KDE) is a statistical tool to create a smooth curve of a given dataset. Hence, instead of representing the data in a histogram, the KDE is drawn from the data to visualize the shape of the distribution. The KDE of multiple times throughout the day are plotted in Figures G.2, G.4, G.6, G.8, G.10, G.12 and G.14 to illustrate the shape change of the simulated data distribution throughout the day. Furthermore, the data points are corrected for their median value at that timestep, such that the KDEs are more easily compared.

It is concluded from Figure G.2 that the simulated inflow data is approximately symmetric and has a kurtosis that corresponds to a normal distribution during the day. However, during the night it seems to be moderately skewed and does not correspond to a normal distribution. The same can be concluded from Figures G.4, G.6, G.8, G.10, G.12 and G.14, in which the distribution seems to be moderately skewed during the night although during the day it is slightly skewed but approximately symmetric. Hence, during the night, the simulated pressure at the sensors do not follow a normal distribution. During the day the simulated pressure sensor data seems to be fairly normal.

G.2.2 Normality tests

In Figures G.3, G.5, G.7, G.9, G.11, G.13 and G.15, the three tests are conducted for the simulated sensor data. The Jarque-Bera (J-B) test, Shapiro and Wilk (S-W) test and the D'Agostino and Pearson (D-P) test.

As can be seen in the Figure G.3, during the night almost all p-values do not exceed the significance level. Hence, during the night, the resulting simulated inflow can not be described by a normal distribution. However, during the day a majority of data points seem to exceed the significance level, meaning that during the day the simulated inflow can be generally described by a normal distribution.

The conducted normality tests of the simulated pressures at the six pressure sensors shown in Figures G.5, G.7, G.9, G.11, G.13 and G.15, show a different result. The p-value of all the conducted normality tests are generally below the significance level of 0.05. However, some data points show a higher p value, with a few high outliers. These timesteps are mostly observed late in the morning and the beginning of the evening. The computed rolling averages reach just above the significance level due to these outliers, though not significantly and usually only for a limited time span. It is therefore concluded that the simulated data from the pressure sensors is considered non-normal throughout the entire day and night.

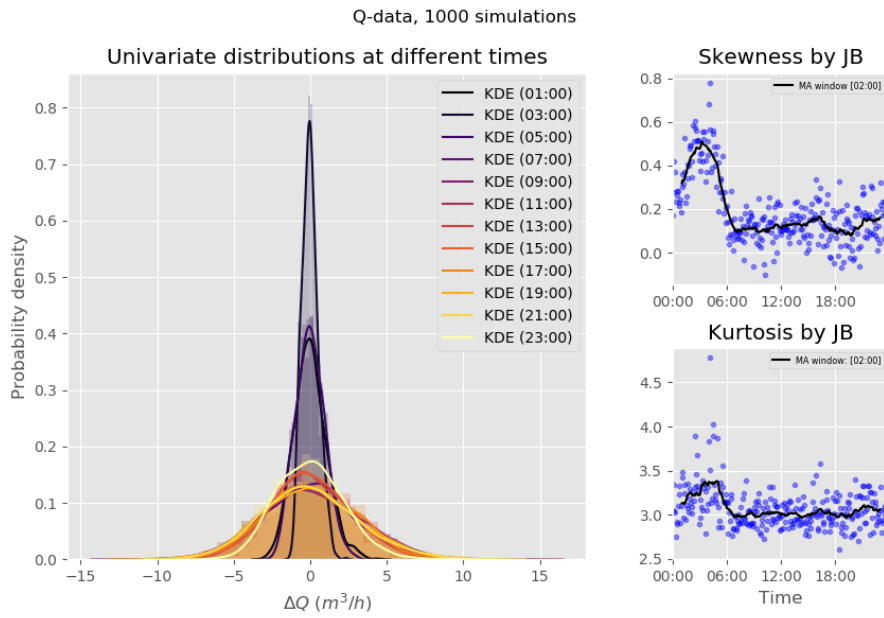### G.2.3   Dstiribution and normality test figures
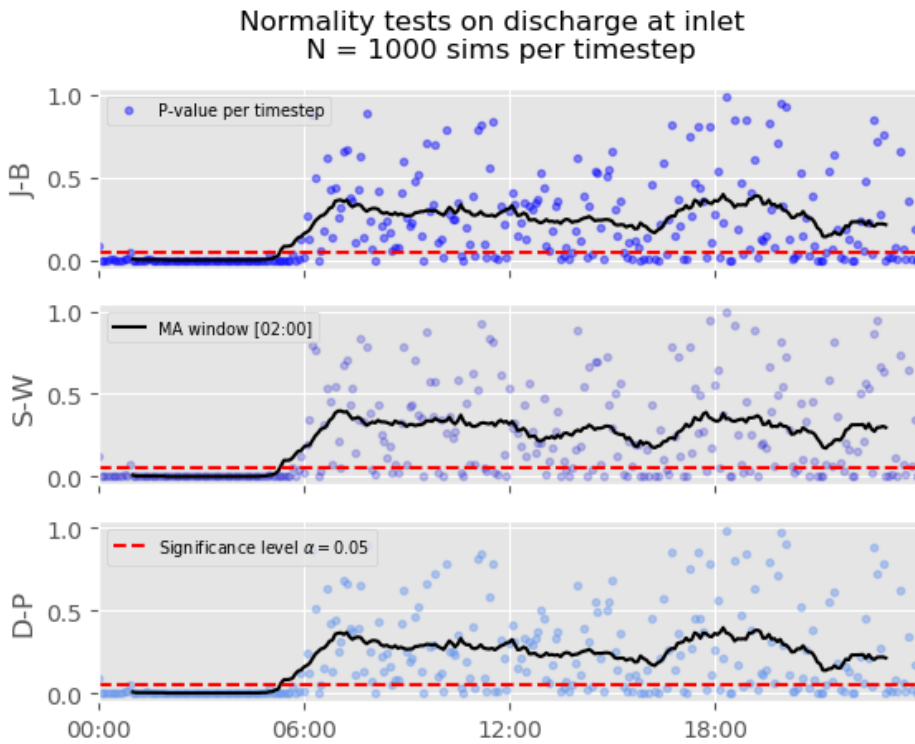

Figure G.2: Distribution shape simulated inflow

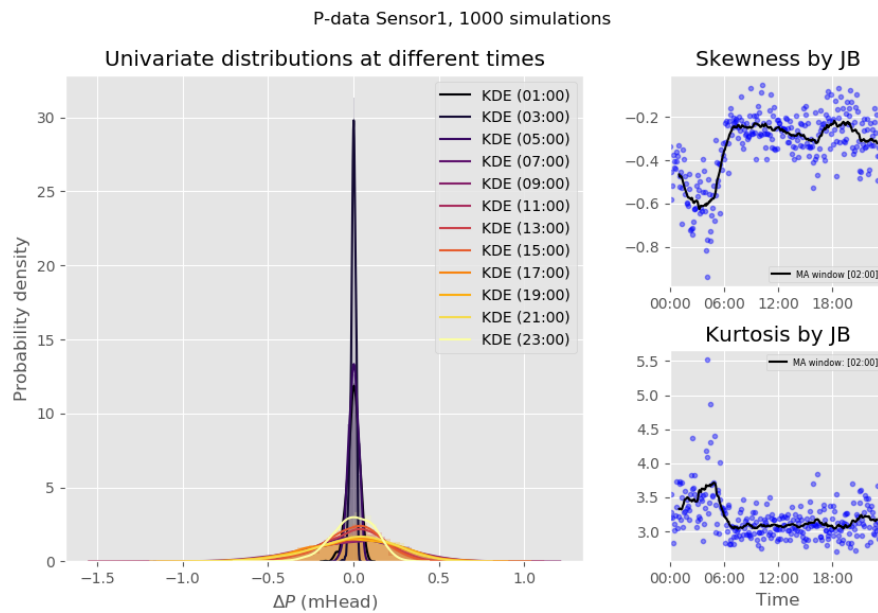Figure G.3: Normality tests simulated inflow

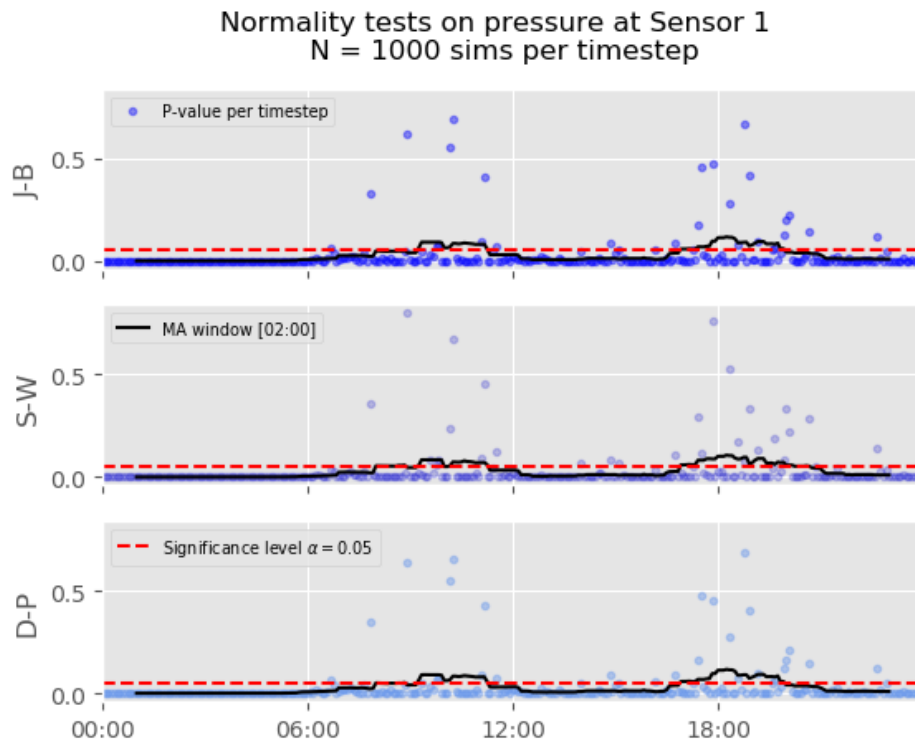Figure G.4: Distribution shape simulated pressure sensor 1

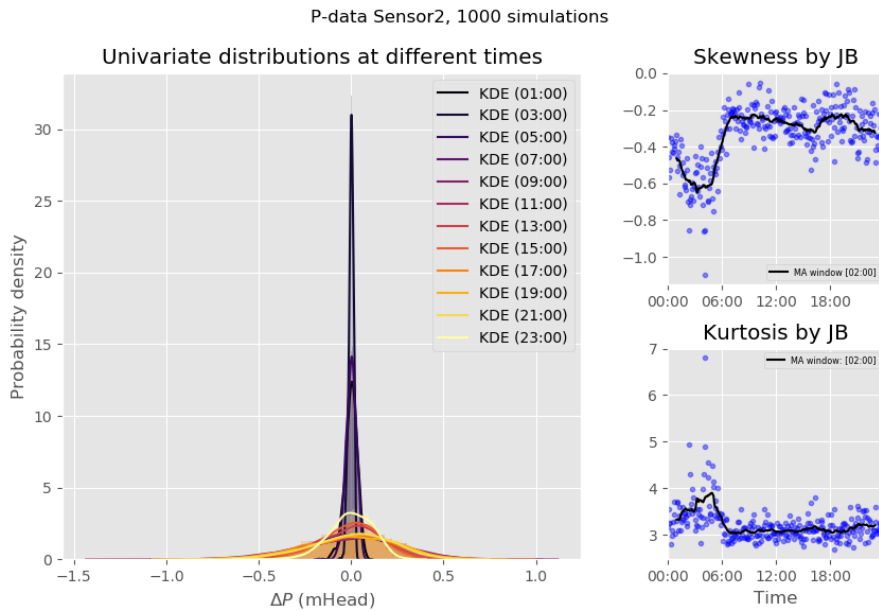Figure G.5: Normality test simulated pressure sensor 1

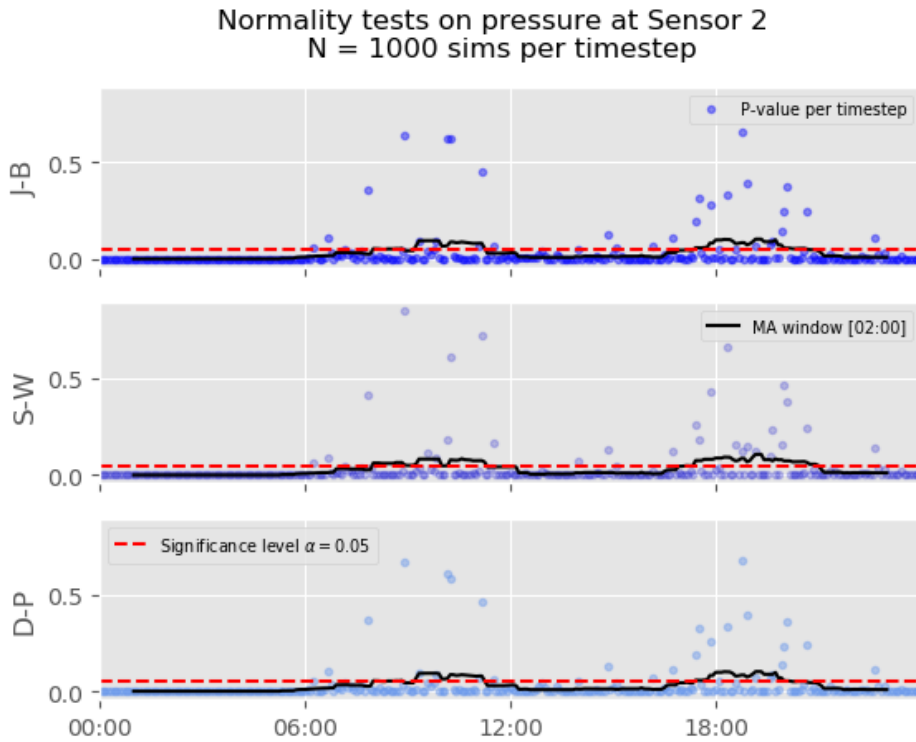Figure G.6: Distribution shape simulated pressure data sensor 2

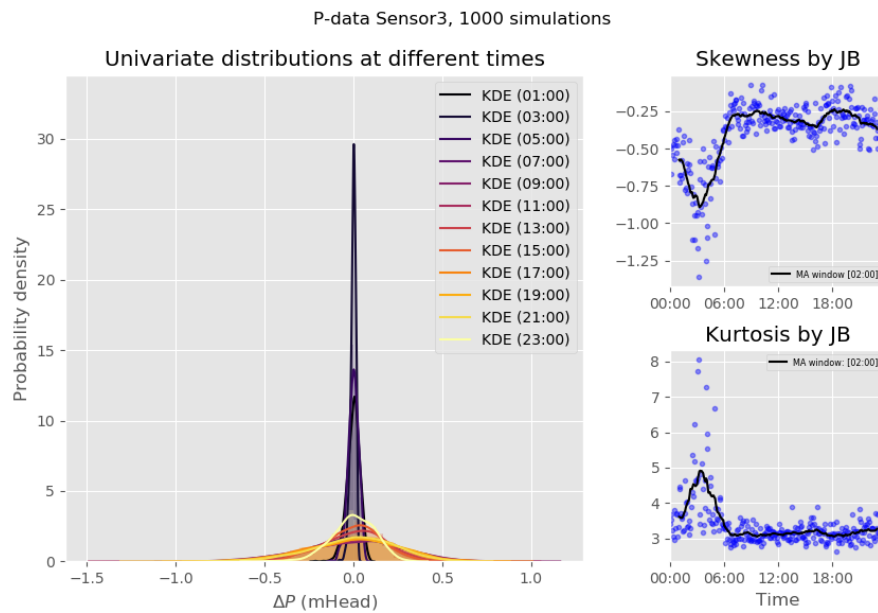Figure G.7: Normality test simulated pressure sensor 2

Figure G.8: Distribution shape simulated pressure sensor 3

Figure G.9: Normality test simulated pressure sensor 3

Figure G.10: Distribution shape simulated pressure sensor 4

Figure G.11: Normality test simulated pressure sensor 4

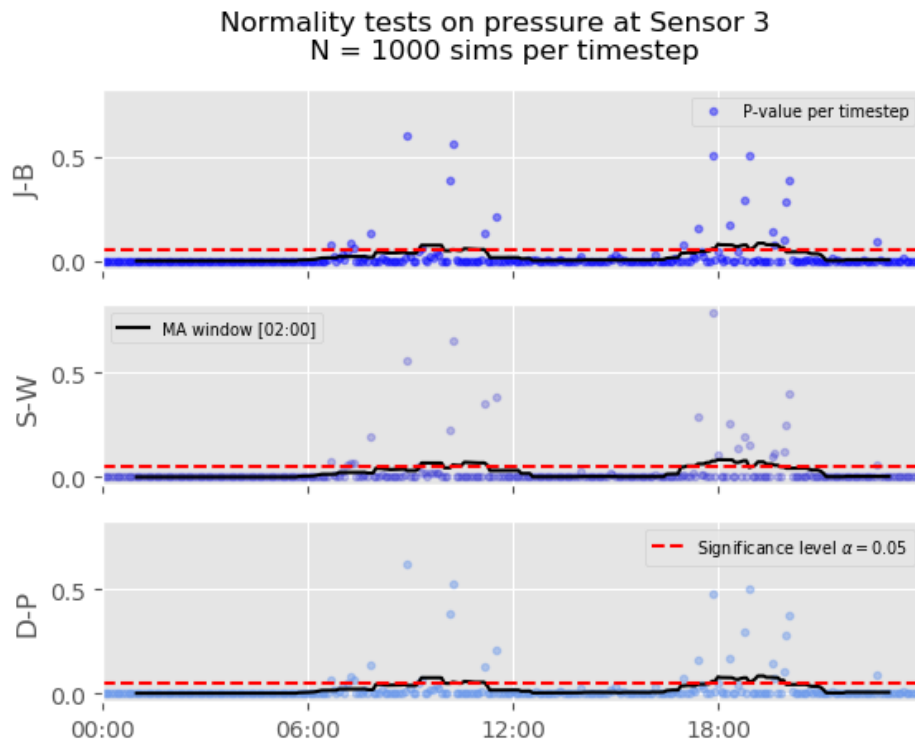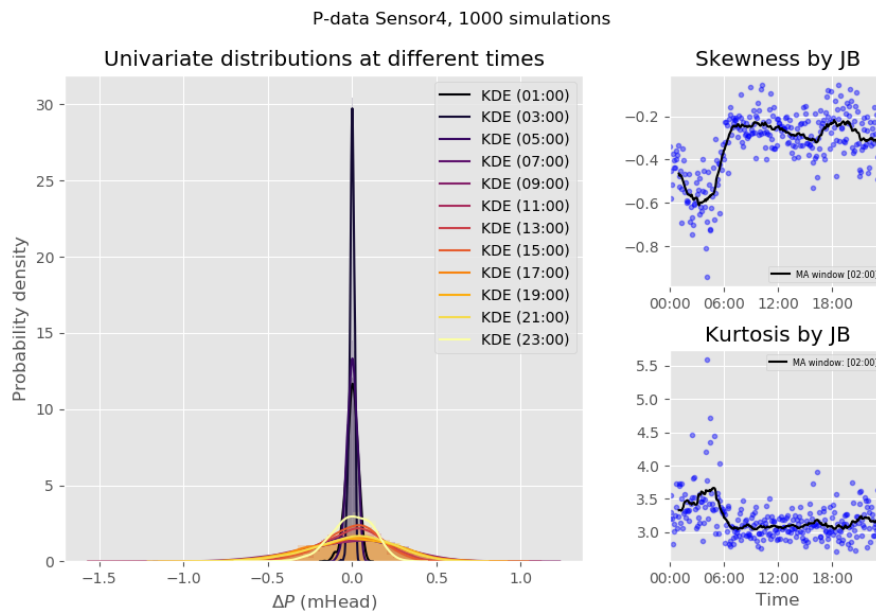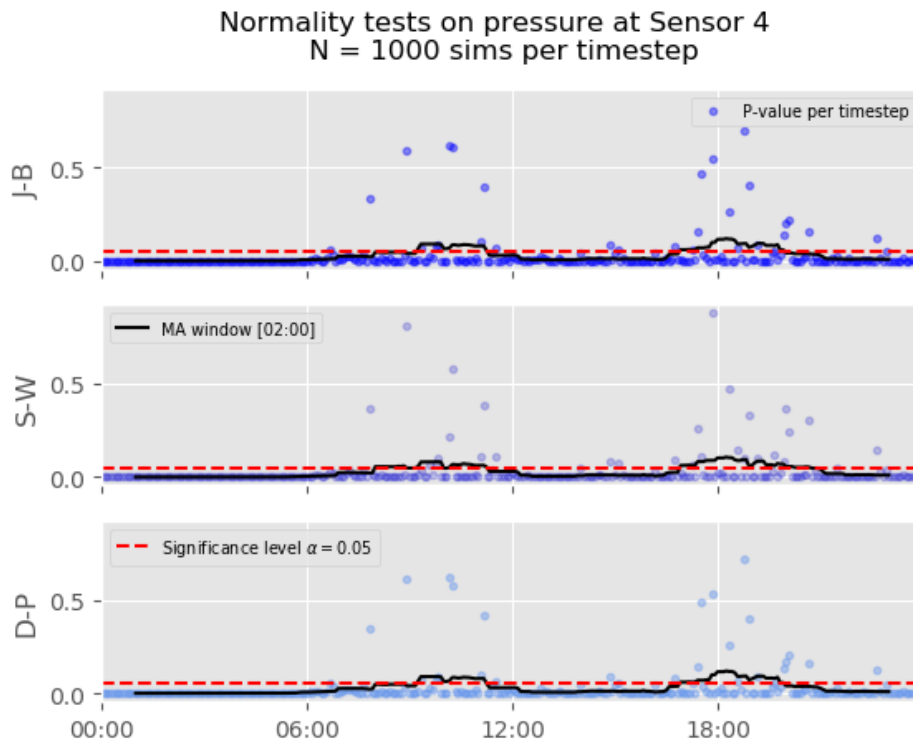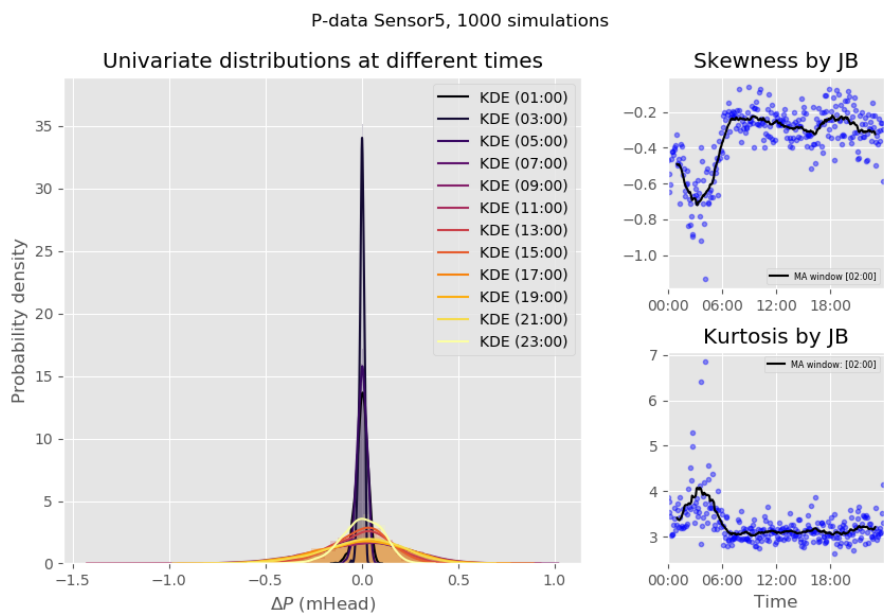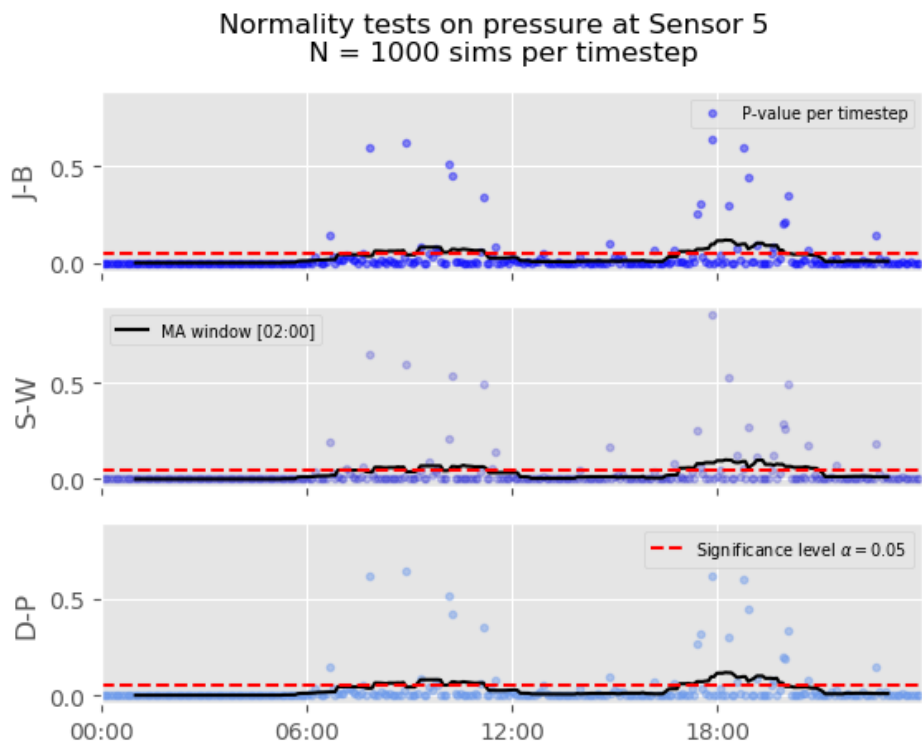Figure G.12: Distribution shape simulated pressure sensor 5

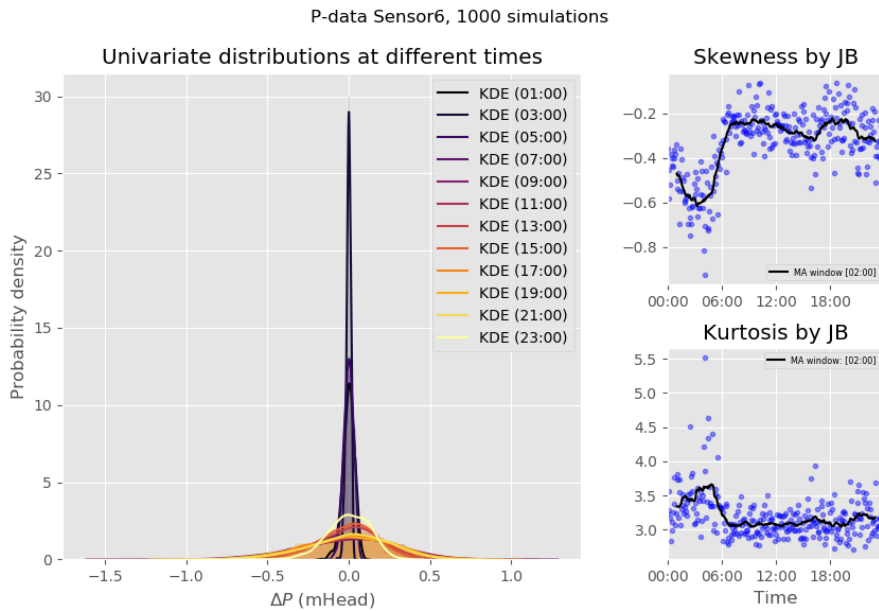Figure G.13: Normality test simulated pressure sensor 5

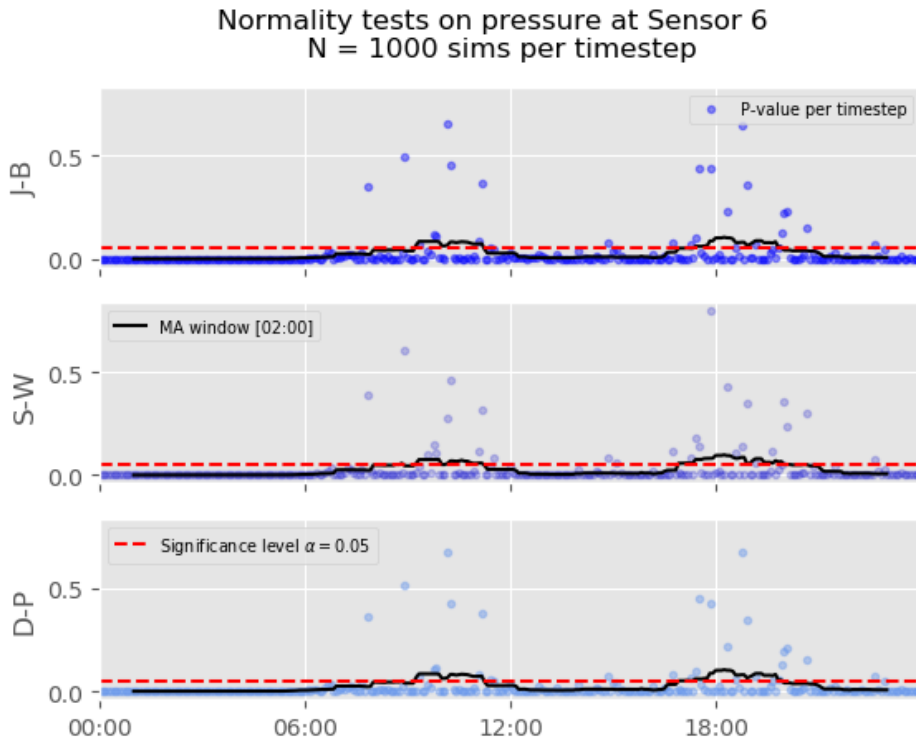Figure G.14: Distribution shape simulated pressure sensor 6

Figure G.15: Normality test simulated pressure sensor 6

H. Leak localization performance

The leak localization is performed for 27 different simulated scenarios in which the position of the leak, the size of the leak and the time at which the leak localization is performed. The three chosen leak positions are illustrated in Figure H.1 as leak A, leak B and leak C. The three chosen leak discharges are $Q_{leak} = 2.5m^3/h$, $Q_{leak} = 5m^3/h$ and $Q_{leak} = 7.5m^3/h$. The three different time intervals at which the leak localization is performed are 03:00-05:00, 07:00-09:00 and 15:00-17:00.
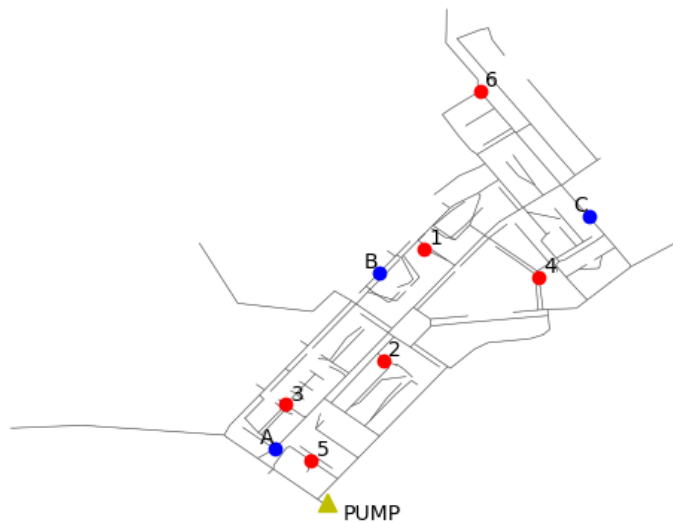
Figure H.1: Simulated leak positions

The first section comprises of tables and figures that illustrate the mean and the standard deviation of the evaluation parameters: D_T in meter, FP_r in percentage and MS in meter, all are taken over 250 simulations and calculated for each scenario. These tables and figures elucidate the differences between the different scenarios. The last three sections show the separate leak localization figures for leak position A,B and C in the different sections. Each plot represents a scenario and the nodal average correlation value of 250 simulations is illustrated with a certain color. The leaknode that is found most often (the highest correlation is found most often at this node) is illustrated with a star, and the percentage of simulations that estimated the leak to be at this node is also represented. The crosses represent the leaknodes which are found less often by the algorithm, relating to its transparency. Hence, a more transparent cross means the corresponding node is less often found by the algorithm. The mean of each evaluation parameters is taken over 250 simulations and denoted for each scenario.

H.1   Average and standard deviation results evaluation parameters

Table H.1: Results topological distance (meter)

	LEAK A
	LEAK B
	LEAK C

Results topological distance (D_T) of 250 simulations
Mean and standard deviations ($\mu \pm \sigma$)

LEAK TIME / LEAK SIZE	03:00 - 05:00	07:00 - 09:00	15:00 - 17:00
2.5 m^3/h	44 ± 37	200 ± 249	186 ± 251
	99 ± 78	284 ± 159	246 ± 142
	127 ± 109	344 ± 223	312 ± 209
5 m^3/h	38 ± 38	97 ± 121	76 ± 63
	40 ± 55	167 ± 83	178 ± 85
	58 ± 110	245 ± 140	194 ± 140
7.5 m^3/h	24 ± 34	70 ± 80	44 ± 47
	13 ± 30	156 ± 78	149 ± 91
	28 ± 79	187 ± 136	127 ± 108

Table H.2: Results false positive rate (%)

	LEAK A
	LEAK B
	LEAK C

Results false positives ($FP_\%$) of 250 simulations
Mean and standard deviations ($\mu \pm \sigma$)

LEAK TIME / LEAK SIZE	03:00 - 05:00	07:00 - 09:00	15:00 - 17:00
2.5 m^3/h	0.5 ± 0.6	19.7 ± 29.9	20.0 ± 31.5
	3.8 ± 2.3	24.4 ± 18.1	18.0 ± 15.8
	4.1 ± 4.3	15.6 ± 9.2	14.4 ± 9.7
5 m^3/h	0.4 ± 0.5	3.7 ± 9.7	1.8 ± 3.0
	1.6 ± 2.1	7.4 ± 6.7	6.9 ± 4.6
	1.2 ± 2.4	10.8 ± 7.2	8.9 ± 6.6
7.5 m^3/h	0.3 ± 0.5	1.6 ± 2.3	1.0 ± 1.3
	0.5 ± 1.3	5.3 ± 3.4	4.8 ± 2.9
	0.4 ± 1.6	8.3 ± 6.4	5.3 ± 5.1

Table H.3: Results maximum spread (meter)

LEAK TIME / LEAK SIZE	03:00 - 05:00	07:00 - 09:00	15:00 - 17:00
	Results maximum spread (MS) of 250 simulations Mean and standard deviations ($\mu \pm \sigma$)		
2.5 m³/h	58 ± 92	783 ± 610	676 ± 624
	263 ± 190	899 ± 415	741 ± 430
	260 ± 252	794 ± 379	721 ± 357
5 m³/h	46 ± 46	290 ± 310	185 ± 221
	118 ± 169	426 ± 259	427 ± 245
	92 ± 177	594 ± 339	497 ± 326
7.5 m³/h	40 ± 69	187 ± 234	114 ± 173
	39 ± 104	342 ± 209	330 ± 210
	33 ± 108	478 ± 337	315 ± 290

LEAK A
LEAK B
LEAK C

Leak localization scenario results
Average topological distance ($N_{sim} = 250$)
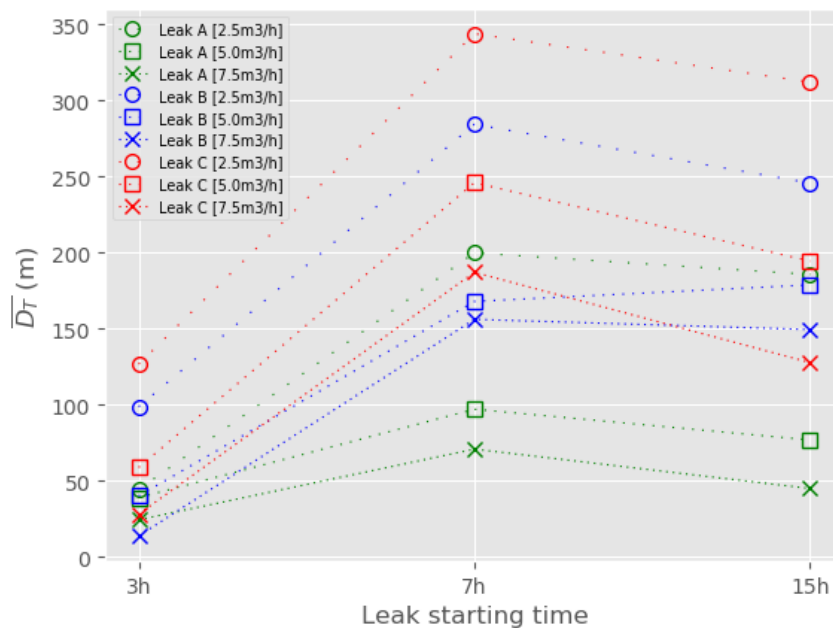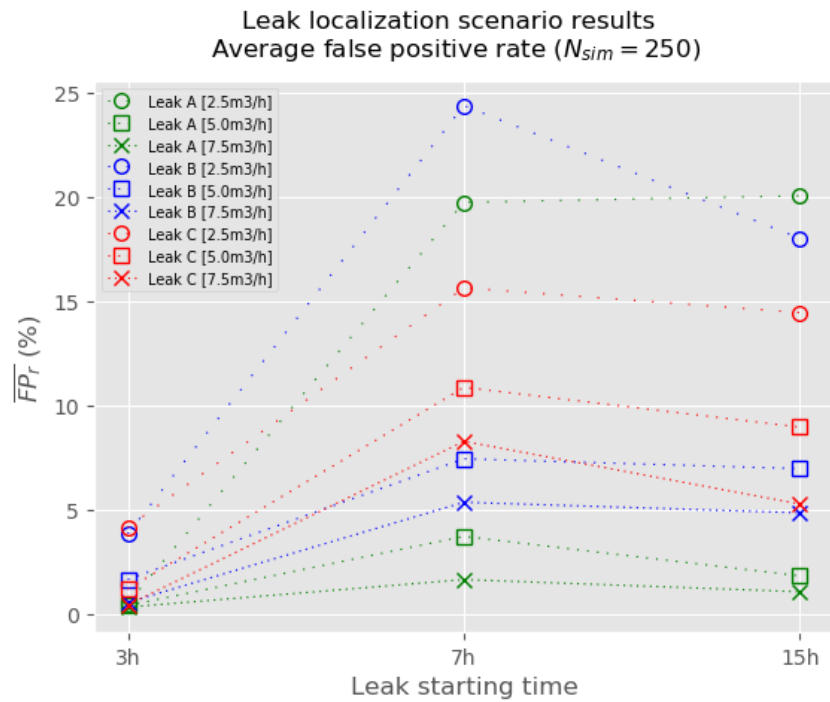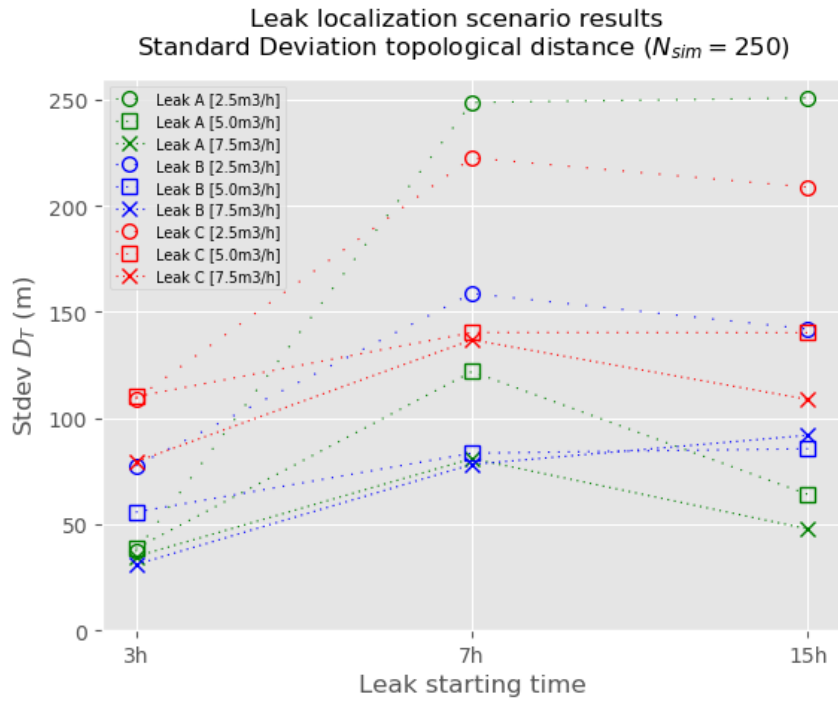
Leak localization scenario results
Standard Deviation topological distance ($N_{sim} = 250$)

Leak localization scenario results
Average false positive rate ($N_{sim} = 250$)

Leak localization scenario results
Standard Deviation false positive rate ($N_{sim} = 250$)
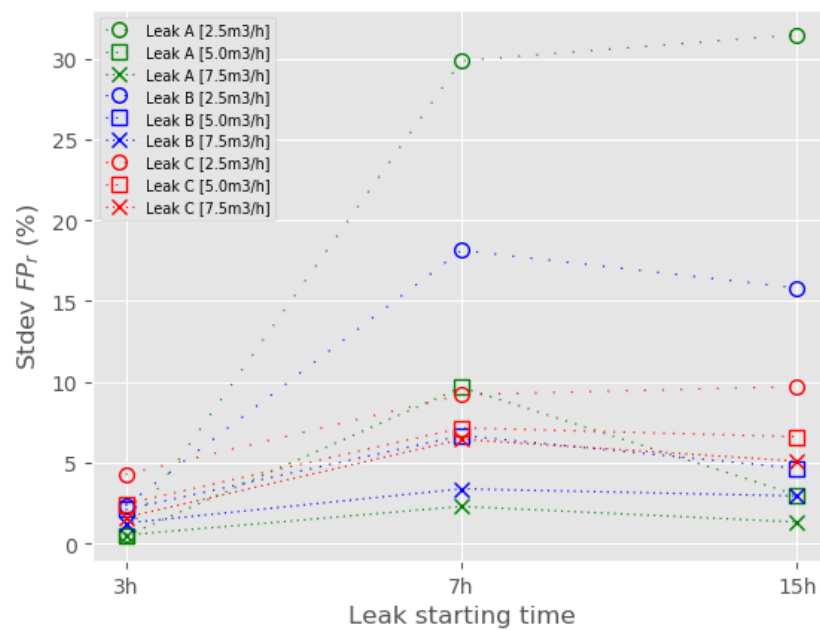
Leak localization scenario results
Average maximum span ($N_{sim} = 250$)

Leak localization scenario results
Standard Deviation maximum span ($N_{sim} = 250$)
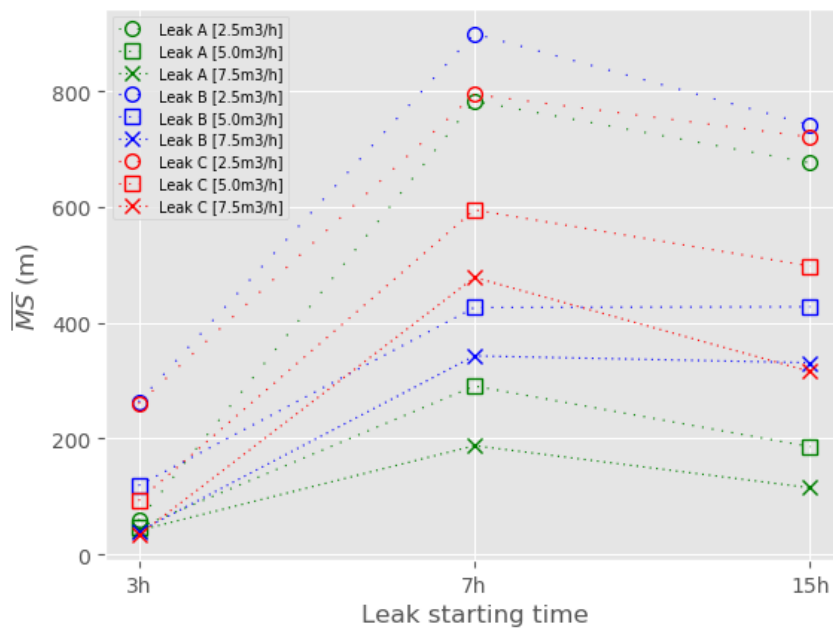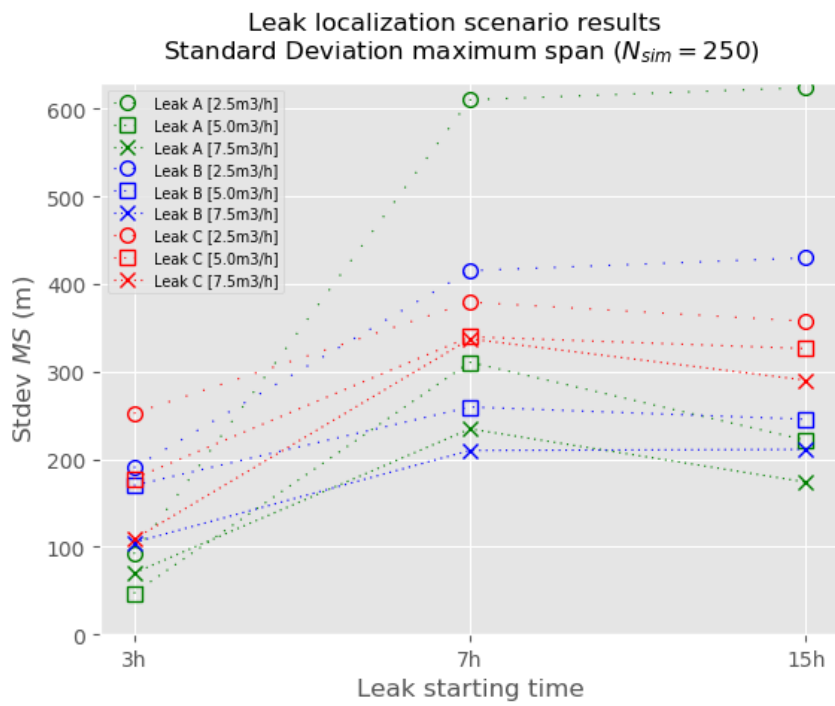
H.2 Leak A

Localization performance for different leak sizes and times of occurrence.

LL AVERAGE: 250 sims
Leak 2.5 m3/h during: [03:00 -- 05:00]

D_T: 44.2 m
FP_r: 0.5 %
MS: 58.4 m
□ Pressure Sensors
○ Actual Leak
☆ Most often found leak (48.4%)
✗ Less often found leak(s)

MEAN of 250 correlation values

LL AVERAGE: 250 sims
Leak 2.5 m3/h during: [07:00 -- 09:00]

D_T: 199.8 m
FP_r: 19.7 %
MS: 782.6 m
□ Pressure Sensors
○ Actual Leak
☆ Most often found leak (14.8%)
✗ Less often found leak(s)

MEAN of 250 correlation values

LL AVERAGE: 250 sims
Leak 2.5 m3/h during: [15:00 -- 17:00]

D_T: 185.6 m
FP_r: 20.0 %
MS: 676.0 m
□ Pressure Sensors
○ Actual Leak
☆ Most often found leak (18.0%)
✗ Less often found leak(s)

MEAN of 250 correlation values

LL AVERAGE: 250 sims
Leak 5 m3/h during: [03:00 -- 05:00]

D_T: 38.9 m
FP_r: 0.4 %
MS: 46.0 m
□ Pressure Sensors
○ Actual Leak
☆ Most often found leak (42.4%)
⊗ Less often found leak(s)

MEAN of 250 correlation values

LL AVERAGE: 250 sims
Leak 5 m3/h during: [07:00 -- 09:00]

D_T: 97.0 m
FP_r: 3.7 %
MS: 290.5 m
□ Pressure Sensors
○ Actual Leak
☆ Most often found leak (20.0%)
⊗ Less often found leak(s)

MEAN of 250 correlation values

LL AVERAGE: 250 sims
Leak 5 m3/h during: [15:00 -- 17:00]

D_T: 76.8 m
FP_r: 1.8 %
MS: 185.7 m
□ Pressure Sensors
○ Actual Leak
☆ Most often found leak (33.2%)
⊗ Less often found leak(s)

MEAN of 250 correlation values

LL AVERAGE: 250 sims
Leak 7.5 m3/h during: [03:00 -- 05:00]

D_T: 24.3 m
FP_r: 0.3 %
MS: 40.9 m
□ Pressure Sensors
○ Actual Leak
☆ Most often found leak (56.8%)
⊗ Less often found leak(s)

LL AVERAGE: 250 sims
Leak 7.5 m3/h during: [07:00 -- 09:00]

D_T: 70.8 m
FP_r: 1.6 %
MS: 187.5 m
□ Pressure Sensors
○ Actual Leak
☆ Most often found leak (28.4%)
⊗ Less often found leak(s)

LL AVERAGE: 250 sims
Leak 7.5 m3/h during: [15:00 -- 17:00]

D_T: 44.9 m
FP_r: 1.0 %
MS: 114.8 m
□ Pressure Sensors
○ Actual Leak
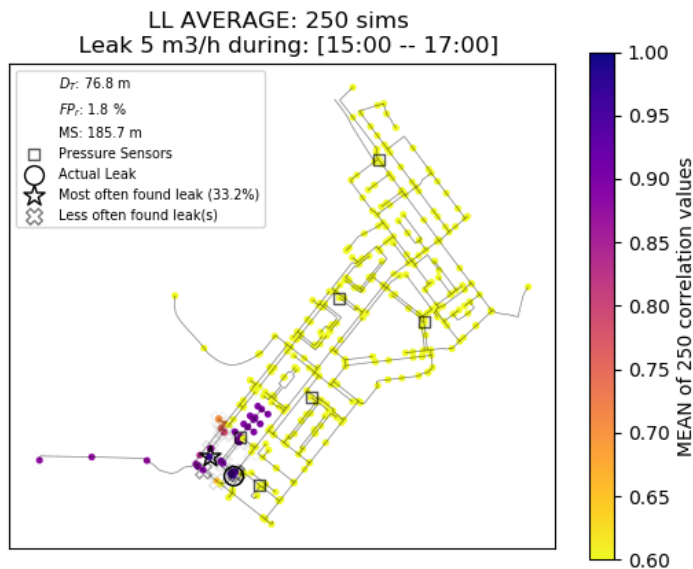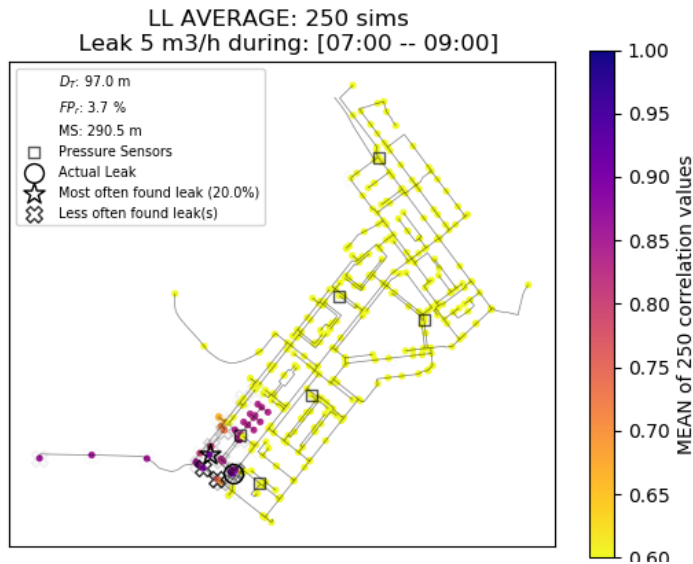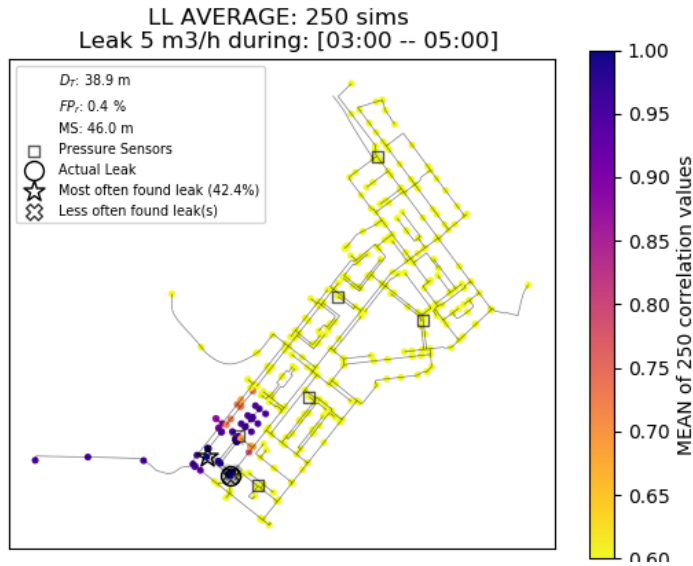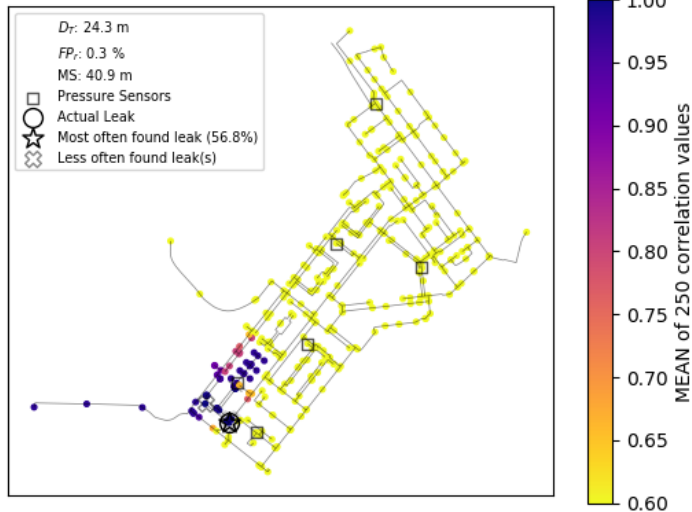☆ Most often found leak (30.8%)
⊗ Less often found leak(s)

H.3 Leak B

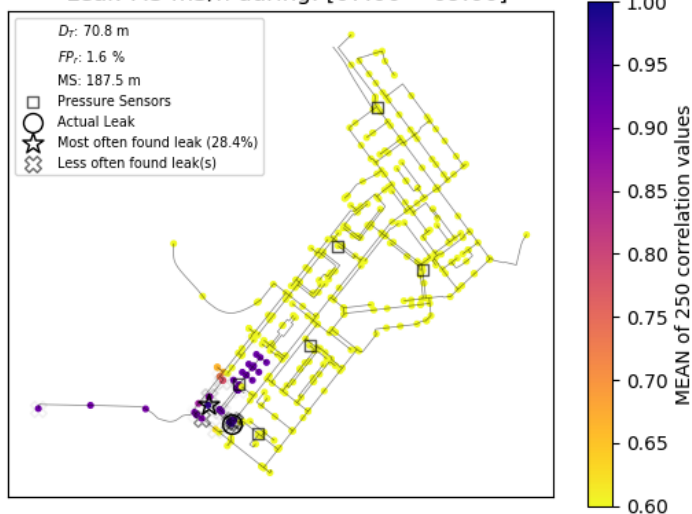Localization performance for different leak sizes and times of occurrence.

LL AVERAGE: 250 sims
Leak 2.5 m3/h during: [03:00 -- 05:00]

D_T: 98.8 m
FP_r: 3.8 %
MS: 263.4 m
□ Pressure Sensors
○ Actual Leak
☆ Most often found leak (14.4%)
⊗ Less often found leak(s)

LL AVERAGE: 250 sims
Leak 2.5 m3/h during: [07:00 -- 09:00]

D_T: 284.3 m
FP_r: 24.4 %
MS: 899.3 m
□ Pressure Sensors
○ Actual Leak
☆ Most often found leak (12.0%)
⊗ Less often found leak(s)

LL AVERAGE: 250 sims
Leak 2.5 m3/h during: [15:00 -- 17:00]

D_T: 245.7 m
FP_r: 18.0 %
MS: 741.4 m
□ Pressure Sensors
○ Actual Leak
☆ Most often found leak (13.2%)
⊗ Less often found leak(s)

LL AVERAGE: 250 sims
Leak 5 m3/h during: [03:00 -- 05:00]

D_T: 40.0 m
FP_r: 1.6 %
MS: 118.7 m
□ Pressure Sensors
○ Actual Leak
☆ Most often found leak (50.8%)
⊗ Less often found leak(s)

LL AVERAGE: 250 sims
Leak 5 m3/h during: [07:00 -- 09:00]

D_T: 167.9 m
FP_r: 7.4 %
MS: 426.2 m
□ Pressure Sensors
○ Actual Leak
☆ Most often found leak (14.8%)
⊗ Less often found leak(s)
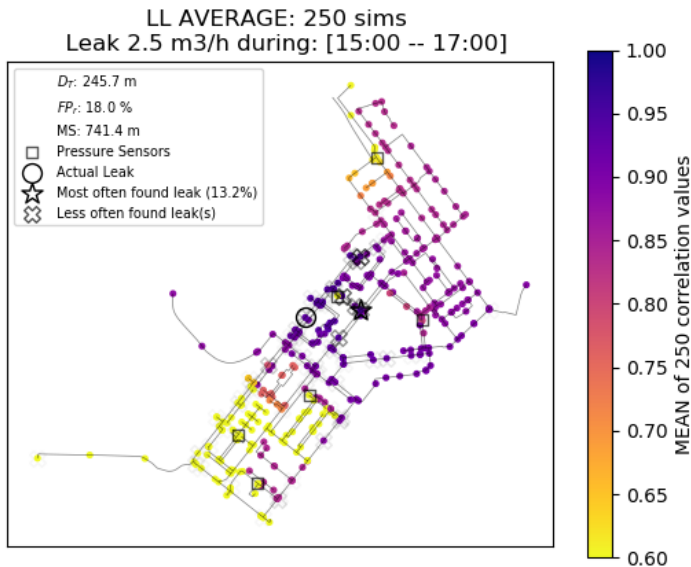
LL AVERAGE: 250 sims
Leak 5 m3/h during: [15:00 -- 17:00]

D_T: 178.8 m
FP_r: 6.9 %
MS: 427.5 m
□ Pressure Sensors
○ Actual Leak
☆ Most often found leak (18.8%)
⊗ Less often found leak(s)

MEAN of 250 correlation values

LL AVERAGE: 250 sims
Leak 7.5 m3/h during: [03:00 -- 05:00]

D_T: 13.7 m
FP_r: 0.5 %
MS: 39.0 m
□ Pressure Sensors
○ Actual Leak
☆ Most often found leak (79.2%)
✕ Less often found leak(s)

MEAN of 250 correlation values

LL AVERAGE: 250 sims
Leak 7.5 m3/h during: [07:00 -- 09:00]

D_T: 156.1 m
FP_r: 5.3 %
MS: 342.5 m
□ Pressure Sensors
○ Actual Leak
☆ Most often found leak (20.0%)
✕ Less often found leak(s)

MEAN of 250 correlation values

LL AVERAGE: 250 sims
Leak 7.5 m3/h during: [15:00 -- 17:00]

D_T: 149.4 m
FP_r: 4.8 %
MS: 330.7 m
□ Pressure Sensors
○ Actual Leak
☆ Most often found leak (16.4%)
✕ Less often found leak(s)

MEAN of 250 correlation values
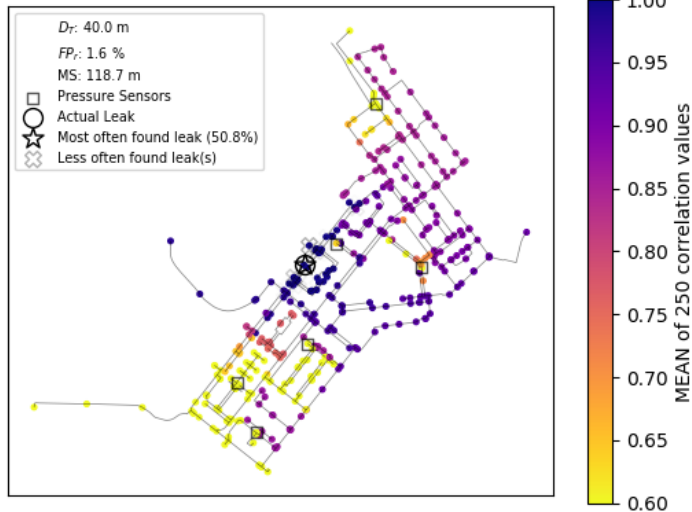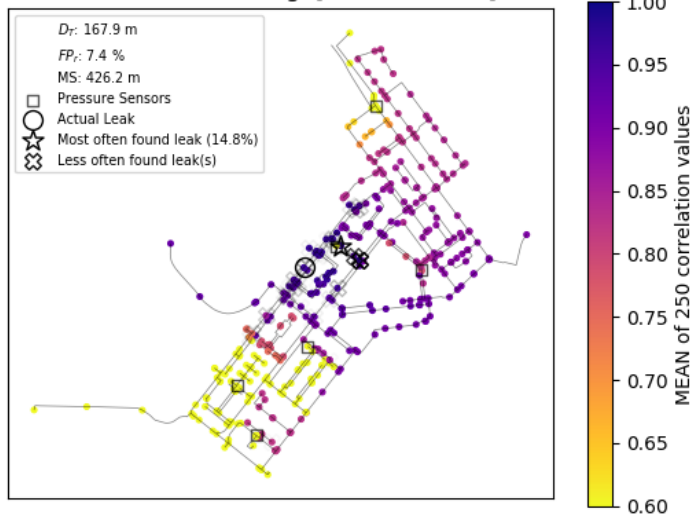
H.4 Leak C

Localization performance for different leak sizes and times of occurrence.

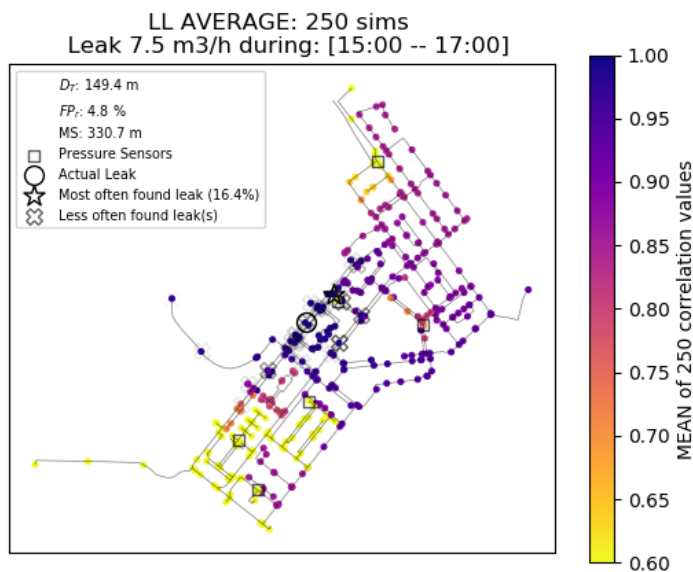LL AVERAGE: 250 sims
Leak 2.5 m3/h during: [03:00 -- 05:00]

D_T: 126.7 m
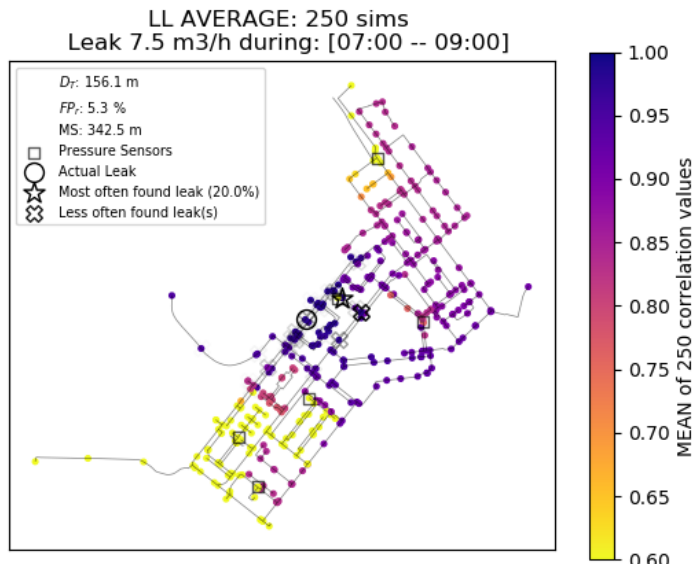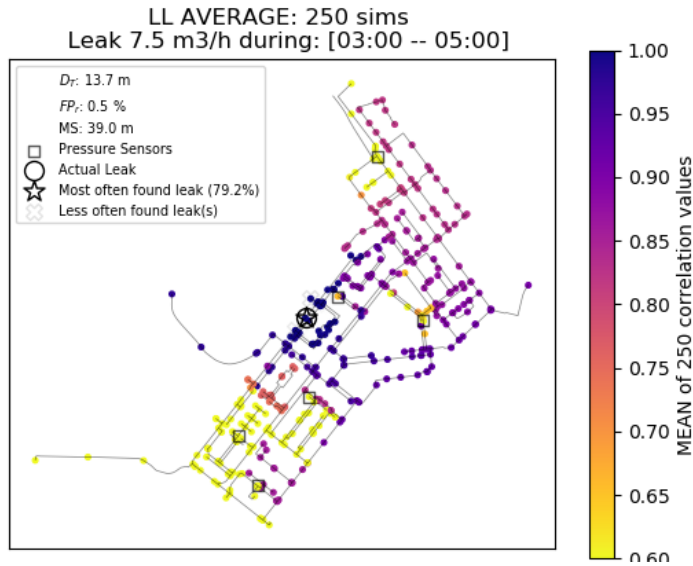FP_r: 4.1 %
MS: 260.1 m
□ Pressure Sensors
○ Actual Leak
☆ Most often found leak (27.6%)
⊗ Less often found leak(s)

MEAN of 250 correlation values

LL AVERAGE: 250 sims
Leak 2.5 m3/h during: [07:00 -- 09:00]

D_T: 343.9 m
FP_r: 15.6 %
MS: 794.3 m
□ Pressure Sensors
○ Actual Leak
☆ Most often found leak (10.4%)
⊗ Less often found leak(s)

MEAN of 250 correlation values

LL AVERAGE: 250 sims
Leak 2.5 m3/h during: [15:00 -- 17:00]

D_T: 312.1 m
FP_r: 14.4 %
MS: 720.6 m
□ Pressure Sensors
○ Actual Leak
☆ Most often found leak (8.4%)
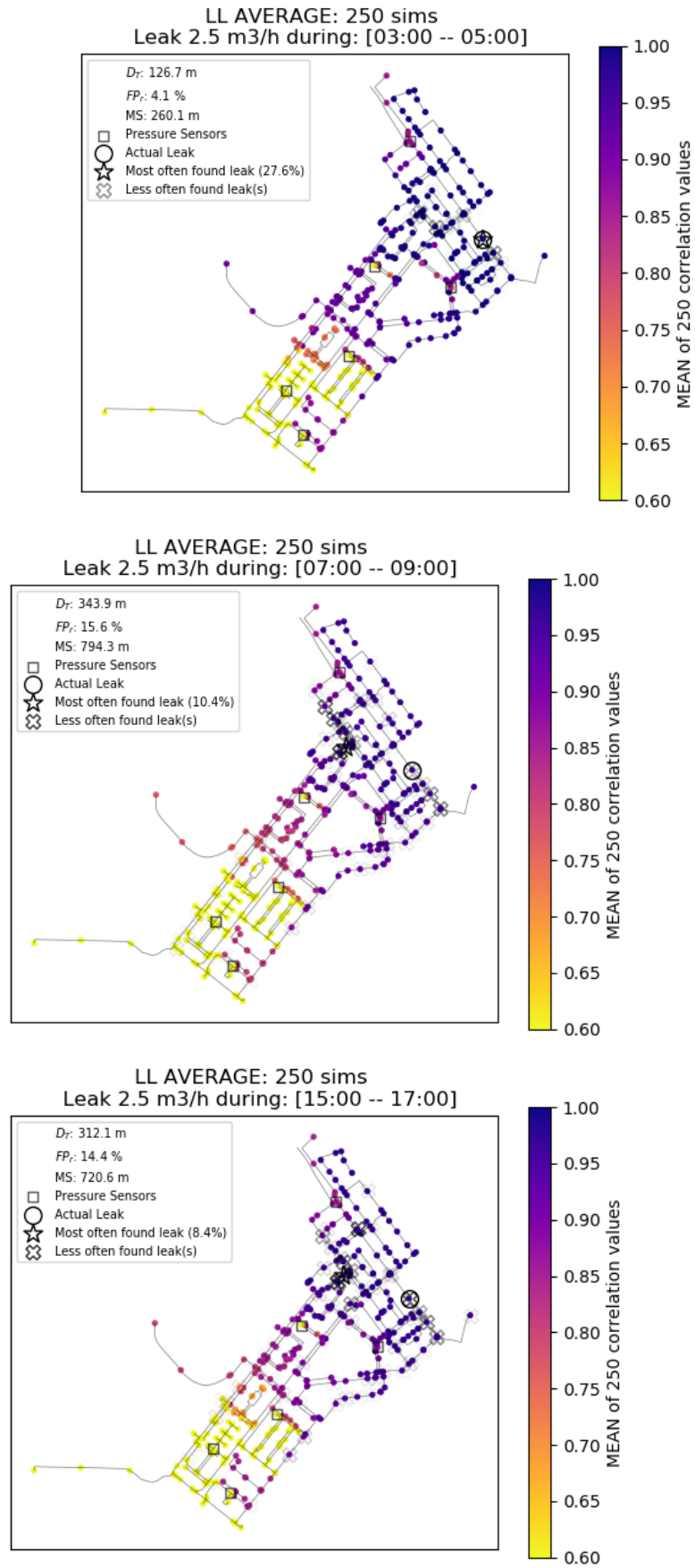⊗ Less often found leak(s)

MEAN of 250 correlation values

LL AVERAGE: 250 sims
Leak 5 m3/h during: [03:00 -- 05:00]

D_T: 58.7 m
FP_r: 1.2 %
MS: 92.6 m
☐ Pressure Sensors
○ Actual Leak
☆ Most often found leak (65.2%)
⊗ Less often found leak(s)

LL AVERAGE: 250 sims
Leak 5 m3/h during: [07:00 -- 09:00]

D_T: 246.0 m
FP_r: 10.8 %
MS: 594.8 m
☐ Pressure Sensors
○ Actual Leak
☆ Most often found leak (10.4%)
⊗ Less often found leak(s)

LL AVERAGE: 250 sims
Leak 5 m3/h during: [15:00 -- 17:00]

D_T: 194.4 m
FP_r: 8.9 %
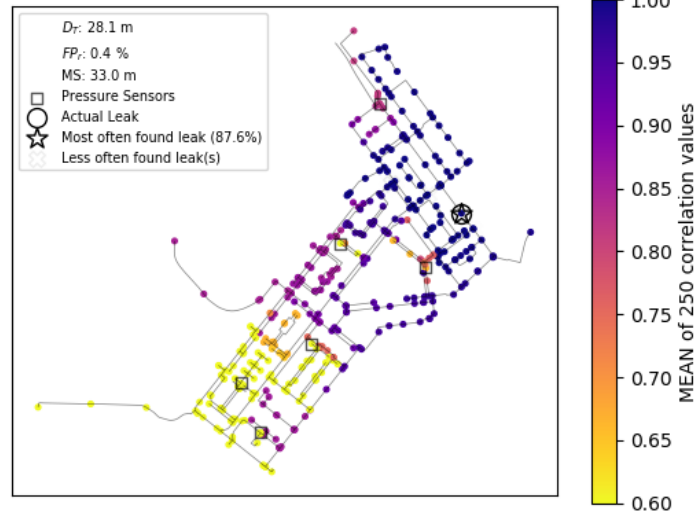MS: 497.6 m
☐ Pressure Sensors
○ Actual Leak
☆ Most often found leak (11.2%)
⊗ Less often found leak(s)

LL AVERAGE: 250 sims
Leak 7.5 m3/h during: [03:00 -- 05:00]

D_T: 28.1 m
FP_r: 0.4 %
MS: 33.0 m
□ Pressure Sensors
○ Actual Leak
☆ Most often found leak (87.6%)
✕ Less often found leak(s)

LL AVERAGE: 250 sims
Leak 7.5 m3/h during: [07:00 -- 09:00]

D_T: 187.0 m
FP_r: 8.3 %
MS: 478.2 m
□ Pressure Sensors
○ Actual Leak
☆ Most often found leak (16.0%)
✕ Less often found leak(s)

LL AVERAGE: 250 sims
Leak 7.5 m3/h during: [15:00 -- 17:00]

D_T: 127.6 m
FP_r: 5.3 %
MS: 315.5 m
□ Pressure Sensors
○ Actual Leak
☆ Most often found leak (22.0%)
✕ Less often found leak(s)

MEAN of 250 correlation values